Master's thesis

NTNU
Norwegian University of Science and Technology
Faculty of Information Technology and Electrical Engineering
Department of Engineering Cybernetics

Henning Levik Ørke

Autodock, Automated tugboat-assisted docking of large vessels

Master's thesis in TTK4900 - Engineering Cybernetics
Supervisor: Jan Tommy Gravdahl
Co-supervisor: Raymond Kristiansen
June 2022

NTNU
Norwegian University of
Science and Technology

Henning Levik Ørke

Autodock, Automated tugboat-assisted docking of large vessels

Master's thesis in TTK4900 - Engineering Cybernetics
Supervisor: Jan Tommy Gravdahl
Co-supervisor: Raymond Kristiansen
June 2022

Norwegian University of Science and Technology
Faculty of Information Technology and Electrical Engineering
Department of Engineering Cybernetics

NTNU
Norwegian University of
Science and Technology

Problem description

This master's thesis focuses on developing advanced automatic control solutions to support automated tugboat-assisted docking operations. The challenging problems related to automatic docking lend themselves to solution through advanced nonlinear automatic control theory, thereby enabling fully automated vessel docking with improved efficiency and reliability. The requirement of highly skilled helmsmen will be relaxed, as the control algorithms will optimally control the tugboats to provide necessary forces for vessel manoeuvring, and optimise time and power consumption as well as safety in the docking operation. In particular, the project includes the following sub tasks:

1. Perform a literature review on automated ship docking and berthing operations.
2. Develop a mathematical model for a specific case of a porting vessel and supporting tugboats, with interaction forces from towlines and stick-slip contact dynamics.
3. Develop control systems for the tugboats, for transit, pulling and pushing operations.
4. Develop guidance and control systems for the porting vessel and supporting tugboats under ideal conditions, with time delayed change between pushing and pulling operations.
5. Through simulations, show the performance of the mathematical model in task 2 and the control and guidance systems developed in task 3 and 4.

Preface

This master's thesis is submitted as a part of the requirement for a two-year master's degree in Industrial Cybernetics at the Department of Engineering Cybernetics at the Norwegian University of Science and Technology (NTNU) in Trondheim, Norway. The master's thesis is a continuation of the work I conducted autumn 2021 in the subject TTK4551 - Engineering Cybernetics, Specialisation Project. The report from the specialisation project is not published, and to give the best reading experience, the theory and methods used are both restated and rewritten in this thesis. The specific chapters and section reused from the specialisation project are mentioned through the thesis and given in the list below.

- Chapter 1 - section 1.1 and 1.3.1
- Chapter 2 - whole chapter except section 2.2.2
- Chapter 3 - whole chapter
- Chapter 4 – section 4.1 and 4.2.3

The Simulink model used in this thesis was developed by me with the tools, Matlab version r2021b and Add-Ons, Stateflow, Optimization Toolbox and Symbolic Math Toolbox, and the MSS toolbox created by Thor I. Fossen for the subject TTK4190 - Guidance, Navigation and Control of Vehicles [1].

I would like to thank my project lead Raymond Kristiansen[1] for this interesting thesis and supportive guidance, and my main supervisor Jan Tommy Gravdahl[2] for supportive guidance. The guidance sessions have provided useful information and support throughout my thesis work. I would also like to credit Thor I. Fossen[2] for answering questions that have helped me understand relevant theory.

Henning Levik Ørke

Trondheim, 2022-06-06

[1] Department of Electrical Engineering, The Arctic university of Norway, Narvik
[2] Department of Engineering Cybernetics, The Norwegian University of Science and Technology, Trondheim

Abstract

Vessels in need of tugboats assistance for docking are usually massive and require multiple tugboats in a manually coordinated operation. Many studies have focused on developing advanced automatic control solutions for controlling tugboats to manoeuvre a large vessel, for automating the docking operation. The common practice among the prior studies is that tugboats are in position to immediately give the desired forces. This thesis focuses on the time delays required to move tugboats in position to provide either pushing or pulling forces and aims to develop guidance and control systems to manoeuvre a large vessel by using tugboats with their own dynamics as thrusters.

First, a mathematical model was developed in Simulink/Matlab by implementing the bulk carrier and tugboat vessel dynamics. Towline dynamics and stick-slip contact dynamics were implemented to simulate the interaction forces between the vessels. Then, the tugboat control systems were developed with several linear and non-linear control laws to get in position and give the desired forces, by using Stateflow logic to switch between them, and control allocation to solve for the necessary directional azimuth thrust forces. Finally, control and guidance systems were developed to control the tugboat operation, by using Stateflow logic to activate the control system when tugboats are in position to compensate for the time delays.

Simulation results show reasonable performance of using tugboats with their own dynamics as thrusters. The mathematical model has plausible dynamics that enlightened certain problems that must be considered when developing guidance and control systems. The results also show limitations for the tugboat control system in operations with increased velocities, while the solutions to handle the time delay was vulnerable to small changes. More work is necessary to create a more realistic model, while control and guidance systems should be developed to handle weather and hydrodynamical forces in harbours.

Sammendrag

Fartøy som trenger slepebåtassistanse for dokking, er vanligvis massive og krever flere slepebåter i en manuelt koordinert operasjon. Mange studier har fokusert på å utvikle avanserte automatiske kontrollsystemer til å kontrollere slepebåter for å manøvrere et stort fartøy, for å automatisere dokking operasjonen. Vanlig praksis blant de tidligere studiene er at slepebåter er i posisjon til å umiddelbart gi de ønskede kreftene. Denne masteroppgaven fokuserer på tidsforsinkelsene som oppstår når slepebåter forflyttes til posisjon for å gi enten skyve- eller trekkrefter, og har som mål å utvikle styrings- og kontrollsystemer for å manøvrere et stort fartøy ved å bruke slepebåter med egen dynamikk som thrustere.

Først ble det utviklet en matematisk modell i Simulink/Matlab ved å implementere fartøysdynamikken for bulkskipet og taubåtene. Slepelinedynamikk og stick-slip-kontaktdynamikk ble implementert for å simulere interaksjonskreftene mellom fartøyene. Deretter ble kontrollsystemet utviklet for taubåtene med flere lineære og ikke-lineære kontrollere for å komme i posisjon og gi de ønskede kreftene, ved å bruke Stateflow-logikk til å bytte mellom dem, og kontrollallokering for å finne de nødvendige retningsbestemte asimutkraftkreftene. Til slutt ble kontroll- og styresystemer utviklet for å kontrollere slepebåtoperasjonen, ved å bruke Stateflow-logikk til å aktivere kontrollsystemet når slepebåtene er i posisjon for å kompensere for tidsforsinkelsene.

Simuleringsresultater viser akseptabel ytelse ved å bruke slepebåter med egen dynamikk som thrustere. Den matematiske modellen har plausibel dynamikk som belyser visse problemer som må vurderes når kontroll- og styresystemer utvikles. Resultatene viser også begrensninger for kontrollsystemet til slepebåtene i operasjoner med økt hastighet, mens løsningene for å håndtere tidsforsinkelsen var sårbare for små endringer. Mer arbeid er nødvendig for å lage en mer realistisk modell, mens kontroll- og styresystemer bør utvikles for å håndtere vær og hydrodynamiske krefter i havner.

Contents

List of Figures

List of Tables

Abbreviations

ADMM Alternating Direction of Multipliers Method.

ASD azimuth stern drive.

ASV Autonomous Surface Vessel.

CG centre of gravity.

CO coordinate origin.

COG course over ground.

DOF degrees of freedom.

DP dynamic positioning.

LOS Line-of-Sight.

LP low-pass.

MBL minimum breaking load.

MCR maximum continuous rating.

MIMO multiple-input and multiple-output.

MPC Model Predictive Control.

NED North-East-Down.

QP quadratic programming.

SOG speed over ground.

SQP sequential quadratic programming.

List of symbols

$\{n\}$ Denotes North-East-Down (NED) reference frame

$\{b\}$ Denotes Body reference frame

$x^{\{\cdot\}}$ Generalised north coordinate
$y^{\{\cdot\}}$ Generalised east coordinate
ψ Generalised heading angle
} as the vector $\boldsymbol{\eta}$

u Linear velocity in surge
v Linear velocity in sway
r Angular velocity in Yaw
} as the vector $\boldsymbol{\nu}$

X Force in surge
Y Force in sway
N Moment in yaw
} as the vector $\boldsymbol{\tau}$

$\boldsymbol{R}$ Rotational matrix between reference frames

$\boldsymbol{M}$ Inertia mass matrix

$\boldsymbol{C}$ Coriolis and centripetal matrix

$\boldsymbol{D}$ Damping matrix

$\boldsymbol{d}(\boldsymbol{\nu})$ Non-linear damping vector

$\boldsymbol{T}$ Thrust coefficient matrix

l Length from thrust force to CO

$f, \boldsymbol{W}$ Control force and weighting matrix

$s, \boldsymbol{Q}$ slack variable and weighting matrix

$\alpha, \boldsymbol{\Omega}$ Azimuth angle and weighting matrix

$\boldsymbol{\Omega_{n,b}}$ Diagonal matrix with, natural frequency ω_n, bandwidths ω_b

$\boldsymbol{Z}$ Diagonal matrix with relative damping ratios ζ

χ ourse angle

y_e cross track error

Δ Lookahead distance

π_p Path course

$C_{B,T}$ Contact point, Bulk and Tug

$T_{B,T}$ Towline connection point, Bulk and Tug

$F_{N,Tow,R,Tot}$ Ineraction forces, Normal, Towline, Friction and Required friction force to stick

$\mu_{s,k}$ Friction coefficients, static, kinetic

μ_0 Critical damping ratio

Chapter 1

Introduction

In this chapter, section 1.2 and section 1.3 are rewritten from section 1.2 and 1.3.1 from the specialisation project [2].

1.1 Background and motivation

Docking refers to the operation of manoeuvring a ship safely to a dock in harbour for loading and/or unloading operations. The docking operation require full knowledge of the ships handling and propulsion system capabilities. The handling is determined from a ships pivot point, the point it rotates about, which changes depending on the forces that act on the ship [3]. Large ships propulsion system usually consists of aft propellers and rudders that require forward velocity to turn, while some are equipped with bow tunnel thrusters to improve manoeuvring at lower velocities (see figure 1.1b). Since the rudder use waterflow from the forward velocity to turn, the turning capability is reduced at low velocity and may cause loss of steering when propellers rotate astern when stopping. Astern moving propellers also cause more noticeable transverse thrust. Transverse thrust is thrust force that causes the stern to move to either port or starboard from the interaction effects between propeller, rudder and hull. This effect can be used to bring the stern alongside the dock as shown in figure 1.1a, but the effect could be hard to predict as the direction can change in shallow waters. [4]

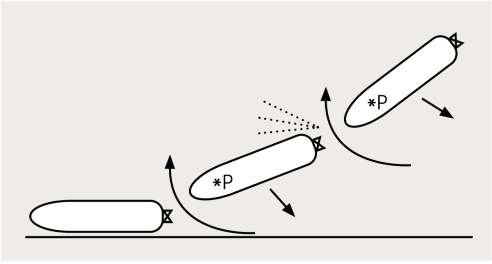

(a) Docking, P=pivot point.

(b) Bow tunnel thrusters.

Figure 1.1: Illustrating docking using transverse thrust in (a) and showing bow tunnel thrusters in (b). Edited from [4]

Harbours have velocity restrictions, dynamic traffic and limited area for manoeuvring. This makes the docking operations challenging for large ships, where the docking operation must be carefully planned out with high enough velocity to steer the ship, but low enough to be able to stop. In addition, wind and ocean currents would also affect the manoeuvring and increase the difficulty of the docking operation. While the forces have larger impact on the

alongside of the ship, the current direction close to the dock can create problems. A current that moves with the ship would require astern motion to stop, while docking against the current could push the ship towards or away from the dock, depending on the ship angle with the dock (see figure 1.2). When the ship closes in on the dock, the restricted waterflow between the ship and dock can cause interactive forces that can suck the ship towards the dock or push it away. Due to the challenges with docking operations, tugboat assistance could be necessary or required. [4]

(a) Pushed away, p=pivot point

(b) Interactive forces

Figure 1.2: Illustrating ocean current effect close to the dock, pushing away in (a) and pushing towards the dock due to suction force of the constrained waterflow in (b). Edited from [4]

Tugboat assisted docking operations often require multiple tugboats that are strategically placed around the hull of the towed ship, where they can apply pushing or pulling forces. The effectiveness of the tug will depend on the position from the pivot point. For a ship moving forward, the pivot point would move ahead, where a tugboat placed closer to the stern would have more effect in rotating the ship than a tugboat closer to the bow [4]. The tugboat operation is coordinated through radio communication by an experienced pilot of the harbour, onboard the towed ship, and skilled helmsmen to manually operate the tugboats. As each operation is unique, due to winds, ocean currents and dynamic traffic in ports, the pilot must adjust the towing operation along the way. The ships that require assistance are usually massive in both size and weight, where every action must be planned and carefully carried out. By automating the operation, the collaboration between the tugboats can be improved

Figure 1.3: Manual tugboat assisted docking of a bulk carrier in Narvik. *Photo: R. Kristiansen*

as the controller will find an optimal solution. This will require solutions through advanced non-linear control theory combined with optimisation problems, to compute the necessary forces and positioning of each tugboat. The coordination through radio communication can therefore be relaxed, and resulting in improved efficiency, time, and safety.

1.2 Relevant studies

There have been many studies on manoeuvring surface vessel by using multiple tugboats as thrusters attached to the hull, with different solutions to the control algorithms. It usually consists of four to six tugboats, opposite paired around the hull, where they can apply pushing forces that have limited rotational capabilities. By using a force allocation strategy, with adaptive control law to compensate for unknown hydrodynamic parameters, asymptotically convergent reference tracking is achieved with six tugboats as thrusters [5]. The thrust allocation is solved as a least square optimisation problem, with linear constraints and is validated through model scale testing. With a similar approach, another study solves the control allocation as an optimisation problem, by using the redistributed pseudo inverse to find desirable directional thrust force for the tugboats [6]. The study uses four tugboats on an unactuated ship, with limited pushing force and directional change, and manage to follow a path with desired velocities in Matlab simulations. An adapting controller is also implemented to account for the uncertainty in draft coefficients of the damping matrix. By using the same method to solve the control allocation problem, another study shows that a sliding mode controller can be used at slow speed trajectory tracking, which have desirable performance in the presence of environmental disturbances [7]. The controller is simulated with a small model, where a non-linear observer is used to estimate position from noisy measurements.

In [8], a floating structure is manoeuvred with three Autonomous Surface Vessel (ASV) in a triangular formation, by combining pushing force at the stern and towline forces on each side. The towline forces are modelled with non-linear dynamics, where the tugboats are attached to the floating structure with two towlines each, one to aft and the other to fore, to allow for surge, sway and yaw control. Simulation results show that a predefined trajectory can be followed, with both static and dynamic obstacles, by using Model Predictive Control (MPC) to control the ASVs and an Alternating Direction of Multipliers Method (ADMM) based approach to make consensus among them.

Dynamic positioning (DP) systems are used to keep overactuated marine vessels in a desired position and heading, by using their own propulsion systems. Studies have focused on improving efficiency and developing robust system capable of handling thruster failures. In [9], an adaptive dynamic control law is developed based on the complex adaptive backstepping method, to compensate for failures or reduced efficiency of thrusters in different control allocation methods. Simulation results show satisfactory performance without information of thruster failures and disturbances. Another study shows that by including hy-

drodynamic interactions from thruster in the thrust allocation problem and solving it as a non-linear sequential quadratic programming (SQP) optimisation problem, the efficiency and performance can be improved [10].

1.3 Prerequisites and assumptions

This thesis is based on tugboat operations in Narvik harbour. Narvik harbour has since 2005 had the title “Motorway of the sea” due to the large quantities of ore shipped out with bulk carriers [11]. From live map at marinetraffic.com, the ore is usually transported in bulk carriers with length 200-300 meters, width 30-45 meters, and carrying capacity between 60 000 to 180 000 tonne. There are three tugboats from "Bukser og Berging" stationed in Narvik, Bulldog, Barents and Rombak, which have either azimuth or voith propulsion systems capable of producing thrust in 360° [12].

The bulk carriers are docked with starboard side when loading ore, as seen in figure 1.4, to reduce manoeuvring when leaving harbour fully loaded. Usually, three tugboats are used on the port side as seen in figure 1.3. There are two main approaches to docking in Narvik, either rotating outside the harbour and then moving astern or moving ahead and turning in a half circle in the harbour area [13].

Due to the location of Narvik, the harbour is affected by the tides, where the height difference between the high tide and low tide usually oscillates with 2-3 [m] [14].

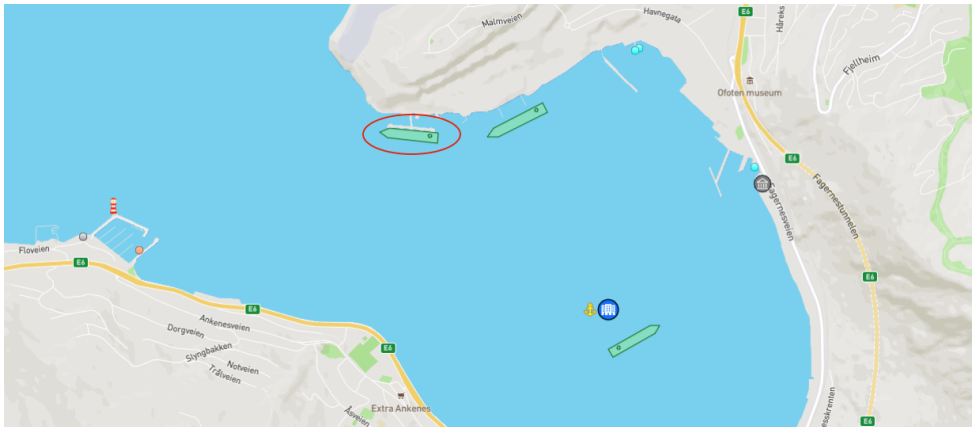

Figure 1.4: Narvik harbour, the red circle shows a bulk carrier loading ore at the dock. Image taken from live map at Marinetraffic.com on 16.November.2021.

1.3.1 Assumptions

Simplifications and assumptions used in this thesis are as followed:

- The marine crafts can only operate in 3-Degrees of freedom (DOF).
- The marine crafts position, orientation and velocities are known.

- Ideal weather conditions, no ocean currents, wind or waves.
- Thrust force has no correlating effect that reduces efficiency.

1.4 Contribution

Many studies have focused on docking operations by coordinating multiple ASV/tugboats to manoeuvre a large ship or structure. Multiple control system solutions have been developed that are capable of handling model parameter uncertainties, environmental disturbances and obstacle avoidance. The common practice among the prior studies is that tugboats are usually placed on both sides of the towed object and in position to immediately give the desired forces.

Since tugboat assisted docking operations may be carried out from one side of the towed object, like in Narvik, the tugboats would require repositioning to change the force direction. This thesis focuses on the time delay required to move tugboats in positions to give either pushing or pulling forces. The contribution of this thesis is a simulator developed in Matlab/Simulink of a bulk carrier and supporting tugboats, with interaction forces between them to simulate towline forces and contact forces with stick-slip dynamics. The necessary control and guidance systems have been developed for the tugboats and bulk carrier, with a proposed strategy to handle the time delay of using tugboats as thrusters.

1.5 Outline

The rest of the thesis is structured as followed:
Chapters 2 and 3 give the theoretical background for developing a mathematical model and a guidance and control system for a surface vessel with supporting tugboats in 3-DOF . Equations and theory, with exception of section 2.2, are based on the "Handbook of marine craft hydrodynamics and motion control" [3], by Thor I. Fossen.

Chapter 4 presents the method of implementing the bulk carrier and tugboat dynamics and the interaction forces between them, while simulation results and discussion of the model and interaction forces are given in chapter 5.

Chapter 6 presents the method of implementing the tugboat control system, while simulation results and discussion of the control system is given in chapter 7.

Chapter 8 presents the method of implementing the bulk carrier control and guidance systems to control the tugboat operation, while simulation results and discussion of the tugboat assisted operation is given in chapter 9.

Chapter 10 concludes the thesis and recommend improvements for further work.

Chapter 2

Mathematical modelling

This chapter presents the theory used to develop the mathematical model of the vessel dynamics and interaction forces. In the chapter, section 2.1 is based on chapter 2 and section 3.2.1 from the specialisation project [2]. The text is rewritten to include the course in section 2.1.1, non-linear damping in section 2.1.3 and fixed pitch propeller dynamics in section 2.1.4.

2.1 Marine craft dynamics

The motion of a marine craft can be described by six body fixed linear and angular velocities, as seen in figure 2.1. By assuming that the rotation in roll and pitch are small, these can be neglected for surface vessels and simplifies the motion of a marine craft to 3-DOF [3]. With 3-DOF, the dynamics of a marine craft is represented in two dimensions with surge, sway and yaw, which are used in this section to find the equations of motion.

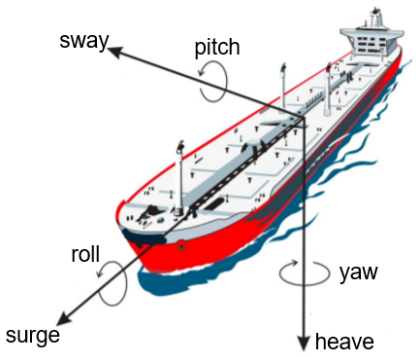

Figure 2.1: The body fixed linear velocities (surge, sway, heave) and angular velocities (roll, pitch, yaw) for a surface vessel. Edited from [3]

2.1.1 Kinematics

The kinematics of a marine craft are usually represented in two reference frames. One to describe the position and orientation, and one to describe linear and angular velocities. For geographical areas of less than 10x10 [km], position and orientation of a marine craft can be represented accurately in the North-East-Down (NED) reference frame [3]. The NED reference frame, denoted $\{n\}$, spans a tangential plane with origin located at the earths reference ellipsoid, with axes pointing to true north x_n, east y_n and the earths centre z_n, [3]. Linear and angular velocities are represented in the Body reference frame, which is fixed to the marine

craft. The Body reference frame, denoted $\{b\}$, usually has the origin at the waterline in the centre of the ship, where the axes point to the bow x_b, starboard y_b and keel z_b [3].

The position and orientation of a marine craft are described by the Body reference frame relative to NED (see figure 2.2a). Position is represented by the coordinates of the Body origin in NED $[x^n, y^n]$, while orientation is given by the angle between true north x_n and the bow direction x_b, which is referred to as heading ψ and is clockwise positive. While heading describes the orientation of the marine craft, the linear movement is represented by the course over ground (COG) χ and can be found with equation (2.1) [3].

$$\chi = \psi + \beta_c \tag{2.1}$$

In the equation, β_c is the crab angle, which is the angle of the speed over ground (SOG) U of the marine craft in Body (see figure 2.2b). The surface velocity is composed of the linear velocity in surge u and sway v, which consist of the ocean current and relative velocity denoted $\{c\}$ and $\{r\}$, as given in equation (2.2). In the absence of ocean currents, the crab angle is equal to the sideslip β, which is caused by the relative velocity of the marine craft.[3]

$$U = U_c + U_r \rightarrow \begin{bmatrix} u \\ v \end{bmatrix} = \begin{bmatrix} u_c + u_r \\ v_c + v_r \end{bmatrix} \tag{2.2}$$

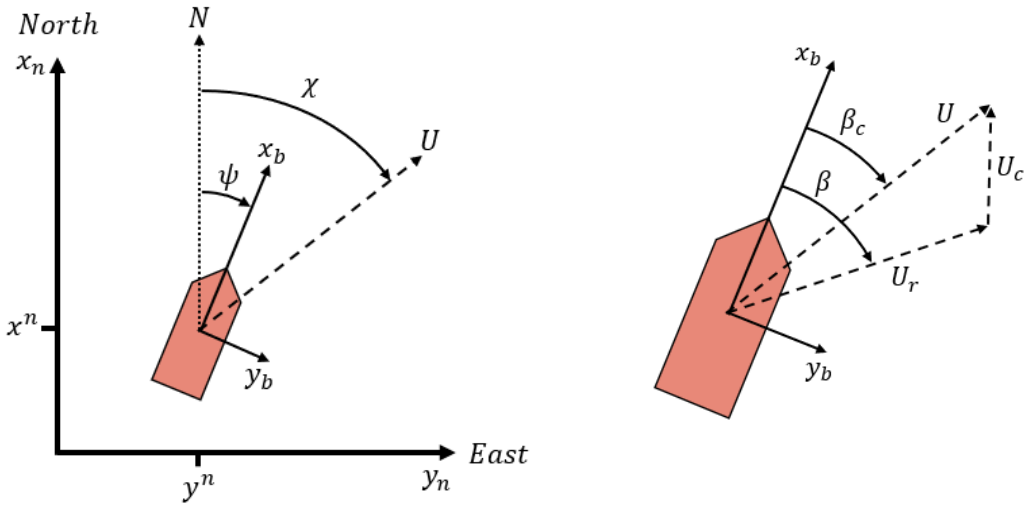

(a) Reference frames **(b)** Velocity

Figure 2.2: In (a), the Body reference frame {b} in NED {n} related by the coordinates $[x^n, y^n]$ and heading angle ψ, with course angle χ. In (b), the surface velocity U composed of relative velocity U_r and ocean current U_c, with crab angle β_c and sideslip β. Edited from [3]

The kinematics of the marine craft are given by the position and orientation vector $\boldsymbol{\eta}$ and linear and angular velocity vector $\boldsymbol{\nu}$, given in equation (2.3), where r is the angular velocity in yaw / heading.

$$\boldsymbol{\eta} = \begin{bmatrix} x^n & y^n & \psi \end{bmatrix}^T, \quad \boldsymbol{\nu} = \begin{bmatrix} u & v & r \end{bmatrix}^T \tag{2.3}$$

The linear and angular velocities $\boldsymbol{\nu}$ can be used to find the change in position and orientation $\boldsymbol{\eta}$ with equation (2.4). In the equation, $\boldsymbol{R}_b^n(\psi)$ is the rotation matrix from Body to NED and is given in equation (2.5) [3].

$$\dot{\boldsymbol{\eta}} = \boldsymbol{R}_b^n(\psi)\boldsymbol{\nu} \tag{2.4}$$

$$\boldsymbol{R}_b^n(\psi) = \begin{bmatrix} \cos(\psi) & \text{-}\sin(\psi) & 0 \\ \sin(\psi) & \cos(\psi) & 0 \\ 0 & 0 & 1 \end{bmatrix} \tag{2.5}$$

The rotation matrix in equation (2.5) is both orthogonal and have determinant of unity, which makes it SO(3), where $\left(\boldsymbol{R}_b^n\right)^T = \boldsymbol{R}_n^b$ [15].

2.1.2 Kinetics

Kinetics describe the translational and rotational motion of a marine craft. The motion is given by the equation of motion in equation (2.6), which is derived by using vectorial mechanics and the Newton-Euler formulation [3].

$$\boldsymbol{M}_{RB}\dot{\boldsymbol{\nu}} + \boldsymbol{C}_{RB}(\boldsymbol{\nu})\boldsymbol{\nu} = \boldsymbol{\tau}_{RB} \tag{2.6}$$

In the equation, $\boldsymbol{M}_{RB}$ is the rigid-body mass matrix , $\boldsymbol{C}_{RB}(\boldsymbol{\nu})$ is the Coriolis and centripetal matrix caused by the rotation between reference frames, while $\boldsymbol{\tau}$ is the external forces and moment vector in Body [3].

$$\boldsymbol{\tau} = [X, Y, N]^T \tag{2.7}$$

The equations of motion are either represented in centre of gravity (CG) or in the coordinate origin (CO). CO is the origin of the body fixed references frame, while CG is located at a distance from CO, given by the vector $\boldsymbol{r}_{bg}^b = [x_g, y_g, z_g]^T$. Guidance and control systems and hydrodynamic forces and moments are often computed in CO, and it can therefore be advantageous to represent the equation of motion in CO [3].

2.1.3 Hydrodynamic forces

Surface vessels float when they displace a volume of water equal to their mass. For the vessel to move, the water has to move around the hull to give space for the vessel and replace the previous displaced volume. This create hydrodynamic forces on the hull, which can be included by expanding equation (2.6) with added virtual mass and damping, giving the manoeuvring equations of motion (2.8) [3].

$$\underbrace{\boldsymbol{M}_{RB}\dot{\boldsymbol{\nu}} + \boldsymbol{C}_{RB}(\boldsymbol{\nu})\boldsymbol{\nu}}_{\text{rigid-body forces}} + \underbrace{\boldsymbol{M}_A\dot{\boldsymbol{\nu}}_r + \boldsymbol{C}_A(\boldsymbol{\nu}_r)\boldsymbol{\nu}_r + \boldsymbol{D}(\boldsymbol{\nu}_r)\boldsymbol{\nu}_r}_{\text{hydrodynamic forces}} = \boldsymbol{\tau} \tag{2.8}$$

In equation (2.8), the hydrodynamic forces consist of damping $\boldsymbol{D}(\boldsymbol{\nu}_r)$ and added mass for the inertial matrix $\boldsymbol{M}_A$ and Coriolis and centripetal matrix $\boldsymbol{C}_A(\boldsymbol{\nu}_r)$. The hydrodynamic forces depend on the relative velocity $\boldsymbol{\nu}_r$, which includes the irrotational ocean currents $\boldsymbol{\nu}_c$ [3] .

Linear damping

The damping $\boldsymbol{D}(\boldsymbol{\nu}_r)$ can be divided into linear damping $\boldsymbol{D}$ consisting of potential damping and skin friction, and quadratic damping $\boldsymbol{D}_n(\boldsymbol{\nu}_r)$. Linear damping causes the velocity to exponentially decay to zero and is important for station keeping and low speed manoeuvring, while quadratic damping dominates at higher velocities [3].

$$\boldsymbol{D}(\boldsymbol{\nu}_r) = \boldsymbol{D} + \boldsymbol{D}_n(\boldsymbol{\nu}_r) \tag{2.9}$$

In manoeuvring models, the closed-loop natural periods for stabilising surge, sway and yaw motion are between 0.03-0.10 [rad/s] [3]. Due to the low frequency, added mass and potential damping can be approximated at zero wave excitation frequency. At zero wave excitation, the potential damping is zero and the linear damping is dominated by the viscous damping. [3]

The viscous damping can be chosen as the diagonal matrix $\boldsymbol{B}_V$ in equation (2.10),

$$\boldsymbol{B}_V(\omega) = \text{diag}\{\beta_1 e^{-a\omega} + N_{\text{ITTC}}(A_1), \beta_2 e^{-a\omega}, \beta_6 e^{-a\omega}\} \tag{2.10}$$

with exponential rate $a > 0$, wave excitation ω, linear surge resistance $N_{\text{ITTC}}(A_1)$ based on equivalent linearisation of equation (2.12) and the linear viscous skin friction coefficients $\beta_{1,2,6}$ [3]. The skin friction coefficients for surge, sway and yaw can be found from the three mass-damper systems in equation (2.11),

$$\beta_{v_1} = \frac{m + A_{11}(0)}{T_1}, \quad \beta_{v_2} = \frac{m + A_{22}(0)}{T_2}, \quad \beta_{v_6} = \frac{I_z + A_{66}(0)}{T_6} \tag{2.11}$$

with time constants $T_{1,2,6}$, mass of the marine craft m, the diagonal elements of the added mass matrix $A_{1,2,6}$ and inertia in yaw I_z [3].

Non-linear damping

The non-linear surge damping can be modelled as,

$$X = -\frac{1}{2}\rho S(1+k)C_f(u_r)|u_r|u_r \tag{2.12a}$$

$$C_f(u_r) = \frac{0.075}{(log_{10}(R_n) - 2)^2 + \epsilon} + C_R \tag{2.12b}$$

$$R_n = \frac{L_{pp}}{\nu}|u_r| \geq 0 \tag{2.12c}$$

where the damping force X depends on the relative surge velocity u_r, with density ρ, wetted hull surface S, viscous correction factor k and the friction coefficient C_f [3]. Typical values of the viscous correction factor are $k = 0.1$ for ship in transit and $k = 0.25$ for DP operations [3], while a tanker have around $k = 0.3$ [16]. The friction coefficient C_f depends on the residual friction C_R, a small number ϵ to keep it well defined and Reynolds number R_n, which are

calculated based on the length between perpendiculars L_{pp} and the kinematic viscosity ν. [3]

The non-linear damping in sway and yaw can be calculated from the cross-flow drag principle. Cross-flow drag is difficult to calculate due to velocity in surge. For very low surge velocities, the effect is less prominent and can be neglected when calculating the transverse movement [16]. The sway force Y and yaw moment N can be found by using a strip theory approach with the equations (2.13) and (2.14),

$$Y = -\frac{1}{2}\rho \int_{-\frac{L_{pp}}{2}}^{\frac{L_{pp}}{2}} T(x) D_d^{2D}(x) |v_r + xr|(v_r + xr) dx \tag{2.13}$$

$$N = -\frac{1}{2}\rho \int_{-\frac{L_{pp}}{2}}^{\frac{L_{pp}}{2}} T(x) D_d^{2D}(x) x |v_r + xr|(v_r + xr) dx \tag{2.14}$$

where it depends on the relative sway velocity v_r, yaw rate r, length between perpendiculars L_{pp}, density ρ, 2D drag coefficient $C_d^{2D}(x)$ and draft $T(x)$, which are calculated at the longitudinal distance x.[3]

2.1.4 Thrust force and moments

Forces and moments for marine crafts are created by effectors and actuators. Effectors are mechanical devices that create time-varying mechanical forces and moments, such as propellers and rudders, while actuators control the magnitude and direction of the effectors with electromechanical devices [17].

Fixed pitch propeller

For a fixed pitch propeller, the thrust force and torque can be calculated from equations (2.15) and (2.16), with density ρ, propeller diameter D, propeller revolution per second n and propeller coefficients for thrust K_T and torque K_Q.

$$\text{Thrust} = \rho D^4 K_T(J_a)|n|n \tag{2.15}$$

$$\text{Torque} = \rho D^5 K_Q(J_a)|n|n \tag{2.16}$$

The coefficients K_T and K_Q depends on the open-water advanced coefficient J_a, which adjust the performance of the propeller depending on the forward velocity u and a wake fraction number w. [3]

$$J_a = \frac{u_a}{nD}, \quad u_a = (1-w)u \tag{2.17}$$

Thruster configuration

The forces and moments from effectors on the marine craft can be computed by summing up the thrust contribution into the DOF they affect. This gives the forces and moment vector

$\boldsymbol{\tau}$ located at the Body fixed origin CO, which includes the surge and sway forces F_x and F_y from the thrusters location in the body reference frame $[l_x, l_y]$. [3]

$$\boldsymbol{\tau} = \sum_{i=1}^{r} \begin{bmatrix} F_{x_i} \\ F_{y_i} \\ F_{y_i} l_{x_i} - F_{x_i} l_{y_i} \end{bmatrix} \tag{2.18}$$

The force and moment vector $\boldsymbol{\tau} \in \mathbb{R}^n$ can be calculated from the input vector $\boldsymbol{u} \in \mathbb{R}^r$ with equation (2.19), where n is DOF and r is the number of effectors. In the equation, $\boldsymbol{B} \in \mathbb{R}^{n \times r}$ is the input matrix that can be divided into a thrust coefficient matrix $\boldsymbol{T} \in \mathbb{R}^{n \times r}$ and force coefficient matrix $\boldsymbol{K} \in \mathbb{R}^{r \times r}$. Depending on the number of DOF and effectors, the system is either fully actuated ($r = n$), underactuated ($r < n$) or overactuated ($r > n$). [3]

$$\boldsymbol{\tau} = \boldsymbol{B}\boldsymbol{u} = \boldsymbol{T}\boldsymbol{K}\boldsymbol{u} \tag{2.19}$$

The number of effectors is increased by using azimuth thrusters. Azimuth thrusters can rotate 360°, which results in a force that can contribution in both surge $F_x = \cos(\alpha)F$ and sway $F_y = \sin(\alpha)F$. The forces depend on the angle of attack α, represented in Body reference frame, which is clockwise positive from the marine crafts heading. [3]

2.2 Interaction forces

2.2.1 Towline force

In towing operations, the towline is attached to pullerts at deck level on the towed structure. For bulk carriers, the towing point is above the tugboat, which can make a significant vertical angle on the towline. The pulling force is not affected by the angle and are equal to the thrust force, but results in a vertical force that lift the tugboat and increases the towline tension. The increased tension cause higher friction forces in the fairleads, which increase the risk of breaking the towline. [18]

A longer towline can reduce the tension, but harbours have restricted space for manoeuvring, which limits the length of the towline. While a shorter towline has faster response time to change tugboat position, it shortens the distance between the tugboat thrust force and the towed ship. The interacting propeller wash from the thrust force can deflect on the hull and disturb the water surrounding the thrusters (see figure 2.3). This effect opposes the thrust force and can cause cavitation with increased effect for shorter towlines. [19].

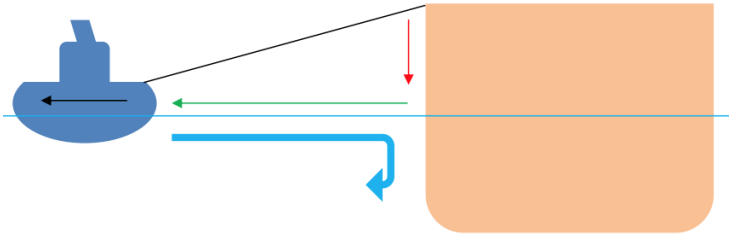

Figure 2.3: Illustration of propeller wash. From [19]

The interacting propeller wash should be accounted for with short towlines, where the required bollard pull can be estimated from an interacting efficiency factor a_{int} with equation (2.20) [20].

$$a_{\text{int}} = \left[1 + 0.015 A_{\text{exp}} / L_{\text{towline}}\right]^{-h} \qquad L_{\text{towline}} > 30[m] \tag{2.20}$$

Where A_{exp} is the projected area on the towed ship [m^2], L_{towline} is the towline length [m] and h is a factor depending on the towed shape, with 1.6 for ship shaped objects and 2.1 for barges [20]. If the towed structure is much larger relative to the tugboat propeller, the effect from the waterflow can result in a negative effect larger than the thrust force, giving motion in the opposite direction [21].

Thrust force close to the bow or stern of the towed ship can also reduce the tow efficiency due to the Coanda Effect [19]. The Coanda Effect is the tendency for a fluid stream to follow a convex surface, instead of going in the initial direction [22]. This effect can create a negative pressure on the opposing side, which can counteract the towing force and even cancel it out, where increasing the pulling force would increase the waterflow and the effect [19].

Towline stiffness

The stiffness of a towline consists of two parts, elastic elongation k_E and change in the catenary geometry k_G [21]. Catenary gives a curvature of the towline depending on the weight, while the elongation depends on the material type. When the towline tension is high, the stiffness due to elastic elongation k_E dominates and can be used to approximate the total stiffness k of the towline [21].

$$k_G = \frac{12 T_0^3}{(wL)^2 L} \tag{2.21a}$$

$$k_E = \frac{EA}{L} \tag{2.21b}$$

$$k = \frac{k_G k_E}{k_G + k_E} \tag{2.21c}$$

Equation (2.21) consist of towline tension T_0 , submerged weight per towline length w , towline length L and nominal cross section area A, while E is Youngs modulus of elasticity. The combined stiffness in equation (2.21c) is only valid for slowly changing motion, with periods over 30 [s] [21].

2.2.2 Contact force

The pushing force from tugboats are limited to certain strong sections on the side of a ship [19]. When the tugboat pushes the ship, the contact force compresses the tugboats rubber fender. The resulting force consist of a normal force perpendicular to the hull, and a friction force tangential to the hull.

Normal force

By using a dissipative contact force model, seen as a linear spring in parallel with a linear damper, the normal force can be computed from equation (2.22) [23].

$$F_N = K\delta + D\dot{\delta} \tag{2.22}$$

In equation (2.22), K is the stiffness parameter related to the elastic force, D is the damping coefficient for the dissipative force and δ are the relative distance of deformation. The equation causes unrealistic behaviour when the damping force contributes while the deformation is zero, $\delta = 0$ and $\dot{\delta} \neq 0$ [23]. For higher material damping, the viscoelastic nature can be represented with a damping factor based on the product of elastic force and velocity [23].

Friction force

Friction reduces or prevents the tugboats from sliding along the hull of the towed ship. The friction force F_R can be calculated from the Coulomb friction model given in equation (2.23), which is not defined for zero velocity $vel = 0$ between the contacting surfaces. Coulomb friction is a static friction model that opposes movement along a surface with a force that is proportional to the normal force F_N, based on the friction coefficient μ [15]. The friction coefficient is a dimensionless number that depends on the material of the contacting surfaces and lubrication between them.

$$F_R = \mu F_N \text{sgn}(vel), \quad vel \neq 0 \tag{2.23}$$

In some static friction models, the friction is larger at zero velocity than under sliding. This can be modelled with a static friction coefficient μ_s when there is no motion and a kinetic friction coefficient μ_k when there is sliding motion [24]. The change in coefficient gives a discontinuous stick-slip motion, where the contacting surfaces sticks together when the velocity is zero and the force is lower than the static friction force, and starts to slide when the static friction force is exceeded. [15].

Chapter 3

Motion Control

This chapter presents the theory used to develop the control and guidance systems for the vessels in the model. The chapter is based on chapter 3 in the specialisation project [2], which is rewritten with minor changes and includes the course autopilot in section 3.2.1 and the implicit constrained control allocation in section 3.3.2

3.1 Guidance system

Guidance systems are used to create setpoints and paths for the marine craft to follow. It is therefore important to have a guidance system that use the marine crafts dynamic to set achievable responses within the limitations of the marine craft.

3.1.1 Trajectory tracking

Trajectory tracking use reference signals with desired position and heading for a marine craft to follow. By using a smooth time varying reference signal, both desired velocity and acceleration can be computed from the time derivatives. For a marine craft represented in 3-DOF, the desired trajectory is obtained by using a controller that minimise the tracking error $\tilde{\boldsymbol{\eta}}$ given in equation (3.1), where $\{d\}$ denotes the desired positions and orientation. [3]

$$\tilde{\boldsymbol{\eta}} = \boldsymbol{\eta} - \boldsymbol{\eta}_d = \begin{bmatrix} x^n - x_d^n \\ y^n - y_d^n \\ \psi - \psi_d \end{bmatrix} \tag{3.1}$$

3.1.2 Reference models

Due to physical limitations of velocity and acceleration of a marine craft, it is important that the guidance system give feasible trajectories. This can be achieved by using a reference model. A reference model can be implemented as a low-pass (LP) filter of desired order, where a position and heading reference model usually are of third order as given in equation (3.2) [3].

$$\frac{\eta_{d_i}}{r_i^n}(s) = \frac{\omega_{n_i}^2}{(1+T_i s)(s^2 + 2\zeta_i \omega_{n_i} s + \omega_{n_i}^2)} \tag{3.2}$$

The 3. order reference model consists of a mass-spring damper system cascaded with a LP filter [3], with time constant $T_i = 1/\omega_{n_i} > 0$, natural frequency ω_n, relative damping ratio ζ_i and reference signal r^n . To obtain good tracking performance and stability, it is important

that the bandwidth of the reference model is lower than the bandwidth of the motion control system [3].

3.1.3 Line-of-Sight path following

In path following, the marine craft follows a given path regardless of time and velocity. The path for a marine craft in 3-DOF can be created by using waypoints with coordinates (x_i^n, y_i^n), and desired heading ψ_d in or out of the waypoint. Waypoints including heading is more used for accurate manoeuvring close to offshore structures, while cross-tracking usually only use coordinates. [3]

Cross-tracking computes the desired heading based on the perpendicular distance a marine craft is to a straight line connecting two waypoints, as illustrated in figure 3.1, where y_e^p is the cross-track error. One method is to use proportional Line-of-Sight (LOS) guidance law to compute the desired course angle χ_d for the marine craft. In proportional LOS, the desired course angle is calculated from,

$$\chi_d = \pi_p - \tan^{-1}(K_p y_e^p) \tag{3.3}$$

with path course π_p, cross-track error and a proportional gain K_p. The proportional gain is usually calculated from the lookahead distance $\Delta > 0$, with $K_p = 1/\Delta$. [3]

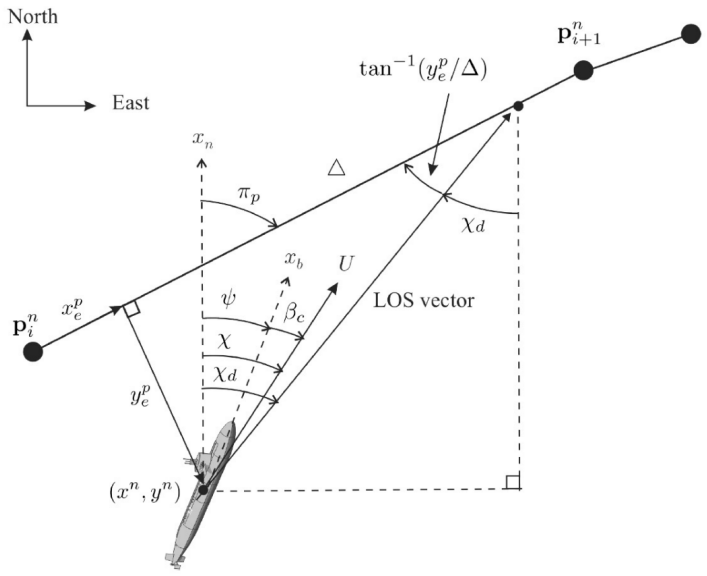

Figure 3.1: Illustration of proportional LOS path following based on the lookahead distance Δ. [3]

3.1.4 Dubins path

A common method of generating paths is by connecting waypoints with straight lines and circular arches. One method is by using Dubins path as illustrated in figure 3.2. Dubins

path is composed of three segments, straights (S) and left (L) and right (R) arches to connect two poses, positions and orientations. The resulting path give the shortest distance between poses for a constant velocity. [3].

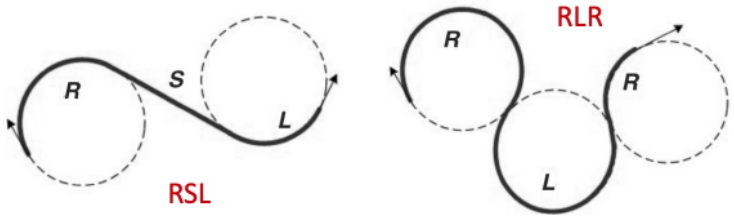

Figure 3.2: Examples of Dubins path between to poses. From [3]

The downside of using straight lines and circular archers is in the transition where the turning rate goes from zero to a constant value. This will create jumps in cross-tracking, which can be prevented by using a Fermat spiral [3]. Fermat spirals can be connected smoothly to straight lines due to their origin having zero curvature[25].

3.2 Control law

3.2.1 Course autopilot

Course auto pilots are used to follow a desired course χ_d that is directly given or computed with north and east coordinates to follow a path. The course angle is given by equation (2.1), as $\chi = \psi + \beta_c$, and differs from heading ψ by the crab angle β_c. By using course instead of heading, ocean currents can be accounted for. The downside with course autopilots is for zero SOG , $U = 0$, when the crab angle in equation (3.4) is not defined.[3]

$$\beta_c = \sin^{-1}(v/U), \qquad U > 0 \tag{3.4}$$

When moving forward, the course can be controlled by a linear PID controller by implementing the crab angle as a disturbance that is compensated for with integral action [3]. By differentiating the course, and comparing the yaw dynamics to a mass-damper system, the linear PID controller for the yaw moment τ_N can be found from,

$$\dot{\chi} = r + \dot{\beta}_c \tag{3.5a}$$

$$(I_z - N_{\dot{r}})\dot{r} - N_r r = \tau_N \tag{3.5b}$$

with yaw rate r, yaw inertia I_z and the hydrodynamic derivatives $N_{\dot{r}}$ and N_r used in manoeuvring models [3]. By writing the yaw dynamics based on the heading $\dot{\psi} = r$, equation (3.5b) turn into,

$$(I_z - N_{\dot{r}})\ddot{\psi} - N_r\dot{\psi} = \tau_N \tag{3.6}$$

which is equivalent to a mass-damper-spring system with mass $m = (I_z - N_{\dot{r}})$, damping $d = -N_r$ and spring stiffness $k = 0$ [3].

The gains $K_{p,d,i}$ for a linear PID control law can be found by applying the control law to a mass-damper-spring system and using the pole placement method, which is summarised in Algorithm 15.1 in [3]. Equation (3.7) shows the algorithm, with design parameters for relative damping $\zeta > 0$ and control bandwidth $\omega_b > 0$. Typical values for relative damping lie between 0.8-1, while the bandwidth is typically 0.1 for smaller vessels and 0.01 for large tankers [3].

$$\omega_n = \frac{1}{\sqrt{1 - 2\zeta^2\sqrt{4\zeta^4 - 4\zeta^2 + 2}}}\omega_b \tag{3.7a}$$

$$K_p = m\omega_n^2 - k \tag{3.7b}$$

$$K_d = 2\zeta\omega_n m - d \tag{3.7c}$$

$$K_i = \frac{\omega_n}{10}K_p \tag{3.7d}$$

3.2.2 Non-linear PID control law

The non-linear PID pole-placement algorithm for multiple-input and multiple-output (MIMO) systems can be designed based on pole-placement algorithms, by using the equations of motion given in equation (2.8) with the non-linear controller $\boldsymbol{\tau}_{\text{PID}}$ [3].

$$\boldsymbol{\tau} = \boldsymbol{R}^T\boldsymbol{\tau}_{\text{PID}} = \boldsymbol{R}^T(-\boldsymbol{K}_p\tilde{\boldsymbol{\eta}} - \boldsymbol{K}_d\dot{\boldsymbol{\eta}} - \boldsymbol{K}_i\int_0^t \tilde{\boldsymbol{\eta}}d\tau) \tag{3.8}$$

In equation (3.8), $\boldsymbol{R}$ is the rotational matrix given in equation (2.5), $\boldsymbol{K}_{p,d,i}$ are the controller gains, while $\tilde{\boldsymbol{\eta}}$ is the error in generalised position from a constant set point $\boldsymbol{\eta}_d$, giving $\tilde{\boldsymbol{\eta}} = \boldsymbol{\eta} - \boldsymbol{\eta}_d$. Simplifying the controller by removing the integral action, setting $\boldsymbol{K}_i = 0$, turns the equation of motion into the close-loop system in equation (3.9) [3].

$$\boldsymbol{M}\dot{\boldsymbol{\nu}} + [\boldsymbol{C}(\boldsymbol{\nu}) + \boldsymbol{D}(\boldsymbol{\nu}) + \boldsymbol{R}^T\boldsymbol{K}_d\boldsymbol{R}]\boldsymbol{\nu} + \boldsymbol{R}^T\boldsymbol{K}_p\tilde{\boldsymbol{\eta}} = 0 \tag{3.9}$$

The velocity vector $\boldsymbol{\nu}$ and its derivative can be found from equation (2.4) by assuming that $\dot{\boldsymbol{R}} \approx 0$, giving $\boldsymbol{\nu} = \boldsymbol{R}^{-1}\dot{\boldsymbol{\eta}}$ and $\dot{\boldsymbol{\nu}} = \boldsymbol{R}^{-1}\ddot{\boldsymbol{\eta}}$ [3]. Turning equation (3.9) into equation (3.10).

$$\boldsymbol{R}^{-T}\boldsymbol{M}\boldsymbol{R}^{-1}\ddot{\boldsymbol{\eta}} + \left(\boldsymbol{R}^{-T}\left[\boldsymbol{C}(\boldsymbol{\nu}) + \boldsymbol{D}(\boldsymbol{\nu})\right]\boldsymbol{R}^{-1} + \boldsymbol{K}_d\right)\dot{\boldsymbol{\eta}} + \boldsymbol{K}_p\tilde{\boldsymbol{\eta}} = 0 \tag{3.10}$$

$$\boldsymbol{R}^{-T}\boldsymbol{M}\boldsymbol{R}^{-1}[\ddot{\boldsymbol{\eta}} + 2\boldsymbol{Z}\boldsymbol{\Omega}_n\dot{\boldsymbol{\eta}} + \boldsymbol{\Omega}_n^2\tilde{\boldsymbol{\eta}}] = 0 \tag{3.11}$$

By comparing equation (3.10) with equation (3.11), the gain parameters $\boldsymbol{K}_{p,d,i}$ for the generalised coordinates and heading can be found with equation (3.12) by specifying the relative damping ratios $\boldsymbol{Z} = \text{diag}\{\zeta_1, \zeta_2, \zeta_6\} > 0$ and bandwidths $\boldsymbol{\Omega}_b = \text{diag}\{\omega_{b_1}, \omega_{b_2}, \omega_{b_6}\} > 0$ in equa-

tion (3.7a) to get the natural frequency $\boldsymbol{\Omega}_n = \text{diag}\{\omega_{n_1}, \omega_{n_2}, \omega_{n_6}\}$. [3]

$$\boldsymbol{K}_p = \boldsymbol{R}^{-T}\boldsymbol{M}\boldsymbol{R}^{-1}\boldsymbol{\Omega}_n^2 \tag{3.12a}$$

$$\boldsymbol{K}_d = 2\boldsymbol{R}^{-T}\boldsymbol{M}\boldsymbol{R}^{-1}\boldsymbol{Z}\boldsymbol{\Omega}_n - \boldsymbol{R}^{-T}[\boldsymbol{C}(\boldsymbol{\nu}) + \boldsymbol{D}(\boldsymbol{\nu})]\boldsymbol{R}^{-1} \tag{3.12b}$$

$$\boldsymbol{K}_i = \frac{1}{10}\boldsymbol{K}_p\boldsymbol{\Omega}_n \tag{3.12c}$$

The system can be proven to be locally asymptotically stable with a non-linear PID-controller, from the assumption that $\dot{\boldsymbol{R}} \approx 0 \Rightarrow \dot{\boldsymbol{K}}_p \approx 0$ and $\dot{\boldsymbol{\eta}}_d = 0$ [3].

3.3 Control allocation

Control allocation is used to find the required input $\boldsymbol{u}$ for a desirable motion of the marine craft. This can be computed based on a given forces and moments vector $\boldsymbol{\tau}$ with equation (2.19), $\boldsymbol{\tau} = \boldsymbol{T}\boldsymbol{K}\boldsymbol{u}$, where $\boldsymbol{T}$ and $\boldsymbol{K}$ are the thrust and force coefficient matrices. [3]

3.3.1 Explicit constrained control allocation

In overactuated systems, when the number of effectors is greater than DOF, the desired motion of a marine craft can be achieved with less input. This means that multiple solutions can exist, where faults in certain effectors can be accounted for. To find the optimal solution, the control allocation is solved as a optimisation problem. The problem is usually constrained, due to physical limitations on effector rate of change and amplitude. One method of solving a constrained control allocation problem is to formulate it as a convex quadratic programming (QP) problem, as given in equation (3.13).[3]

$$\begin{aligned} J = \min_{\boldsymbol{f}} \{ & \boldsymbol{f}^T\boldsymbol{W}\boldsymbol{f} + \boldsymbol{s}^T\boldsymbol{Q}\boldsymbol{s} + \beta\bar{f}\} \\ & \text{Subject to} \\ & \boldsymbol{T}\boldsymbol{f} = \boldsymbol{\tau} + \boldsymbol{s} \\ & \boldsymbol{f}_{\min} \leq \boldsymbol{f} \leq \boldsymbol{f}_{\max} \\ & -\bar{f} \leq f_1, f_2, \ldots, f_r \leq \bar{f} \end{aligned} \tag{3.13}$$

In equation (3.13), $\boldsymbol{W}$ and $\boldsymbol{Q}$ are positive definite weighting matrices for the control forces $\boldsymbol{f} = \mathbf{Ku}$ and the slack variables $\boldsymbol{s}$, on how "expensive" they are to use. In control allocation, this will resemble the fuel consumption of using a specific thruster or tugboat. The constraints $\boldsymbol{f}_{\min/\max}$ saturate the control force, while $\bar{f}$ minimises the largest force depending on the constant $\beta \geq 0$. By using a slack variable, the solution of the generalised force $\boldsymbol{T}\boldsymbol{f}$ can deviate from the desired force $\boldsymbol{\tau}$. The slack variables should be kept close to zero, which can be achieved by setting $Q \gg W > 0$ [3].

3.3.2 Implicit constrained control allocation

For azimuth thrusters, both angle of attack α and input force f must be computed. Since azimuth thruster can rotate, the constraints should include physical limitations on actuator turning rate and feasible directions [3]. In applications like DP, the marine crafts controllability is lost when the thrusters are pointing in the same direction. This can be avoided by using singularity avoidance penalty in the optimisation problem, but will result in a non-convex non-linear problem [26].

The non-convex non-linear optimisation problem can be approximated by solving a local convex QP-problem, as given in equation (3.14) [26]. This is done by assuming that the input force is close to the last input with a quadratic term $f = f_0 + \Delta f$, while a linearisation about the last azimuth angle $\alpha = \alpha_0 + \Delta\alpha$ can be used to approximate the singularity avoidance penalty [3].

$$
\begin{aligned}
J = \min_{\boldsymbol{\Delta f}, \boldsymbol{\Delta\alpha}, \mathbf{s}} \Bigg\{ & (\boldsymbol{f}_0 + \boldsymbol{\Delta f})^T \mathbf{P} (\boldsymbol{f}_0 + \boldsymbol{\Delta f}) + \mathbf{s}^T \mathbf{Q} \mathbf{s} + \boldsymbol{\Delta\alpha}^T \boldsymbol{\Omega} \boldsymbol{\Delta\alpha} + \frac{\partial}{\partial \boldsymbol{\alpha}} \left(\frac{\varrho}{\varepsilon + \det(\mathbf{T}(\boldsymbol{\alpha}) \mathbf{W}^{-1} \mathbf{T}^T(\boldsymbol{\alpha}))} \right) \Bigg|_{\boldsymbol{\alpha}_0} \boldsymbol{\Delta\alpha} \Bigg\} \\
& \text{Subject to:} \\
& \mathbf{s} + \mathbf{T}(\boldsymbol{\alpha}_0) \boldsymbol{\Delta f} + \frac{\partial}{\partial \boldsymbol{\alpha}} \Big(\mathbf{T}(\boldsymbol{\alpha}) \boldsymbol{f} \Big) \Big|_{\boldsymbol{\alpha}_0, \boldsymbol{f}_0} \boldsymbol{\Delta\alpha} = \boldsymbol{\tau} - \mathbf{T}(\boldsymbol{\alpha}_0) \boldsymbol{f}_0 \\
& \boldsymbol{f}_{\min} - \boldsymbol{f}_0 \leq \boldsymbol{\Delta f} \leq \boldsymbol{f}_{\max} - \boldsymbol{f}_0 \\
& \boldsymbol{\alpha}_{\min} - \boldsymbol{\alpha}_0 \leq \boldsymbol{\Delta\alpha} \leq \boldsymbol{\alpha}_{\max} - \boldsymbol{\alpha}_0 \\
& \boldsymbol{\Delta\alpha}_{\min} \leq \boldsymbol{\Delta\alpha} \leq \boldsymbol{\Delta\alpha}_{\max}
\end{aligned}
\tag{3.14}
$$

In equation (3.14) $\mathbf{P}$, $\mathbf{Q}$ and $\boldsymbol{\Omega}$ are the weighting matrices for change in input force $\boldsymbol{\Delta f}$, slack variable $\mathbf{s}$ and change in angle of attack $\boldsymbol{\Delta\alpha}$. The last term in the minimisation problem is the singularity avoidance penalty, where $\varrho > 0$ is a scalar weight that increases manoeuvrability with power consumption, while $\varepsilon > 0$ is used to avoid division by zero [3].

Chapter 4

Implementing the model dynamics

The simulation model used in this thesis was design and implemented in Simulink with Matlab version R2021b, by using the MSS toolbox by Thor I. Fossen from Github [1], and the Matlab Add-Ons, Stateflow, Optimization Toolbox and Symbolic Math Toolbox. The simulation model is divided into three categories, model dynamics, tugboat control system (see chapter 6) and bulk carrier control and guidance systems (see chapter 8).

In this chapter, the implementation method for the model dynamics is described, while relevant Simulink models and Matlab codes are given in appendix B. The chapter explains the mathematical models for the bulk carrier and tugboat dynamics, and the interaction forces between them caused by direct contact and from the towline (see figure 4.1).

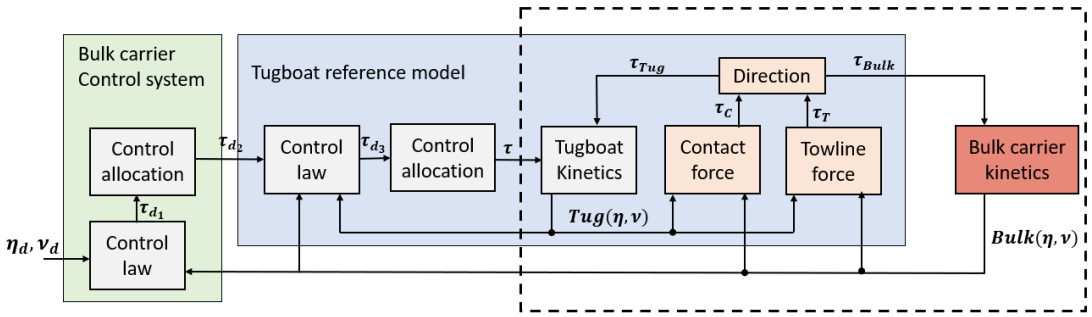

Figure 4.1: Illustration of the vessel kinetics and interaction forces in the Simulink model covered in chapter 4, within the dotted line.

4.1 Implementing the vessel dynamics

The vessel dynamics were implemented by using the Symbolic Math Toolbox in Matlab, where the code for the tugboat and bulk carrier are given in appendix B.1.3 and appendix B.2.1. The bulk carrier dynamics in section 4.1.1 are from section 4.1 in the specialisation project, and was reused since it was concluded that the model would have bad performance in a real application but had credible dynamics that could be used to validate the control system [2].

4.1.1 Bulk carrier dynamics

To simulate the dynamics of a bulk carrier, the dynamics are based on data from a Wamit file of a tanker, created by Thor I. Fossen, and obtainable from the MSS toolbox at Github [1]. Wamit is a computer program that solves 3D potential theory by dividing the hull in contact

with water into elements. This method is suitable for offshore applications at zero-forward velocity and can be used to find frequency dependant added mass and potential damping.[3] The specification of the Tanker is given in table 4.1 and the 3D-surface model of the ship is shown in figure 4.2.

Table 4.1: Specification of the Wamit files, Tanker and FPSO, from MSS toolbox [1]. Length is the length between the perpendiculars.

Vessel	Length	Width	Draft	weight
Tanker	246 m	46 m	10 m	94 620 t
FPSO	200 m	46 m	10 m	100 410 t

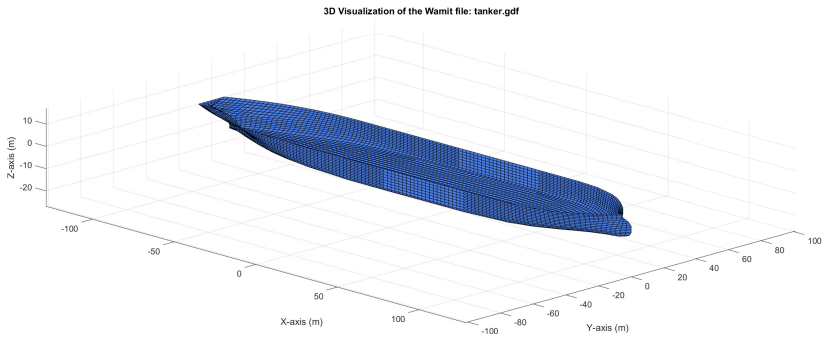

Figure 4.2: Illustration of the 3D-surface model of the Tanker from the MSS toolbox.[1]

The rigid body mass matrix $\boldsymbol{M}_{RB}$ and Coriolis and centripetal matrix $\boldsymbol{C}_{RB}(\boldsymbol{\nu})$, represented in CO with $\boldsymbol{r}_{bg}^{b} = [3.9, 0]^T$, was found with the function "rbody" from MSS toolbox [1]. To convert the matrices into 3-DOF the effect from heave, roll and pitch were neglected, resulting in the matrices in equation (4.1).

$$\boldsymbol{M}_{RB} = \begin{bmatrix} m & 0 & 0 \\ 0 & m & mx_g \\ 0 & mx_g & I_z \end{bmatrix} \quad \boldsymbol{C}_{RB}(\boldsymbol{\nu}) = \begin{bmatrix} 0 & -mr & -mx_g r \\ mr & 0 & 0 \\ mx_g r & 0 & 0 \end{bmatrix} \tag{4.1}$$

Both the rigid body added mass matrix $\boldsymbol{M}_A$ and the potential damping matrix $\boldsymbol{D}_p$ was found at zero wave excitation frequency $\omega = 0$, while the added mass Coriolis and centripetal matrix $\boldsymbol{C}_A(\boldsymbol{\nu}_r)$ was computed from $\boldsymbol{M}_A$ with the function "m2c" from MSS toolbox [1]. The matrices used are shown in equation (4.2), and since there are ideal conditions with no ocean currents, $\boldsymbol{\nu}_r = \boldsymbol{\nu}$.

$$
\begin{aligned}
\boldsymbol{M}_A &= -\begin{bmatrix} X_{\dot{u}} & 0 & 0 \\ 0 & Y_{\dot{v}} & Y_{\dot{r}} \\ 0 & N_{\dot{v}} & N_{\dot{r}} \end{bmatrix} = \begin{bmatrix} A_{11}(0) & 0 & 0 \\ 0 & A_{22}(0) & A_{26}(0) \\ 0 & A_{62}(0) & A_{66}(0) \end{bmatrix} \\
\boldsymbol{C}_A(\boldsymbol{\nu}_r) &= \begin{bmatrix} 0 & 0 & Y_{\dot{v}} v_r + Y_{\dot{r}} r \\ 0 & 0 & -X_{\dot{u}} u_r \\ -Y_{\dot{v}} v_r - Y_{\dot{r}} r & X_{\dot{u}} u_r & 0 \end{bmatrix} \\
\boldsymbol{D}_p &= 0
\end{aligned} \tag{4.2}
$$

There is no potential damping at zero wave excitation, and thus the linear damping only consists of viscous damping $\boldsymbol{D}_v$. The viscous damping given in the tanker Wamit file needed adjustments and was instead calculated from equation (2.10) with time constants of a mass-damper system. As the FPSO tanker has relatively similar proportions as the tanker file, see table 4.1, the time constants of the FPSO, $T_1 = 100$, $T_2 = 17$ and $T_6 = 18$ was used as a starting point. First the time constant T_1 was increased, since the FPSO is built for standing still on DP and compared to the tanker has a relatively flat front area. While the tanker is longer, the FPSO has flatter surfaces and thus increased resistance for moving in water. The constants, T_2 and T_6, was therefor set similarly to the FPSO. Resulting in a diagonal damping matrix given in equation (4.3), computed with the time constants $T_1 = 160$, $T_2 = 19$ and $T_6 = 21$. The surge resistance term $A_{\text{ITTC}}(A_1)$ was neglected since it is a linearisation of the quadratic damping in surge, which should be small due to low velocity.

$$
\boldsymbol{D} = -\begin{bmatrix} X_u & 0 & 0 \\ 0 & Y_v & 0 \\ 0 & 0 & N_r \end{bmatrix} = \begin{bmatrix} \beta_{v_1} & 0 & 0 \\ 0 & \beta_{v_2} & 0 \\ 0 & 0 & \beta_{v_6} \end{bmatrix} \tag{4.3}
$$

4.1.2 Tugboat dynamics

The simulated tugboat was based on Bulldog from "Bukser og Berging", which is stationed in Narvik. Bulldog is an azimuth stern drive (ASD) tug that is equipped with two azimuth thrusters for main propulsion, and a tunnel thruster at the bow to increase manoeuvrability at low velocities. The effectiveness of the tunnel thrusters can be lost between 1-2.5 [m/s] [4]. ASD tugs have towline connection at the bow and are equipped with rubber fenders around the bow, as seen in figure 4.3.

The tugboat model was implemented by using the 3-DOF manoeuvring model given in equation (2.8), with non-linear damping $\boldsymbol{d}(\boldsymbol{\nu})$,

$$
\boldsymbol{M}\dot{\boldsymbol{\nu}} + (\boldsymbol{C} + \boldsymbol{D})\boldsymbol{\nu} + \boldsymbol{d}(\boldsymbol{\nu}) = \boldsymbol{\tau} \tag{4.4}
$$

where $\boldsymbol{M} = \boldsymbol{M_{RB}} + \boldsymbol{M_A}$, $\boldsymbol{C} = \boldsymbol{C_{RB}} + \boldsymbol{C_A}$, and $\boldsymbol{D}$ have the same form as the bulk carrier given in section 4.1.1.

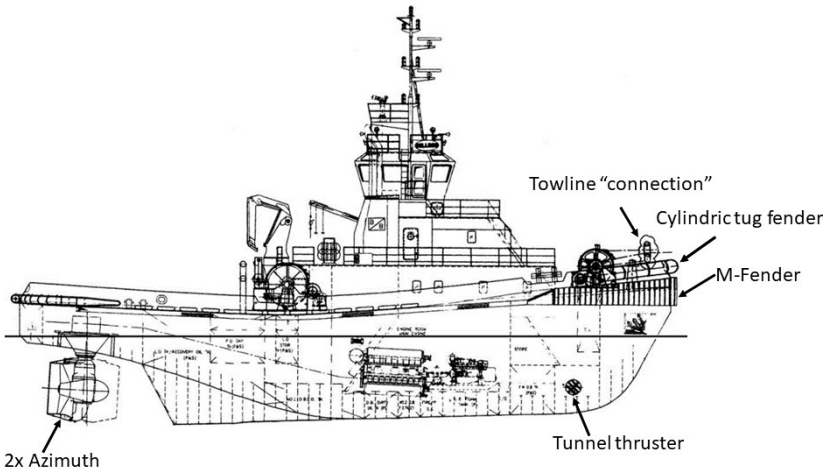

Figure 4.3: Illustration of BB Bulldog. Edited from appendix A.1

Due to limited data on the tugboat, the implemented model was based on the vessels in table 4.2. While a naval vessel has large hull differences compared to a tugboat, the hydrodynamic coefficients of the naval vessel was used to find the added mass inertial matrix $\boldsymbol{M_A}$. This was since the hydrodynamic coefficients for the escort tugboat model were dimensionless [27], and to reuse the implementation method of the bulk carrier for simplicity, values of the naval vessel was chosen. The full scale data of a tugboat model was used to find more realistic values for the tugboat displacement and wetted surface area, which was used to calculate the inertial matrix $\boldsymbol{M_{RB}}$ and non-linear damping in surge.

Table 4.2: Data on vessels used to implement the model of BB Bulldog. Navel vessel from the MSS toolbox [1], and a similar tugboat model used for escort operations with full scale from [27]. Length is the length between the perpendiculars.

Vessel	Length	Width	Draft	Displacement	Wet surface
Naval vessel	51.5 m	8.6 m	2.3 m	362 m^3	-
Tug model (FS)	27.5 m	12 m	3.7 m	659 m^3	392 m^2

The draft of the tugboat was approximated from figure 4.3, by measuring the distance from the waterline in certain points and interpolating between them. This gave the resulting draft in figure 4.4, where the hull and keel are separated. The hull and keel were separated to calculate the tugboat displacement from the hull draft, and cross-flow drag from both. While the azimuth thrusters would have affected both displacement and cross-flow drag, they were neglected to simplify the implementation.

Finding the rigid body matrices

The rigid body matrices in equation (4.1), $\boldsymbol{M_{RB}}$ and $\boldsymbol{C_{RB}}$, was found from the mass m, the vector from CO to CG in surge direction x_g and the moment of inertia I_z. The mass was calculated from the displaced volume by combining the cross section areas along the tugboat hull with the trapezoidal rule. Each section on the tugboat was assumed to have form of a half ellipse, with breadth of the tug $B = 11.5$ [m] and height from the draft in figure 4.4. The

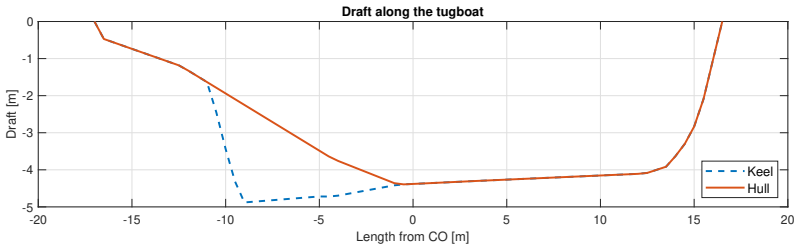

Figure 4.4: Draft along the tugboat based on the illustration in figure 4.3.

calculated displacement was reduced by 10%, resulting in mass $m = 790$ [t]. To simplify the calculations, $CG = CO \Rightarrow x_g = 0$, and the moment of inertia was calculated from the moment of inertia of a plate, and reduced by 40% by assuming that most of the weight is caused by the engines that are placed close to the CO, giving $I_z = 4.96 \cdot 10^7$ [kgm^2].

Finding the hydrodynamic matrices

The hydrodynamic matrices in equation (4.2), $\boldsymbol{M_A}$ and $\boldsymbol{C_A}$, was found based on the hydrodynamic coefficients of the naval vessel given in table 4.3. Since the tugboat had a wider and larger front area, the added mass in surge $X_{\dot{u}}$ was increased. For the added mass in sway $Y_{\dot{v}}$, the values were set similarly, by assuming that the side area was around the same size, while the added mass in yaw $N_{\dot{r}}$ was lowered, as the tugboat is shorter. For the cross terms, $Y_{\dot{r}}$ and $N_{\dot{v}}$, they were set with the same sign and lowered, by assuming that added mass would have less impact on the stern of the hull, where acceleration in sway would cause some rotation.

This resulted in a non-symmetric inertial matrix $\boldsymbol{M}$. The non-symmetric inertial matrix is positive definite if the symmetric part $\boldsymbol{M}_s = 1/2(\boldsymbol{M} + \boldsymbol{M}^T)$ is positive definite, which can be proven from positive eigenvalues [28]. Based on the symmetric part, the inertia matrix was positive definite. Similar to the linear damping $\boldsymbol{D}$ of the bulk carrier in equation (4.3), the

Table 4.3: Hydrodynamic coefficients for the navel vessel in table 4.2, obtained from the MSS toolbox [1], and the used coefficients for Bulldog.

Vessel	$\boldsymbol{X_{\dot{u}}}$	$\boldsymbol{Y_{\dot{v}}}$	$\boldsymbol{Y_{\dot{r}}}$	$\boldsymbol{N_{\dot{v}}}$	$\boldsymbol{N_{\dot{r}}}$
Naval vessel	$-1.74 \cdot 10^4$	$-3.93 \cdot 10^5$	$-1.40 \cdot 10^6$	$5.38 \cdot 10^5$	$-3.87 \cdot 10^7$
Bulldog	$-8.00 \cdot 10^4$	$-3.90 \cdot 10^5$	$-1.00 \cdot 10^6$	$5.00 \cdot 10^5$	$-3.00 \cdot 10^7$

linear damping for the tugboat was calculated from equation (2.11), with the time constants $T_1 = 50$, $T_2 = 80$ and $T_3 = 10$ [29].

Calculating non-linear damping

To use the non-linear damping in the tugboat dynamics $\boldsymbol{d}(\boldsymbol{v})$ (see equation (4.4)), the sign in the functions for non-linear surge damping and cross-flow drag, given in section 2.1.3, was changed.

From equation (2.12), the non-linear surge damping was calculated with the wetted surface

area S, a viscous correction factor $k = 0.25$ and a friction coefficient $C_f(u_r)$. The friction coefficient was adjusted to a max speed of 13 knots given in appendix A.1. The wetted surface area was calculated from a box with dimension $B \cdot L \cdot T = 11.5 \cdot 33.5 \cdot T(x_b)$, where the draft T is given in figure 4.4, and reduced by a factor of 25% resulting in $S = 672$ [m^2].

The cross-flow drag was calculated from the strip theory approach in equation (2.13) and equation (2.14). At each strip, the draft from figure 4.4 was used, while the 2D drag coefficient C_d^{2D} was found with the function "hoerner" in MSS toolbox [1], by using the breadth $B = 11.5$. The relation between breadth and draft for the coefficient are shown in figure 4.5, where C_d^{2D} was set to 0.5 when $B/2T > 4$.

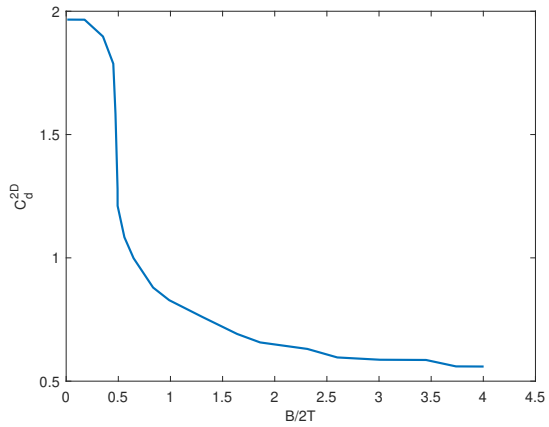

Figure 4.5: Graph of the 2D cross flow coefficient C_d^{2D} as a function of the ratio between breadth and draft $B/2T$. The plot is created with data from the function "hoerner" in MSS toolbox [1].

4.2 Implementing the interaction forces

The interaction forces from vessel contact and the towline was modelled in the tugboat reference model, where the implementation in Simulink is shown in appendix B.1.

4.2.1 Implementing contact force

The contact force was simulated between the tugboat bow and bulk carrier hull. To model the contacting surfaces, the hull of the bulk carrier was modelled as two straight lines, while the bow of the tugboat was assumed to have a half circular shape. The contacting point on the tug C_T and bulk carrier C_B was found by using the starboard pointing vector y_b in the bulk carrier reference frame. This gave the point closest to the hull that would make contact first (see figure 4.6).

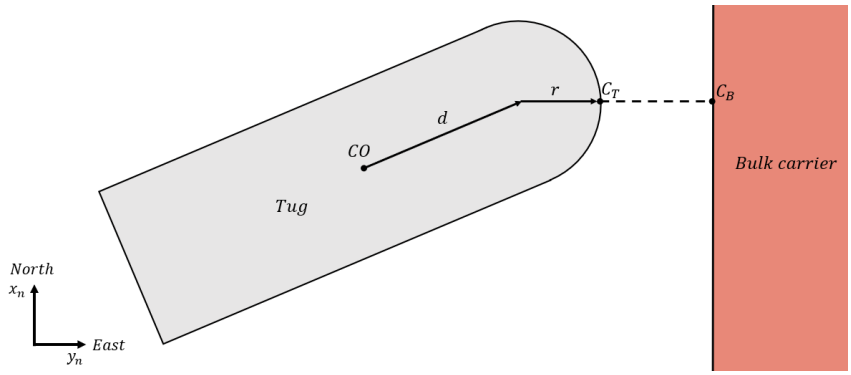

Figure 4.6: The contacting points on the bulk carrier hull C_B and the tugboat fender C_T, which is on a half circle with radius $r = 5.75$ [m] with centre at a distance $d = 11.75$ [m] from the CO.

The normal force F_N was calculated with the dissipative contact force model in equation (2.22), based on the overlapping of the contacting points (illustrated in figure 4.8).

$$F_N = K_N(C_B - C_T) + D_N(\dot{C}_B - \dot{C}_T) \tag{4.5}$$

In equation (4.5), the stiffness parameter K_N was curve fitted to give the reaction force of the M600-fender in figure 4.7, by assuming that the contact point was one meter of fender. The damping coefficient was set to $D_N = \mu_0\sqrt{4mK_N}$, and was based on contact damping from Abaques simulation program [30], with tugboat mass m and a critical damping fraction μ_0 assumed to be 0.1.

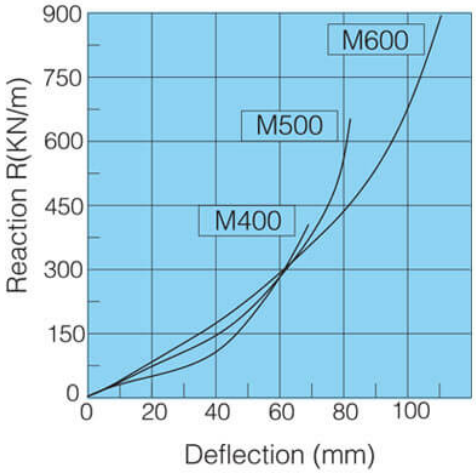

Figure 4.7: Performance curve for three M-type fenders from a general manufacture [31], with no connection to the tugboat modelled.

4.2.2 Implementing friction force

The friction force was used to counteract two forces between the tugboat and bulk carrier (see figure 4.8). First, the tangential force F_T in the contact point on the bulk carrier, caused by the tugboat pushing force. Second, the force required to stick the tugboat contacting point C_T at the bulk carrier hull F_{Stick}.

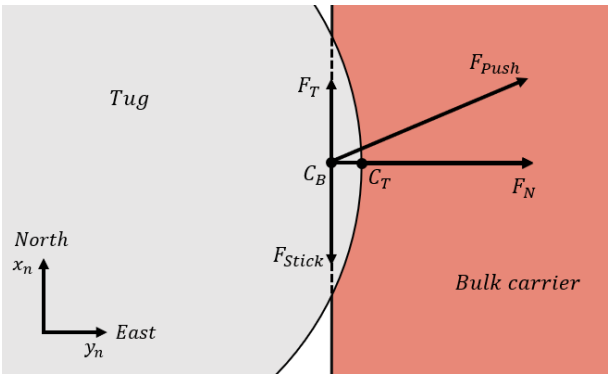

Figure 4.8: Illustrating the contacting forces on the bulk carrier (moving in north direction) from the tugboat, where the direction of F_{Push} is the tugboat heading. F_{Stick} is the force required to stick the tugboat to the hull, while F_T is the tangential pushing force.

For the tugboat to stick to the bulk carrier, the tugboat contact point C_T must have the same velocity and direction as the surge velocity of the bulk contact point C_B. Since the tugboat is seen as a rigid body, this meant that the tugboat must follow in the same direction, without rotation. By using the manoeuvring model of the tugboat dynamics given in equation (4.4), the required force to stick the tugboat to the hull F_{Stick} was found with the force required to move the tugboat with the contact point velocity and direction. In the manoeuvring model, the velocity and acceleration were found based on the velocity of the contact points,

$$\boldsymbol{\nu} = \boldsymbol{R}_T^T \boldsymbol{R}_B \begin{bmatrix} \dot{C}_B & 0 & 0 \end{bmatrix}^T \qquad \dot{\boldsymbol{\nu}} = \boldsymbol{R}_T^T \boldsymbol{R}_B \begin{bmatrix} (\dot{C}_B - \dot{C}_T)/dt & 0 & 0 \end{bmatrix}^T \tag{4.6}$$

where $\boldsymbol{R}$ is the rotational matrix in equation (2.5), for the bulk carrier $\{B\}$ and tugboat $\{T\}$, while the acceleration was calculated with a small time duration dt to give the large force required to stick instantly. This method was based on the contact model used in the boarding control system on offshore wind turbines [32], where the contact friction is modelled as a spring-damper system to capture the elasticity of the rubber fender, which uses a small mass to represent the contact point under sliding.

The total force between the vessels was then $F_{Tot} = F_{Stick} - F_T$, and the tugboat would stick to the bulk carrier if the force was lower than the friction force. The friction between the tugboat and the bulk carrier was simulated based on the Coulomb friction law given in equation (2.23), with both static and kinetic friction coefficient. To have a smooth transition between static friction when still and kinetic friction when the tugboat started to slide along the bulk carrier hull, an exponential term was implemented to the equation. This exponential transition between coefficients is also used in Abaqus simulation program [33]. The resulting friction force was,

$$F_R = \left((\mu_s - \mu_k) e^{-K_{v_r} v_r} + \mu_k\right) \cdot F_N \tag{4.7}$$

where v_r is the relative velocity between the contacting points C_T and C_B in the direction along the bulk carrier hull, and K_{v_r} is a constant. The friction coefficients were based on the

kinetic friction coefficient between rubber and wet asphalt, between $\mu_k = 0.25 - 0.75$ [24], to simulate a wet hull. For a relatively low stick and slip limit, the kinetic and static friction coefficients were set to $\mu_k = 0.25$ and $\mu_s = 0.4$.

The direction of the friction force was decided based on the direction of the total force F_{Tot}, where the resulting friction force on the tugboat was,

$$F_R = \begin{cases} F_{Tot} & \text{if } |F_{Tot}| \leq F_R \\ F_R \cdot \text{sign}(F_{Tot}) & \text{else} \end{cases} \tag{4.8}$$

while the friction force on the bulk carrier was in the opposite direction. Based on the condition, the vessels would stick together when $|F_{Tot}| \leq F_R$, and slide when $|F_{Tot}| > F_R$.

4.2.3 Implementing towline force

In this model, the towline is assumed to be connected in a horizontal plane. The increased towline force caused by the height difference between the bulk carrier and tugboat are not accounted for in the simulations. Instead, the towline is set relatively long, with a minimum of 60 [m], and the force is assumed to have a small increase and therefore neglected. By having a longer towline, the impact of the propeller wash is also reduced, as seen in equation (2.20). The effect of the propeller wash is not included in the simulations, but the tugboats are kept relatively far from the hull to reduce the effects. Figure 4.9 illustrates the towing operation, with a connection point on the bulk carrier T_B that could be placed along the length on either side, and the connection point on the tugboat T_T that was set to the bow centre.

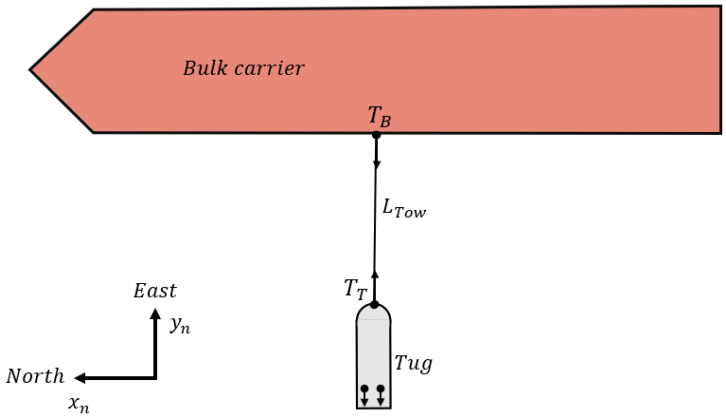

Figure 4.9: Illustration of the towing operation with connection point on tug T_T and bulk carrier T_B.

The towline was chosen based on the minimum requirements given in equation (4.9), where K_{Tow} is a safety factor based on the designed bollard pull T_b [kN] [34].

$$F_{\min} = K_{Tow} T_b, \qquad K_{Tow} = 2.625 - \frac{T_b}{1600} \tag{4.9}$$

From the tugboat specifications given in appendix A.1, the designed bollard pull is 653 [kN], which require a towline that can handle a minimum of 1447 [kN]. Based on specifications on one type of fibre ropes used as main towlines given in appendix A.2, this required a towline with diameter 48 [mm], which has weight of 1.37 [kg/m] and minimum breaking load (MBL) of 1620 [kN].

Due to the relatively low weight of the towline, and assumed high towline tension in operations, the stiffness of the towline only consisted of the stiffness due to elastic elongation $K_E = \frac{EA}{L}$ from equation (2.21). The implemented towline was assumed to be used and had a linear elongation depending on the force, with 2% elongation at MBL (see appendix A.2). Based on this, the stiffness was calculated from Hooks law, with $\Delta L = 0.02$ [m] and $F = 1620$ [kN],

$$F = K_E \Delta L \rightarrow K_E = \frac{F}{\Delta L} \tag{4.10}$$

giving $K_E = 6.63 \cdot 10^7$ [kN/m]. To implement internal friction of the towline, the towline force was modelled with a dissipative damping term similar to the fender contact force in section 4.2.1, but with a lower critical damping fraction μ_0.

$$F_{Tow} = K_E(T_T - T_B) + \mu_0 \sqrt{4mK_E} \cdot (\dot{T}_T - \dot{T}_B) \tag{4.11}$$

Chapter 5

Simulation results of the interaction forces

Simulation results shown in this chapter was created with Simulink, by using automatic solver selection, which chose ode3, with fixed step size of 0.025. The results show the interaction effect between a tugboat and bulk carrier generated from the contact and towing forces from chapter 4.

5.1 Impact force simulations

To simulate the impact force and settling time of the contact force, the tugboat was approaching the bulk hull with a constant velocity of 0.2 [m/s], from a distance of 5 [m]. From the results in figure 5.1, the damping term causes undesired effect and can be seen from Run A, where there is a negative force on the bulk carrier when the tugboat moves away from the hull. This effect is removed with an "if" statement on the normal force F_N as seen with Run B, and has a small effect on the settling time. By increasing the force when contact is achieved, as seen with Run C, the force settles faster.

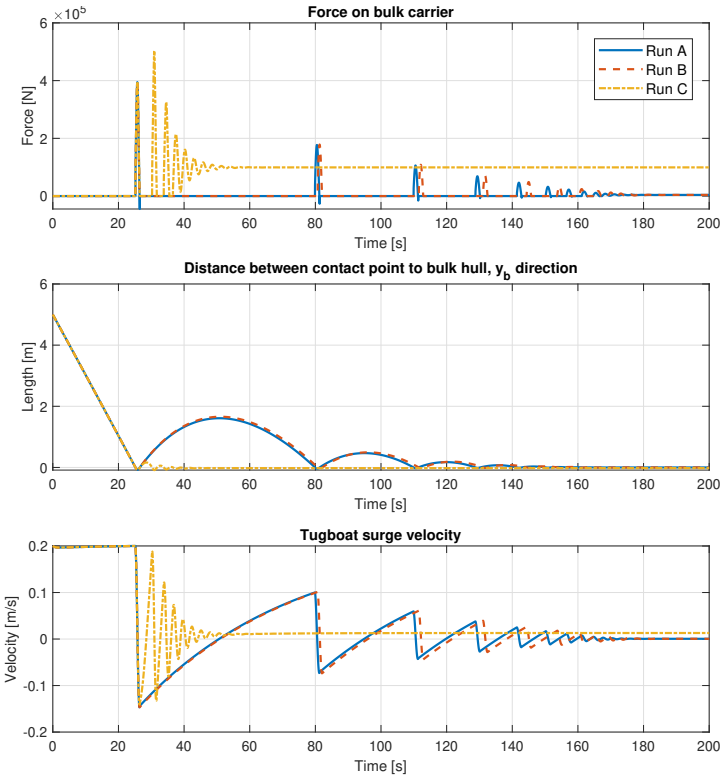

Figure 5.1: Simulation results of the impact force on the bulk carrier. Run A has a constant force of 4 [kN], Run B use if $F_N < 0 \Rightarrow F_N = 0$ and Run C set a desired force of 100 [kN] after the first contact.

Impact forces are sudden and often very large and can be difficult to simulate. In this model, the force depends on the overlapping distance and velocities, where the force could vary depending on when the first overlapping between contact surfaces is registered. The simulation results should be more consistent by using a smaller time step, but will results in longer computational time. While a time step of 0.025 [s] is small, the overlapping distance have a relatively large effect due to the high stiffness of the contacting fender. The negative force around the zero overlapping, on the return of the impact, shows that the implementation method is not accurate around the crossing. The accuracy of the model depends on the parameters used, and without real data, the actual response is difficult to simulate. While it is difficult to assume how it should be without experimental test results, high contact forces could also cause deformation on the hull and would increase the dissipative damping forces. While this may not be necessary to model, it should be considered to prevent damage on the vessels in a real system.

5.2 Friction force simulations

To simulate the friction forces between the vessels, the tugboat was starting in contact facing directly at the bulk carrier hull with a desired push force, while the bulk carrier had a constant velocity around 0.4 [m/s] heading north.

5.2.1 Period duration simulations

To see how the period duration dt to calculate the acceleration for the tugboat stick force F_{Stick} affected the behaviour, the tugboat was simulated with a desired force of 500 [kN]. The results are shown in figure 5.2, where $dt = 0.025$ gives a unstable behaviour that can be seen from the fluctuations on the bulk carrier force. By increasing the time duration, $dt = 0.1$ and $dt = 1$, the force is more stable, but the initial force required to stick the tugboat to the hull is much lower. From the position of the bulk contact point, it seems like the lowest time duration $dt = 0.025$ drifts more after settling, compared to the other two.

While the acceleration of the rigid contact point should be "instant", to give the required stick force, there are some computational limitations. This is best seen from the unstable results with $dt = 0.025$, where the forces fluctuate. This unstable behaviour could be caused by how the vessels moves compared to each other, where if one moves before the other in the simulations, a small change in velocity will generate a large force. By using a higher period duration, the initial force is reduced, but if this force is much larger than the friction force, the resulting force between the vessels should be similar. If there are large contact forces, due to pushing force or impact force, there may be larger differences. With a time duration $dt = 0.1$, the required force to stick get relatively large, which should be enough for a more realistic behaviour, as the rubber fender is flexible were the contact point would have a small change to accelerate.

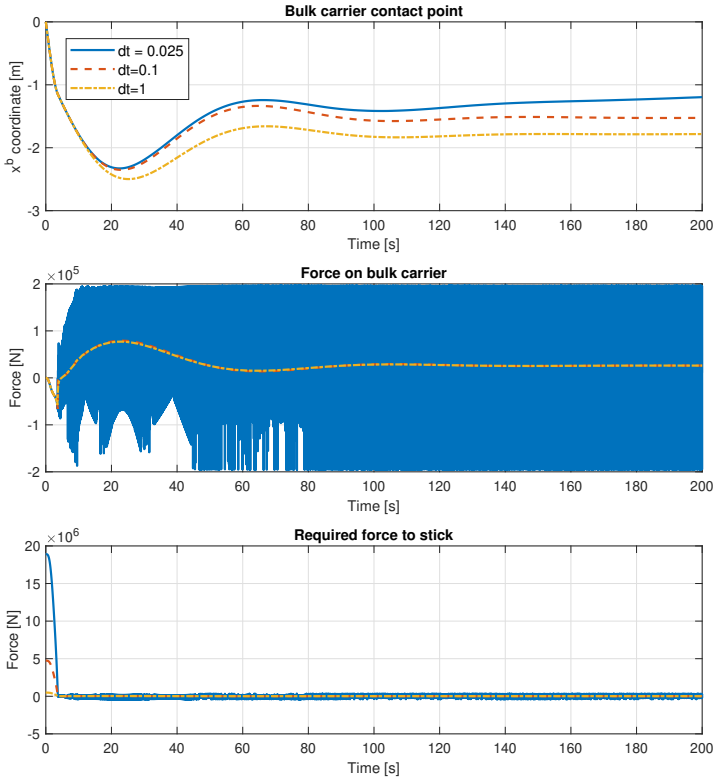

Figure 5.2: Simulating contact friction with different period duration dt to calculate the acceleration based on the relative velocity between contact points (see equation (4.6)).

5.2.2 Stick-slip dynamic simulations

The stick dynamics was simulated by using a desired tugboat force of 60 [kN] and is shown in figure 5.3. First, the tugboat slide along the hull since the required stick friction F_{Tot} is larger than the friction limit F_R, which is due to the jump in relative velocity. At around 8 [s], the tugboat bow stick to the hull, where the change in bulk contact point should be caused by the tugboat bow rolling along the hull, which can be seen by comparing the contact point and the tugboat heading. When the tugboat heading changes in the direction of the motion, the required friction force changes. The required friction gets close to the friction force limit, where the tugboats is close to slipping at around 80 [s], before settling at an angle of around 60°. After stabilising, there is a slow drift in contact position.

A lower desired tugboat force of 40 [kN] was used to show the slip dynamics of the friction force, where the simulation results are shown in figure 5.4. The slip dynamics simulation is similar to the previous stick dynamics, up until about 70 [s], where the tugboat starts to slide along the hull of the bulk carrier. By using a lower pushing force, the friction force limit is lower, which is enough for the required friction force to surpass the limit. When the limit is reached, the limit reduces until the relative velocity and heading starts to stabilise.

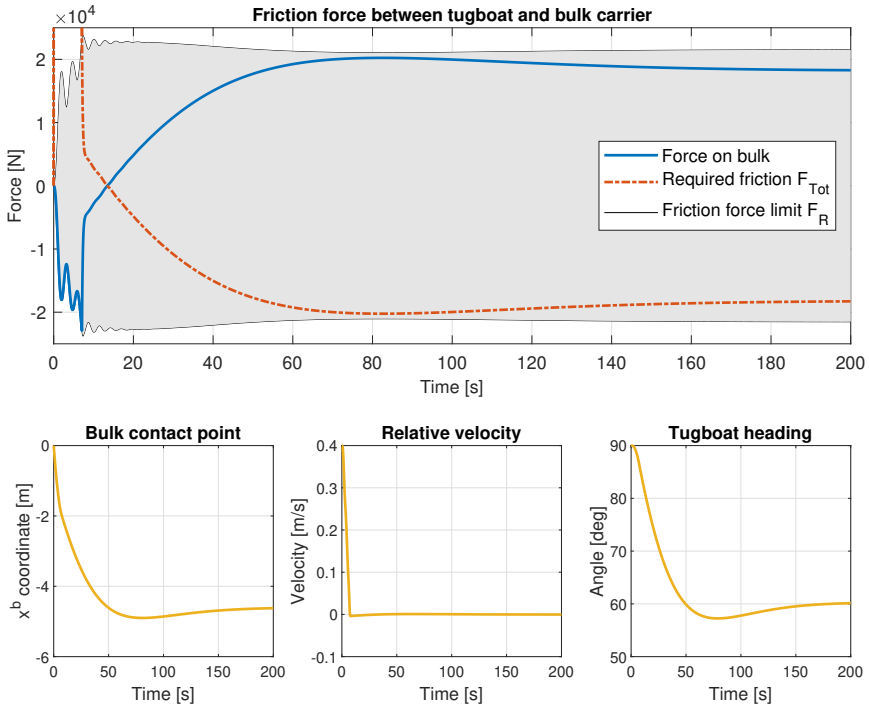

Figure 5.3: Friction force simulation results of the tugboat sticking to the bulk carrier hull. The relative velocity is along the hull between contacting points.

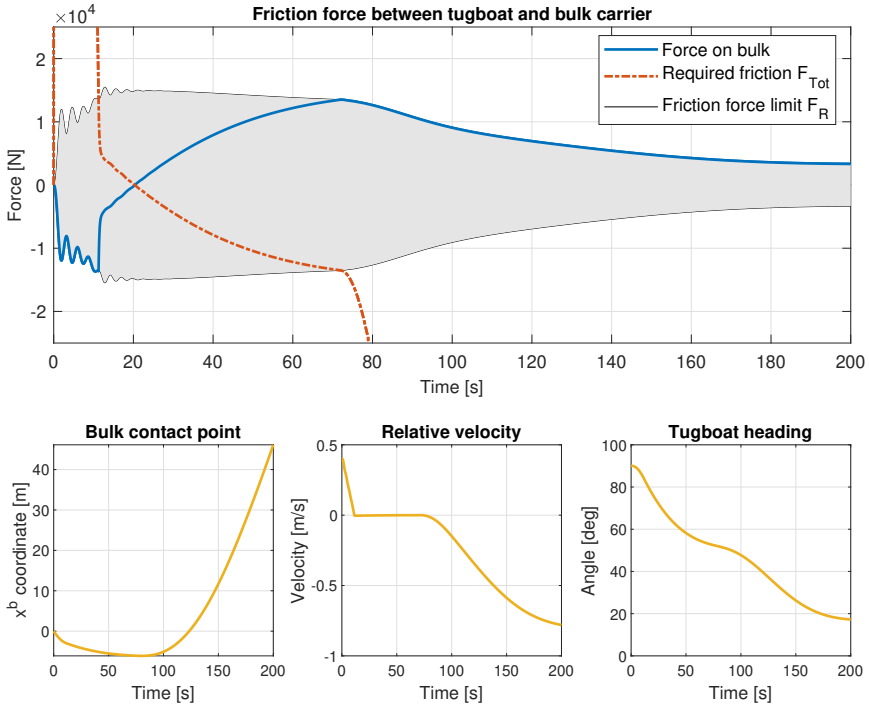

Figure 5.4: Friction force simulation results of the tugboat sliding along the bulk carrier hull. The relative velocity is along the hull between contacting points.

By using the tugboat dynamics to find the required friction force to stick against the hull of the bulk carrier, the transition between stick and slip seemed to be smooth. The fast decrease in the friction force limit when slipping should be explained by the exponential change between static and kinetic friction coefficient, which changes fast when there is motion, combined with the increasingly reduction of the contact force based on the heading.

The heading angle that the tugboat stabilises on, should be explained by how the required friction force is found. Since the required friction force is based on the velocity and direction the tugboat moves through the water, the stabilising angle should be at the point when the propulsion thrust force generates a moment about the contact point equivalent to the required friction force. The heading would therefore move towards a surge direction, which has less resistance than sway direction, and stabilise if the resulting contact force is high enough.

The drift from the stick dynamics is small and would be 10-20 [cm] in the next 800 [s], if the simulations kept going. The reason for the drift is unknown, as it could be the simplification of not using yaw rate or yaw acceleration in the calculations, or if it is due to the simulation method. While the drifting could increase depending on the velocity and desired force, the small drift should have little to no impact, as it can be compared to around 1-2° roll of the tugboat bow.

5.3 Towline tension simulations

To simulate the forces generated by the towline tension, the tugboat started still at the towline length of 60 [m] from the bulk carrier, amidship (see figure 4.9), and had a desired force of -100 [kN]. From the simulation results shown in figure 5.5, the towline force on the bulk carrier oscillates around the desired pulling force. Without the internal friction of the towline, when the critical damping fraction $\mu_0 = 0$, the damping is only caused by the damping in the tugboat dynamics. By using a relatively low damping term, with $\mu_0 = 0.001$ and $\mu_0 = 0.01$, the oscillations settle quicker and have little impact on the total force given to the bulk carrier, which can be seen by the change in east position.

The dissipative damping term used to simulate the internal friction in the towline may be much larger than in a real towline, but by removing oscillations there is shown little impact on the change in bulk position. A higher damping term could therefore be more favourable in the simulations. While the total force on the bulk carrier is similar, the change should have a larger difference when the towline stretches with tugboat velocity. The effect should be similar as shown for the impact force in figure 5.1. For a more accurate model, the stiffness due to catenary geometry should have been implemented, which could reduce the velocity before a sudden stretching of the towline. Since the catenary stiffness depend on the towline weight, and the towline is relatively light, this effect may be to small for a short towline too make a difference.

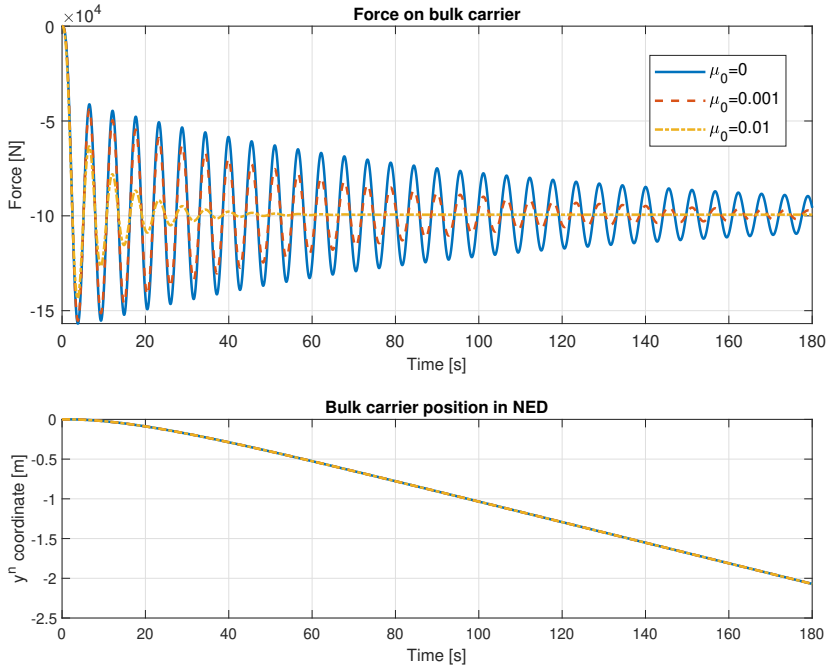

Figure 5.5: Simulation results of the towline force with length 60 [m] modelled with different critical damping fractions μ_0 for the dissipative damping term in equation (4.11)

5.4 Model discussion

From the simulation results of the towline tension and impact force, the dissipative damping is difficult to model, as small changes can make large differences. While the responses would differ in a real system, there would be large impact forces and oscillations to some degree. Combined with the stick-slip dynamics of the friction force, it should provide plausible dynamics that must be considered during a real operation. This should enlighten certain problems that must be considered in the control system designs, for using tugboats as dynamical thrusters.

The bulk carrier model dynamics was reused from the specialisation project, where it was concluded that the model would have bad performance in a real application but had credible dynamics that could be used to validate the control system. For the tugboat model, due to limited data on hydrodynamic forces, the linear dynamics was based on the linear hydrodynamic forces on a different hull shape and should not be accurate. Since the non-linear damping was based on the hull shape, the non-linear damping could give more plausible tugboat dynamics at higher velocities. The model should therefore give some limitations to the motion, while it may not be accurate, the real system should have similar limitations at different values. Accurate models would be hard to implement as they require experimental testing, which can be expensive. However, by having more accurate models, adaptive controllers developed in other studies (see section 1.2), should have better performance when the models have less deviation from the actual dynamics.

Since the contacting surfaces for the vessels is simplified, with straight lines for the entire bulk carrier length and a perfect circular arc for the tugboat bow, some constraints should be considered in simulations. For the bulk hull, there are certain strong sections that should be used for contact pushing, which are marked and often coincide with the towing pullerts. The strong section can be seen in figure 1.3, which lies on the midway from amidships to the bow and stern. While the tugboat bow can have a circular shape, it may have a flatter front area and narrowing sides, which should be possible to implement in a similar method. Since the tugboat sides are not modelled, the tugboat cannot make contact with the sides to follow along.

The simulation model was implemented with ideal conditions, where ocean currents, waves and wind forces are neglected. Ocean currents from the tides in Narvik and wind could have significant impact on the behaviour of the vessels, while the waves should be relatively small in harbour and have less effect. In addition, hydrodynamic interaction forces could also result in undesired motion of the vessels. One is the interaction forces caused by the tugboat propulsion system, propeller wash and the Coanda effect, where these combined can cause motion in the opposite direction of the desired force. While the propeller wash can be included in the required bollard pull, as an efficiency factor based on the towline length and projected area, the angle the propeller wash is to the bulk carrier hull should affect the projected area and may be challenging to model. Another is transverse thrust, which can move the stern if the towed bulk carrier is to use its own propulsion. Since the transverse thrust could change the direction in shallow waters, the force could also be challenging to model. There could also be other hydrodynamic forces that may have a significant impact on the vessels, which should require more investigation and experience from the harbour to know about.

Chapter 6

Tugboat control system design

In this chapter, the control system design for the tugboat is described, while relevant Simulink models and Matlab code are given in appendix C. The control system was implemented in the tugboat reference model (see figure 6.1), which consist of control allocation to optimise the thrust force among the thrusters and a control law to get the tugboat into position and give the desired force from the bulk carrier control system.

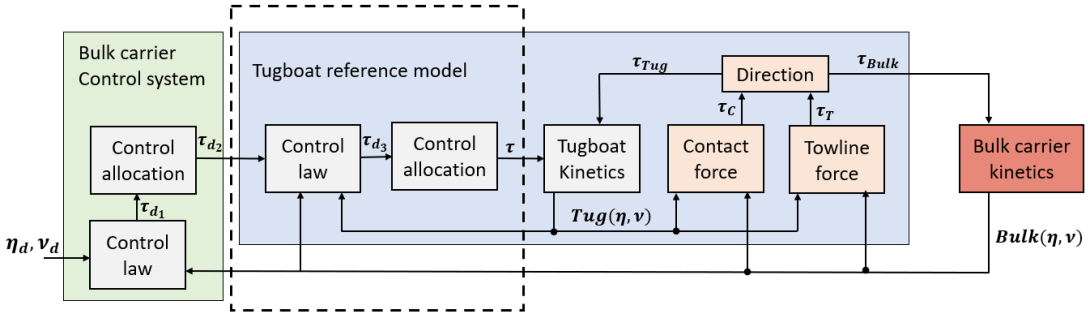

Figure 6.1: Illustration of the control systems in the Simulink model covered in chapter 6, within the dotted line.

6.1 Tugboat control allocation

6.1.1 Tugboat thrust force

Since the tugboat is equipped two azimuth thrusters and a bow tunnel thruster, the system is overactuated for 3-DOF. Both azimuth thrusters can rotate 360°, but have reduced performance when propeller wash disrupt the surrounding water of the opposite thruster. This is illustrated in figure 6.2, where the red sectors are not desirable. While the red sectors can be avoided by using restrictions, this creates a non-convex problem. Instead, the azimuth thrusters are restricted to only operate in 180°, from straight ahead to astern.

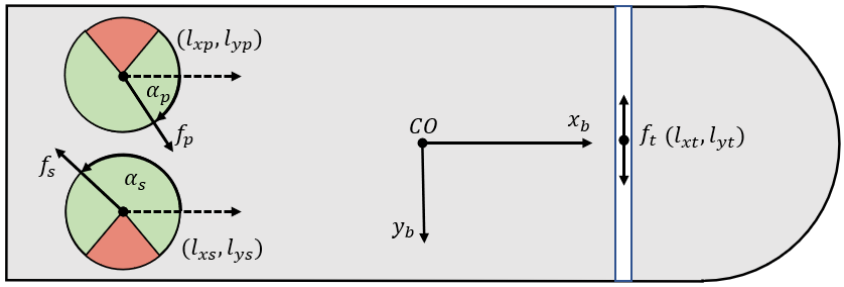

Figure 6.2: Illustration of tunnel thruster and the azimuth thrusters position (l_x, l_y) on the tug, with tunnel $\{t\}$, port $\{p\}$ and starboard $\{s\}$, where the undesired angle of attack α due to propeller wash are in the red sectors.

For fixed pitch propellers, the thrust force can be calculated from equation (2.15) based on rpm and a thrust coefficient $K_T(J_a)$ that depends on the surge velocity. By calculating the thrust force at zero surge velocity, $K_T(0)$ is constant and the thrust force can be approximated with equation (6.1), by using curve fitting based on the maximum rpm and thrust force achieved from a bollard pull test [35].

$$\text{Thrust} = T_{|n|n}|n|n \rightarrow T_{|n|n} = \frac{\text{Thrust}_{\max}}{|n_{\max}|n_{\max}} \tag{6.1}$$

The azimuth thrust force was calculated from the bollard pull given in appendix A.1, with 66.5 [t] at maximum continuous rating (MCR) and a maximum of 1000 [rpm] based on the engine data [36]. To simulate delay of the azimuth thrust force, a LP filter was implemented on the desired rpm, where saturation was used on the error to limit the rate of change (see appendix C.1.1). Since the bow tunnel thruster is only listed with 252 [hp] in appendix A.1, the thrust force and rpm was based on a tunnel thruster with similar size from [37], giving a thrust force of 27 [kN] at maximum 1800 [rpm].

6.1.2 Tugboat control allocation optimisation problem

The control allocation for the tugboat was solved based on equation (3.14), which solve a non-linear non-convex problem by solving a local approximation with a QP problem. In the equation, the singularity term is used to prevent thrusters from pointing in the same direction, to prevent controllability loss when no force can be achieved in certain directions. This term was neglected for the tugboat control, where the controllability loss was not seen as a problem, since the thrusters are used in the same direction for pushing and pulling. In addition, the change in thrust force was also limited. The resulting optimisation problem is given in equation (6.2),

$$
\begin{aligned}
J = \min_{\Delta \boldsymbol{f} \Delta \boldsymbol{\alpha}, \mathbf{s}} & \left\{ \Delta \boldsymbol{f}^T \mathbf{W} \Delta \boldsymbol{f} + \mathbf{s}^T \mathbf{Q} \mathbf{s} + \Delta \boldsymbol{\alpha}^T \boldsymbol{\Omega} \Delta \boldsymbol{\alpha} + 2 \Delta \boldsymbol{f}^T \mathbf{W} \mathbf{f}_0 \right\} \\
& \text{Subject to:} \\
& \mathbf{s} + \mathbf{T}(\boldsymbol{\alpha}_0) \Delta \boldsymbol{f} + \frac{\partial}{\partial \boldsymbol{\alpha}} \Big(\mathbf{T}(\boldsymbol{\alpha}) \boldsymbol{f} \Big) \Big|_{\boldsymbol{\alpha}_0, \boldsymbol{f}_0} \Delta \boldsymbol{\alpha} = \boldsymbol{\tau} - \mathbf{T}(\boldsymbol{\alpha}_0) \boldsymbol{f}_0 \\
& \boldsymbol{f}_{\min} - \boldsymbol{f}_0 \leq \Delta \boldsymbol{f} \leq \boldsymbol{f}_{\max} - \boldsymbol{f}_0 \\
& \Delta \boldsymbol{f}_{\min} \leq \Delta \boldsymbol{f} \leq \Delta \boldsymbol{f}_{\max} \\
& \boldsymbol{\alpha}_{\min} - \boldsymbol{\alpha}_0 \leq \Delta \boldsymbol{\alpha} \leq \boldsymbol{\alpha}_{\max} - \boldsymbol{\alpha}_0 \\
& \Delta \boldsymbol{\alpha}_{\min} \leq \Delta \boldsymbol{\alpha} \leq \Delta \boldsymbol{\alpha}_{\max}
\end{aligned}
\tag{6.2}
$$

where the thrust coefficient matrix $\mathbf{T}(\boldsymbol{\alpha})$, including the tunnel thruster, and its partial derivative $\frac{\partial \mathbf{T}(\boldsymbol{\alpha})}{\partial \boldsymbol{\alpha}}$ are given in equation (6.3), with the vector force $\boldsymbol{f}$ and angle of attack vector $\boldsymbol{\alpha}$. In the matrices l is the distance from the CO, while the notations are tunnel $\{t\}$, port $\{p\}$ and starboard $\{s\}$.

$$
\mathbf{T}(\boldsymbol{\alpha}) = \begin{bmatrix} 0 & \cos(\alpha_p) & \cos(\alpha_s) \\ 1 & \sin(\alpha_p) & \sin(\alpha_s) \\ l_{xt} & -l_{yp}\cos(\alpha_p) + l_{xp}\sin(\alpha_p) & -l_{ys}\cos(\alpha_s) + l_{xs}\sin(\alpha_s) \end{bmatrix}
$$

$$
\frac{\partial \mathbf{T}(\boldsymbol{\alpha})}{\partial \boldsymbol{\alpha}} = \begin{bmatrix} -\sin(\alpha_p) & -\sin(\alpha_s) \\ \cos(\alpha_p) & \cos(\alpha_s) \\ l_{yp}\sin(\alpha_p) + l_{xp}\cos(\alpha_p) & l_{ys}\sin(\alpha_s) + l_{xs}\cos(\alpha_s) \end{bmatrix}, \quad \boldsymbol{f} = \begin{bmatrix} f_t \\ f_p \\ f_s \end{bmatrix}, \quad \boldsymbol{\alpha} = \begin{bmatrix} \alpha_p \\ \alpha_s \end{bmatrix}
\tag{6.3}
$$

The constraints used in the optimisation problem are listed in table 6.1. Both azimuth thrusters were limited to only giving thrust in one direction, no reversing. This caused an error when the initial position of the azimuth thruster was more than 90° from the desired direction, as the minimisation problem takes the force to zero instead of rotating the azimuth thrusters. To fix this problem, a small value was set on the minimum thrust force for the azimuth thrusters, which gave the problem something to minimise. Since the optimisation problem was locally approximated, a step limit was set on the force $\Delta \boldsymbol{f}$, similar to the angle step $\Delta \boldsymbol{\alpha}$. The step limits were assumed to be 10 [s] to turn the azimuth thrusters 180°, 10 [s] to give 250 [kN] from each azimuth thrusters and 2 [s] to maximum tunnel thrust.

Table 6.1: Constraints used in the optimisation problem given in equation (6.2).

Thruster	$f_{\min/\max}$ [kN]	$\Delta f_{\min/\max}$ [kN/s]	$\alpha_{\min/\max}$ [°]	$\Delta\alpha_{\min/\max}$ [°/s]
Tunnel	-27/27	13.5	–	–
Port	0.00001 / 300	25	0 / 180	18
Starboard	0.00001 / 300	25	-180 / 0	18

The optimisation problem was solved with the Matlab function "quadprog" (see appendix C.1.2

for implementation), on the form given in equation (6.4),

$$\min_{\mathbf{z}} \frac{1}{2}\mathbf{z}^T\mathbf{H}\mathbf{z} + (\mathbf{R}\mathbf{p})^T\mathbf{z} \text{ such that } \begin{cases} \mathbf{A}_1 \cdot \mathbf{z} = \mathbf{C}_1\mathbf{p} \\ \mathbf{A}_2 \cdot \mathbf{z} \leq \mathbf{C}_2\mathbf{p} \\ \mathbf{lb} \leq \mathbf{z} \leq \mathbf{ub} \end{cases} \tag{6.4}$$

with the vectors,

$$\mathbf{z} = \left[\Delta \boldsymbol{f}^T, \Delta \boldsymbol{\alpha}^T, \mathbf{s}^T\right]^T, \quad \mathbf{p} = \left[\boldsymbol{\tau}^T, \boldsymbol{f}_{\min}^T, \boldsymbol{f}_{\max}^T, \boldsymbol{\alpha}_{\min}^T, \boldsymbol{\alpha}_{\max}^T, \boldsymbol{\alpha}_0^T, \boldsymbol{f}_0^T\right]^T$$

and the weights $\boldsymbol{H} = \text{diag}([\boldsymbol{W}, \boldsymbol{\Omega}, \boldsymbol{Q}])$. The weights were chosen based on , $\boldsymbol{\Omega} < \boldsymbol{W}$ to favour rotation of the azimuth thrusters, and $\boldsymbol{W} << \boldsymbol{Q}$ for the slack variables $\boldsymbol{s}$ to go to zero.

6.2 Tugboat control law

The tugboat control law consists of two main controllers, one for transit and another for giving the required force to the bulk carrier. The transit controller was used to steer the tugboat into position, for either pushing or pulling, where the controller was switched to the required force control by using a Stateflow chart in Simulink.

6.2.1 Tugboat transit controller

To get the tugboat close to the desired position on the bulk carrier hull, while maintaining a direct heading, the transit controller was implemented with 3-DOF trajectory tracking and a surge controller. The trajectory tracking was used to get to the desired position x_d^b and desired heading ψ_d, while the surge controller was implemented to reach the desired position y_d^b (see figure 6.3).

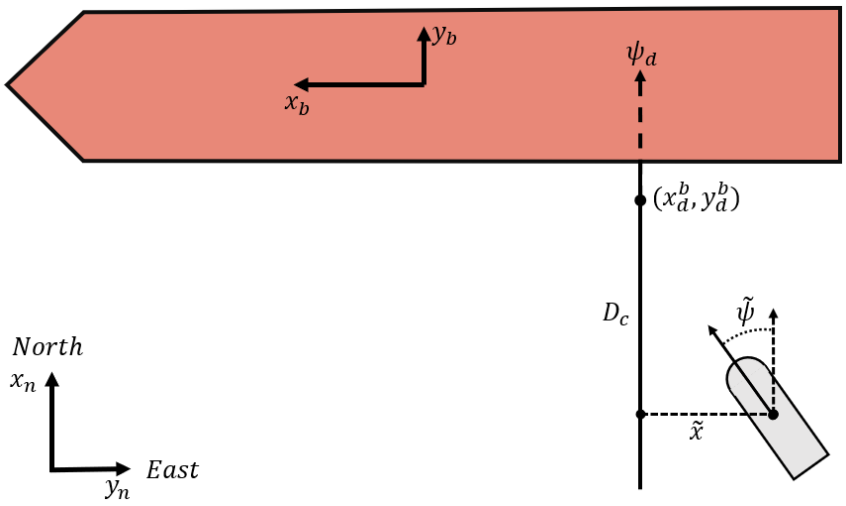

Figure 6.3: Illustrating the desired position and orientation of the tugboat, for a pushing operation.

3-DOF trajectory tracking

The 3-DOF trajectory tracking was designed based on the non-linear PID control law in section 3.2.2 and was implemented in Simulink as shown in appendix C.2.1. Since tugboats have high manoeuvrability, it was assumed that time derivative of the rotation matrix $\dot{\boldsymbol{R}} \not\approx 0$. Using $\dot{\boldsymbol{R}} \not\approx 0$ for 3-DOF was seen in several studies [5, 6, 7], where asymptotically stability of the tracking error was proven from Lyapunov analysis.

The time derivative of the rotation matrix can be represented in reference frame $\{a\}$ or $\{b\}$, as shown equation (6.5) [15].

$$\dot{\boldsymbol{R}}_b^a = (\boldsymbol{\omega}_{ab}^a)^\times \boldsymbol{R}_b^a = \boldsymbol{R}_b^a (\boldsymbol{\omega}_{ab}^b)^\times \tag{6.5}$$

Since the the marine craft was operating in 3-DOF, the angular velocity is equal in the NED and Body reference frame, giving $\boldsymbol{\omega}_{ab}^a = \boldsymbol{\omega}_{ab}^b = \begin{bmatrix} 0 & 0 & r \end{bmatrix}^T$. Due to the SO(3) properties of the rotation matrix given in equation (2.5), $\boldsymbol{R}^T = \boldsymbol{R}^{-1}$ and $\boldsymbol{R}^{-T} = \boldsymbol{R}$, the acceleration could be written as,

$$\dot{\boldsymbol{\nu}} = \boldsymbol{R}^T \ddot{\boldsymbol{\eta}} - \boldsymbol{R}^T (\boldsymbol{\omega})^\times \boldsymbol{R} \boldsymbol{R}^T \dot{\boldsymbol{\eta}}$$

which gave the resulting gains in equation (6.6). Since the gains was used on position and heading errors, the natural frequencies for north and east position was tuned equally $\omega_{n_1} = \omega_{n_2}$, while the heading was tuned separately ω_{n_6}. In equation (6.6), the natural frequencies are given as $\boldsymbol{\Omega}_n = \text{diag}([\omega_{n_1}, \omega_{n_2}, \omega_{n_6}])$, while the damping $\boldsymbol{Z}$ was set as the identity matrix to give critical damping.

$$\boldsymbol{K}_p = \boldsymbol{R}\boldsymbol{M}\boldsymbol{R}^T \boldsymbol{\Omega}_n^2 \tag{6.6a}$$

$$\boldsymbol{K}_d = 2\boldsymbol{R}\boldsymbol{M}\boldsymbol{R}^T \boldsymbol{Z}\boldsymbol{\Omega}_n - \boldsymbol{R}[\boldsymbol{C}(\boldsymbol{\nu}) + \boldsymbol{D}(\boldsymbol{\nu})]\boldsymbol{R}^T + \boldsymbol{R}\boldsymbol{M}\boldsymbol{R}^T (\boldsymbol{\omega})^\times \tag{6.6b}$$

$$\boldsymbol{K}_i = \frac{1}{10} \boldsymbol{K}_p \boldsymbol{\Omega}_n \tag{6.6c}$$

For the 3-DOF trajectory tracking to be unaffected from the surge control, the desired position was given in the bulk carrier reference frame, with the error,

$$\tilde{\boldsymbol{\eta}} = \begin{bmatrix} x_{tug}^b - x_d^b \\ 0 \\ \psi_{tug} - \psi_d \end{bmatrix} \tag{6.7}$$

where the north coordinate in Body x_d^b was set from the desired contact point. This resulted in a constant coordinate, with a variable desired heading based on the bulk carrier heading.

The controller gains given in equation (6.6) use the rotation matrix to determine the values. This mean that the gain matrices are designed for the NED reference frame. Since the trajectories was given in the bulk carrier reference frame, the rotation matrix used to calculate the gains had to be calculated from the difference in heading, $\psi = \psi_{Tug} - \psi_{Bulk}$.

To get feasible trajectories, the desired trajectories was obtained from the 3. order reference mode given in equation (3.2). This was implemented in Simulink as shown in appendix C.2.1, by saturating the acceleration and velocity, where the velocity was saturated in the integrator to prevent integrator windup. By using the desired change in position $\dot{\tilde{\boldsymbol{\eta}}}$ from the reference model, and $\boldsymbol{R}_T^T\boldsymbol{R}_B$ to convert the forces from the bulk carrier reference frame to the tugboat reference frame, the final control law was given as shown in equation (6.8).

$$\boldsymbol{\tau} = \boldsymbol{R}_T^T\boldsymbol{R}_B\boldsymbol{\tau}_{\text{PID}} = \boldsymbol{R}_T^T\boldsymbol{R}_B(-\boldsymbol{K}_p\tilde{\boldsymbol{\eta}} - \boldsymbol{K}_d\dot{\tilde{\boldsymbol{\eta}}} - \boldsymbol{K}_i\int_0^t \tilde{\boldsymbol{\eta}}d\tau) \tag{6.8}$$

Surge control

The surge controller was used to reach the contact point, either bulk carrier hull or the towing distance, at a reasonable velocity. This was implemented by having a desired surge velocity u_d that would exponentially decay with the distance D_c (see figure 6.3). By using velocity control instead of position, errors from navigation systems would have less impact on the performance as the exact position is not required. To ensure that the tugboat would reach the contact point, a low velocity of 0.1 [m/s] were added. For the desired velocity to be idle until the tugboat was in position, the desired velocity was based on the deviation from coordinate $\tilde{x}$ and heading $\tilde{\psi}$ from the 3-DOF trajectory tracking controller. The desired velocity was found with,

$$u_d = u + \Big(\pm\left(K_{Surge}(1-e^{-(D_cK_c)}) + 0.1\right) - u\Big)e^{-(\tilde{x}K_{\tilde{x}})}e^{-(\tilde{\psi}K_{\tilde{\psi}})} \tag{6.9}$$

where K is tuneable constants and $\pm$ is determined from push and pull operation. This resulted in a desired velocity that changed with the error and distance, where the change in distance depended on the velocity towards the hull.

The surge controller was designed based on the linear surge dynamics of the tugboat $(m - X_{\dot{u}})\dot{u} + X_u u = \tau_X$ (see section 4.1.2). To compensate for the change in desired velocity, the controller was set as a PI-regulator with a feed forward term F_f, where the parameters was found based on the comparison method [38], giving the gains in equation (6.10).

$$\begin{aligned}
&M\dot{u} + Du = F_f + K_p(u_d - u) + K_i\int_0^t (u_d - u)dt, \quad e = u_d - u \\
&M\dot{e} = \cancel{M\dot{u}_d} - \cancel{F_f}^{\,0} - M\dot{u} = -(K_p e + K_i\int_0^t e dt - Du_d + De) \\
&M\ddot{e} + (K_p + D)\dot{e} + K_i e = 0 \Leftrightarrow \ddot{x} + 2\zeta\omega_n\dot{x} + \omega_n^2 x = 0 \\
&K_p = 2\zeta\omega_n(m - X_{\dot{u}}) - X_u, \quad K_i = (m - X_{\dot{u}})\omega_n^2, \quad F_f = (m - X_{\dot{u}})\dot{u}_d
\end{aligned} \tag{6.10}$$

For the desired velocity u_d and acceleration $\dot{u}_d$ to be smooth, the reference model should be of order two [3]. This is equivalent to the third order reference model in equation (3.2), without the low pass filter $(1/(1+T_i s)$. Since the desired velocity change $\dot{u}_d \neq 0$, the change in reference signal $\dot{r}^b$ was added in the reference model to reduce overshoot. This was modelled

as,

$$\frac{u_d}{r^b}(s) = \frac{2\zeta\omega_n s + \omega_n^2}{s^2 + 2\zeta\omega_n + \omega_n^2} \tag{6.11}$$

and implemented in simulink as seen in appendix C.2.2.

6.2.2 Switching between tugboat controllers

To switch between the different tugboat controllers, a Stateflow chart was implemented in Simulink (see appendix C.3). The logic of the Stateflow chart is shown in figure 6.4, where it starts in idle and goes into transit mode for pushing or pulling, depending on the required force. When the tugboat contacts the hull or stretches the towline, the controller was changed to pushing or pulling mode, respectively. To prevent rapid changes between the controllers, due to impact bouncing (see results of impact simulations figure 5.1), both pushing and pulling mode was set with a delay before turning back to transit, when contact or stretch was lost. This allowed for the desired force to stabilise the tugboat in either pushing or pulling mode. To prevent sudden unrealistic jump in desired force, when changing force direction, a time delay was set in the force change block that was activated when the force crossed zero. This allowed the azimuth thrusters to slow down and start to turn, before the other controller was activated.

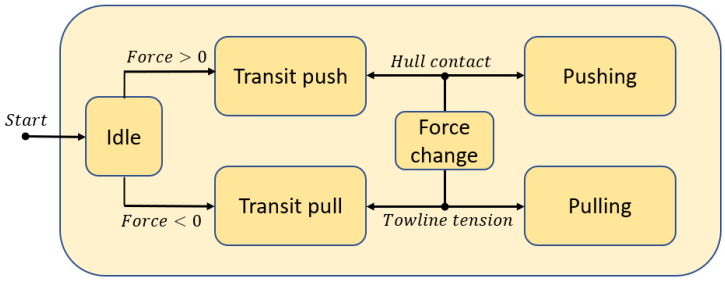

Figure 6.4: Illustration of the Stateflow chart with logic used to switch between controllers.

The change in controllers was performed by using boolean signals from the Stateflow chart, to activate enabled subsystems. By setting the enabled subsystems to reset, the values were deleted each time it was activated, but the output was frozen at the last active step. To remove this, the signal was sent through a LP filter and multiplied with the output, to reduce the output smoothly to zero. The tunnel thruster was only active under transit operations, to control the pushing and pulling mode with the azimuth thrusters.

6.2.3 Tugboat force controller

The force controller was used to give the desired force to the bulk carrier at a given angle, and was implemented in Simulink as shown in appendix C.4. The desired force was obtained through a LP filter with saturation, where the limitations of the QP-solver was used. This was to prevent the desired force in changing to rapidly for the thrusters to follow, and prevent rotation of the azimuth thrusters, if the surge force was lowered to fast. To achieve a given

angle, two controllers was implemented. One for the angle of attack α under towing and another for hull contact (see figure 6.5).

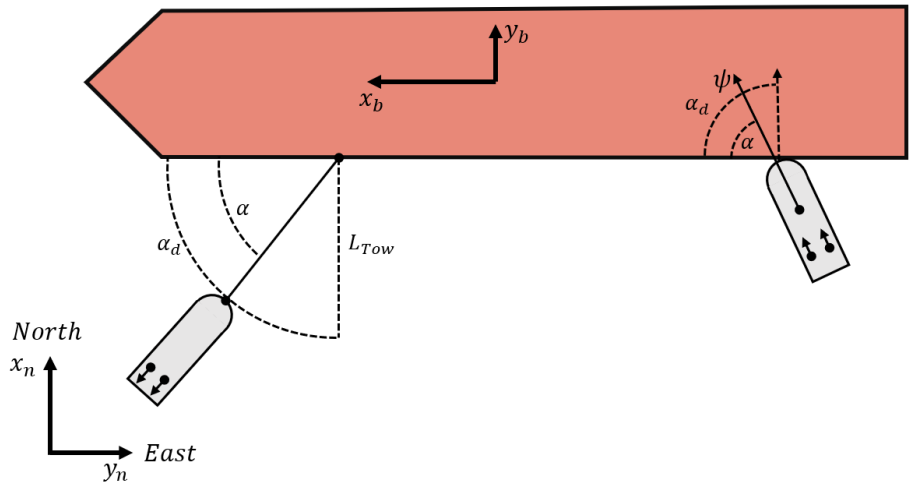

Figure 6.5: Illustration of the desired angle of attack α_d, for towing and pushing operation.

Towing angle controller

The towing angle controller was implemented to prevent the tugboat from giving undesired motion to the bulk carrier, by holding the desired force angle. The towing angle was controlled by using the arch length to the desired angle, at the distance of tugboat CO, as the error to control the sway motion of the tugboat. This was based on that in a towing operation the pulling force would be sufficiently large, so that a relatively small thrust force in sway direction from either azimuth would give a pure sway motion. By using the arch length as the error in sway direction $\tilde{y}$ and assuming a constant desired angle $\dot{\alpha}_d = 0$,

$$\tilde{y} = (\alpha - \alpha_d) \cdot (L_{Tow} + L_{CO}), \qquad \dot{\tilde{y}} = \dot{\alpha} \cdot (L_{Tow} + L_{CO}) \tag{6.12}$$

where L_{CO} is the distance to the tugboat CO from the towing connection. The angular velocity $\dot{\alpha}$ was found by setting reference frames for the actual and desired angle of attack and using the sway velocity (see appendix C.4.1 for implementation).

The control law was implemented as a linear PID controller, by separating the sway motion from the yaw motion and comparing it to a mass-spring-damper system. This was similar to the 3-DOF gains without the rotation matrices (see section 6.2.1), giving

$$\begin{gathered}(m - Y_{\dot{v}})\ddot{y} + (-Y_v)\dot{y} = \tau_Y = -K_p\tilde{y} - K_d\dot{y} - K_i\int_0^t \tilde{y}dt \\ (m - Y_{\dot{v}})\ddot{y} + (K_d - Y_v)\dot{y} + K_p\tilde{y} \Leftrightarrow \ddot{x} + 2\zeta\omega_n\dot{x} + \omega_n^2 x = 0 \\ K_p = \omega_n^2(m - Y_{\dot{v}}), \qquad K_d = 2\zeta\omega_n(m - Y_{\dot{v}}) + Y_v, \qquad K_i = \frac{\omega_n}{10}K_p\end{gathered} \tag{6.13}$$

where the gains were based on the hydrodynamic coefficients in section 4.1.2. To limit the sway force and prevent large azimuth angles, a 3. order reference model was implemented. The reference model was similar to the one used for 3-DOF trajectory tracking, with saturation on the velocity and acceleration.

Contact angle controller

The contact angle controller was implemented to ensure that the tugboat would face directly at the hull while pushing. This was to optimise the pushing force and reduce the friction force. Since the desired pushing force was given in the tugboat surge direction, an angle would not give the desired force to the bulk carrier. The force would instead increase the force along the hull, which could make the tugboat slide, as seen in the stick-slip simulation results in section 5.2.2.

To control the tugboat contact heading, a similar PID controller used for the towing angle was implemented. The error was seen as the arch between the angles, at the distance from the final contact point at the bow tip, to the CO. This was possible since the tugboat bow was implemented as a perfect half circle, while the real tugboat has a circular shape of changing radius. The change in error was found from the tugboat velocity in sway, by assuming that the tugboat rotated about the bow tip, with the yaw rate r of the tugboat. This gave the error,

$$\tilde{y} = (\alpha - \alpha_d) \cdot L_{CO}, \qquad \dot{\tilde{y}} = -L_{CO} \cdot r \tag{6.14}$$

where the gains for the PID controller was calculated as shown in equation (6.13).

While the towing angle could be controlled by assuming a pure sway motion, this was not working for the contact angle as there was more rotation. The problem was found in the QP-solver, which tried to solve for an increasing sway force with zero yaw moment. This gave an increased desired force, which was mostly compensated for by slack variables in the QP-solver, but resulted in increased surge force. To prevent this, a yaw moment was added with the desired sway force. The yaw moment was calculated from the desired sway force at the distance of the azimuth thrusters from the CO.

Chapter 7

Tugboat control system simulations

Simulation results shown in this chapter was created with Simulink, by using automatic solver selection, which chose ode3, with fixed step size of 0.025. The results show the performance of the tugboat control system from chapter 6.

7.1 Tugboat control allocation simulations

To see how the control allocation handled a large change in force direction, the desired force was set to -10 [kN], while both thrusters had an angle of attack $\alpha = 0$. From the simulation results in figure 7.1, the force is at the minimum value, while desired force is taken up by the slack variable. This can be explained by the thruster angle, where up until 5 [s], the azimuth angle is more than 90° from the optimal heading of 180°. Since the azimuth angle rotates at a limited rate, the desired force is larger than the required force, where a relatively small portion contributes to the desired direction, and the rest is wasted to each side. This cause the azimuth thrust force to have a peak before settling, where the actual force is delayed from the desired force. The delay should be caused by the rate of change used in the QP-problem, being faster than the dynamics set for the azimuth thruster rate of change with the LP filter.

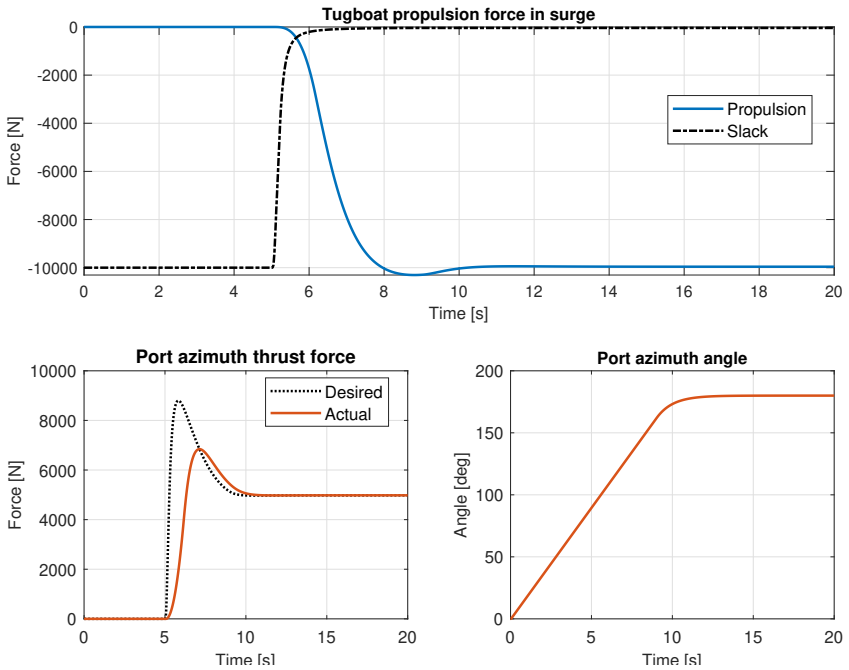

Figure 7.1: Simulation results for a desired force of -10 [kN] in surge direction. The starboard thruster have a identical desired and actual force, while the angle is equal but inverse.

7.2 Tugboat transit controller simulations

7.2.1 3. order reference model simulations

The 3. order reference model used in the 3-DOF trajectory tracking controller was tested at different deviations from the reference in north coordinate x and heading ψ. Figure 7.2 show the performance of the reference model with desired trajectories (see position and heading), and how the change in position is saturated (see velocity and yaw rate). The graphs shows that the position have varying performance up until a distance of 30 [m] (x_2) from the desired position, while the heading have varying performance up until 90° (ψ_4) from the desired heading. The performance is similar after these points, due to the saturation limits.

The saturation allows the controller to be more aggressive close to the desired trajectories, while maintaining feasible motion at larger distances. From the velocity and yaw rate graphs, the acceleration saturation gives a linear increase, which should be easier to follow for the tugboat, and reduce the deviation build up with the integral action. The velocity saturation gives sudden stop to the desired yaw rate and velocity, which should be difficult for the tugboat to follow.

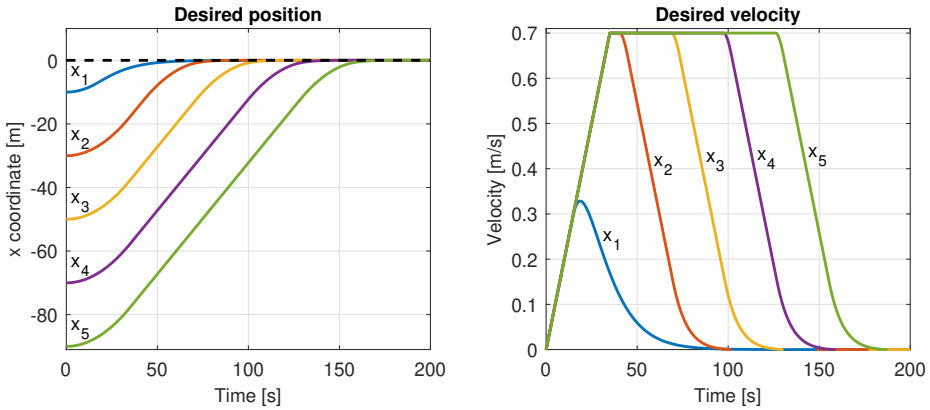

(a) Position: $\omega_n = 0.1$, $\zeta = 1$, $\dot{x}_d^b(\max) = 0.7$ [m/s] and $\ddot{x}_d^b(\max) = 0.02$ [m/s^2]

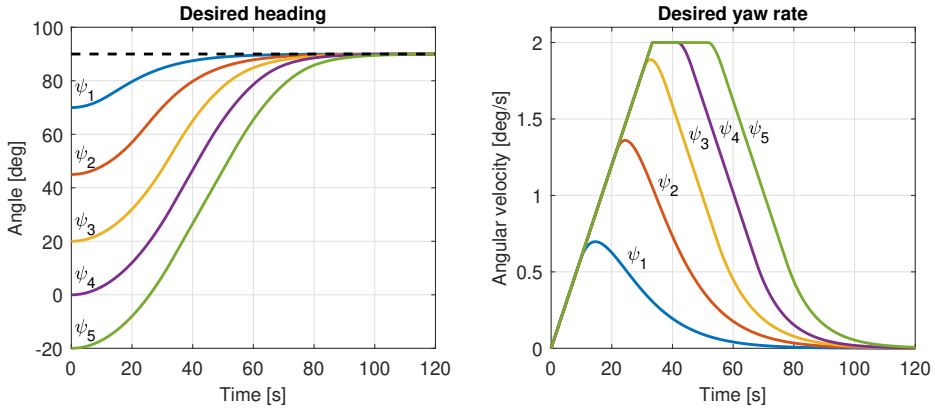

(b) Heading: $\omega_n = 0.1$, $\zeta = 1$, $\dot{\psi}_d(\max) = 2$ [deg/s] and $\ddot{\psi}_d(\max) = 0.06$ [deg/s^2]

Figure 7.2: Simulation results of a 3. order reference model for position in (a) and heading in (b), with the parameters and saturation values used.

7.2.2 3-DOF trajectory tracking simulations

In the 3-DOF trajectory tracking simulations, the tugboat starts with both thrusters pointing straight ahead, giving the angle of attack $\alpha = 0$.

Still trajectory

To see if the tugboat could follow the desired trajectories from the 3. order reference model, the bulk carrier was still, while the tugboat started by pointing towards the desired position with a heading of 45°. The results are shown in figure 7.3, and shows the tugboat performance by including the desired velocities $\dot{\boldsymbol{\eta}}_d$ of the trajectories in the control law. Without the desired velocities, the controller adjusts the deviation by using the integral action more, which can be seen with a slower increase and an overshoot of the reference. While the controller is improved by including the desired velocity, it should require a more impulsive force in the start. Impulse forces could be hard to follow, as the tugboat is limited by the available force and how fast the thrust force can increase with the current azimuth thruster positions.

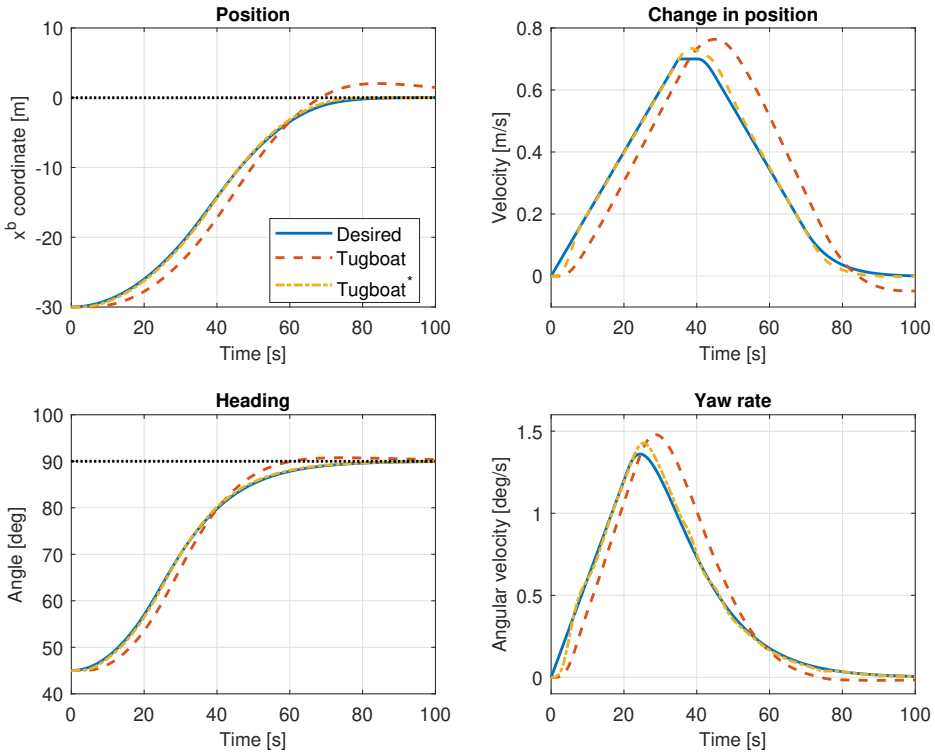

Figure 7.3: Simulation result of the 3-DOF trajectory tracking, by tracking the desired trajectories x_2 and ψ_2 from figure 7.2. The control law is run with (*) and without $\dot{\boldsymbol{\eta}}_d$ (see equation (6.8)).

Moving trajectory

While the tugboat manages to follow the desired trajectories, the heading influence the limitations of the controller. This was tested by starting the bulk carrier from still with a desired forward thrust force, to see how the tugboat could follow a moving trajectory.

Figure 7.4 show the results with an initial heading of 90°, which points the tugboat directly at the bulk carrier hull. By starting the tug in 90°, the motion should only be in the sway direction, which is limited by the tunnel thruster force and the force from the azimuth thruster to counteract the tunnel thruster moment. While the tugboat manages to follow the desired trajectory and then the bulk carrier when it moves (see position, x coordinate, note that the desired trajectory is in the bulk reference frame), the tugboat moves closer to the hull (see position, y coordinate). This can be explained from the tugboat surge and sway force. The initial peak in surge force should be caused by the angle of the azimuth thrusters, which need to get in position, while the large peak corresponds to the desired sway force that exceeds the limitation of the thrust force. Since the controller is set with constant east error $\tilde{y} = 0$, the tugboat can move freely towards the bulk carrier hull, which can give unstable performance and result in collision. From the initial sway forces, the tugboat is close to the thrust force limit, which shows that the controller is not well suited for only sway motion at larger distances. The thrust force is also delayed, which can be explained from the control allocation results (see section 7.1).

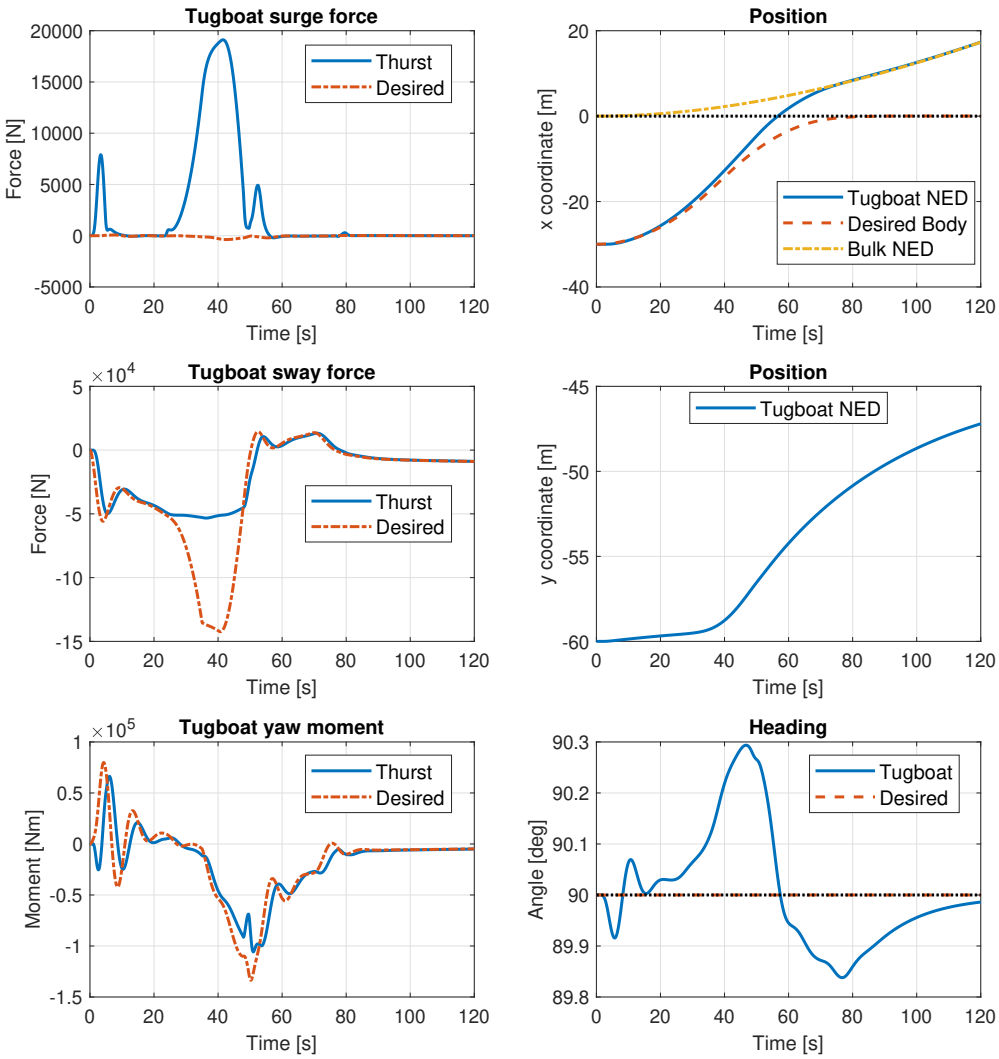

Figure 7.4: Simulation result of the 3-DOF trajectory tracking, by starting the tugboat at -30 [m] with the heading 90°. The bulk carrier is starting still and set with a surge force of 300 [kN].

By starting the tugboat at an angle of 45°, the motion can be divided between surge and sway motion, until the heading is facing directly at the hull. The simulation results are shown in figure 7.5, where the tugboat manage to follow the desired trajectory in a similar trend as the previous result, but with less motion towards the bulk carrier hull (see position, y coordinate). This can be explained by the force being divided to give more feasible desired thrust force in sway. Compared to the previous simulation, the tugboat thrust force in sway has a larger peak. This can be explained by the desired yaw moment. Since there is a desired yaw moment in a favourable direction, the azimuth thruster can surpass the moment of the tunnel thruster and thus increase the maximum allowed sway force.

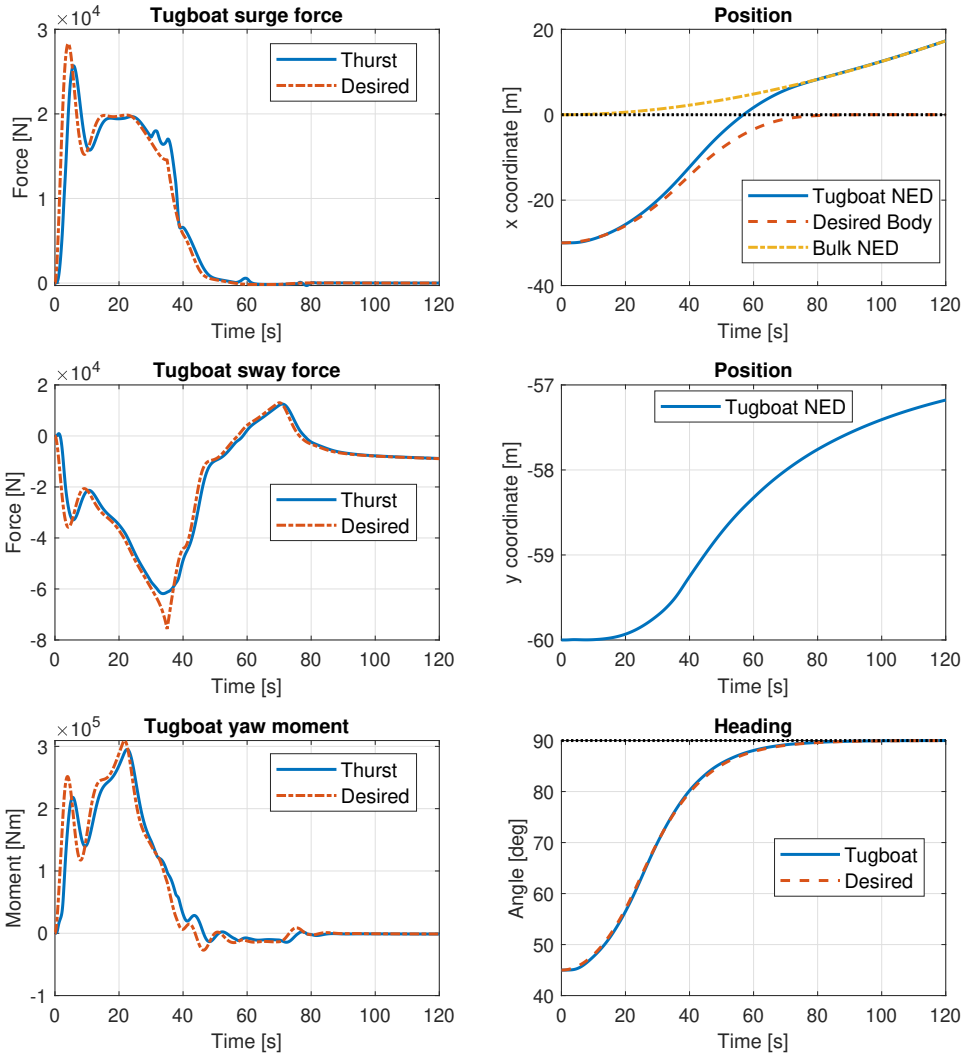

Figure 7.5: Simulation result of the 3-DOF trajectory tracking, by starting the tugboat at -30 [m] with the heading 45°. The bulk carrier is starting still and set with a surge force of 300 [kN].

7.2.3 Surge controller simulations

In the surge control simulations, the tugboat starts with the azimuth thrusters in the port and starboard directions, giving the angle of attack $\alpha = \pm 90^{\circ}$. The simulations show how the tugboat handle a sudden desired velocity, a sudden change in direction, and in combination with the 3-DOF trajectory tracking controller.

Figure 7.6 show the response of the surge controller under transit to a pushing operation. From the results, the reference value has a sudden jump that requires a relatively large force. The desired velocity has a maximum before reaching the reference value. This can be explained by the reference signal rate of change used in the 2. order reference model. By having the rate of change of the reference value, the desired velocity manages to follow the reference value without an overshoot. Since there is no overshoot, the surge force has smooth decay, until it hits the bulk carrier hull at 90 [s] with a velocity of 0.1 [m/s]. To follow the reference velocity, the thrust force turns negative. Before turning negative, the azimuth thruster must turn 180° and results in a sudden change in force. While the negative thrust force is relatively small, the value can be changed from different values for the exponential decay. The tugboat could either be slower without requiring negative thrust force, or have a quicker response and use more negative force.

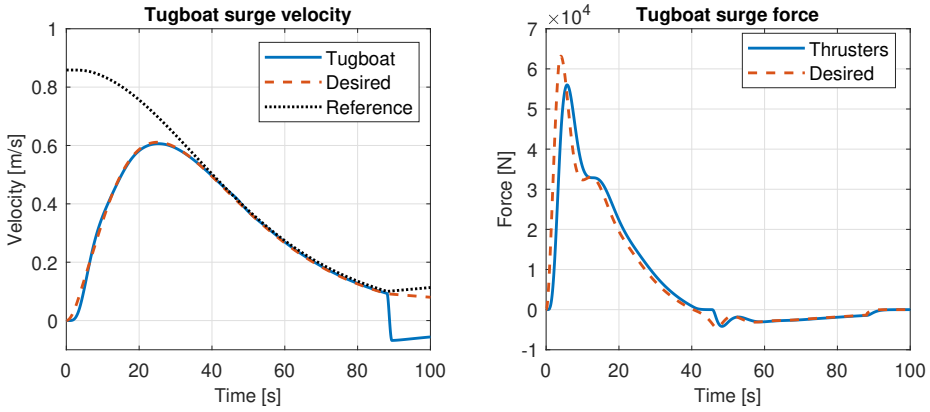

Figure 7.6: Simulation result of the surge controller when starting the tugboat 30 [m] from the bulk carrier hull in transit to pushing mode.

To see how the tugboat responded with a sudden change in transit operation, the desired operation was changed from pushing to pulling at the tugboat peak velocity. The result is shown in figure 7.7, where the desired force have a large negative peak, since the azimuth thrusters need time to rotate. After the large negative peak, the desired force has a positive peak. This should explain the small plateau in the tugboat velocity around 45 [s]. Since a change in thruster direction require the azimuth thrusters to rotate, they should have started to rotate for the positive peak, but since the peak quickly becomes negative, they went back again and results in unnecessary rotation.

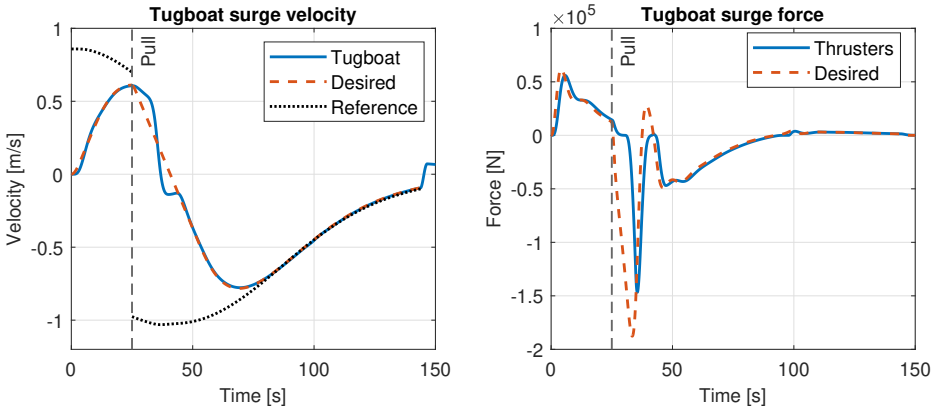

Figure 7.7: Simulation result of the surge controller when starting the tugboat 30 [m] from the bulk carrier hull in pushing mode, and after 25 [s] changing to pulling mode with a 60 [m] towline.

The reference velocity in the surge controller also depended on the error in position and heading from the 3-DOF controller. Figure 7.8 show the tugboat response when starting the tugboat 30 [m] from the tugboat hull, with the errors $\tilde{x} = -30$ and $\tilde{\psi} = -45$ in the 3-DOF controller, combining the simulation from figure 7.3 and figure 7.6. Instead of a sudden jump in reference velocity, the value increases based on how fast the 3-DOF controller reaches the desired values. Since the change is increasing, this results in a slight overshoot, which is compensated by using negative thrust. The small increase in reference velocity until 60 [s] should be the tugboat velocity towards the hull, which is used to have the surge control idle.

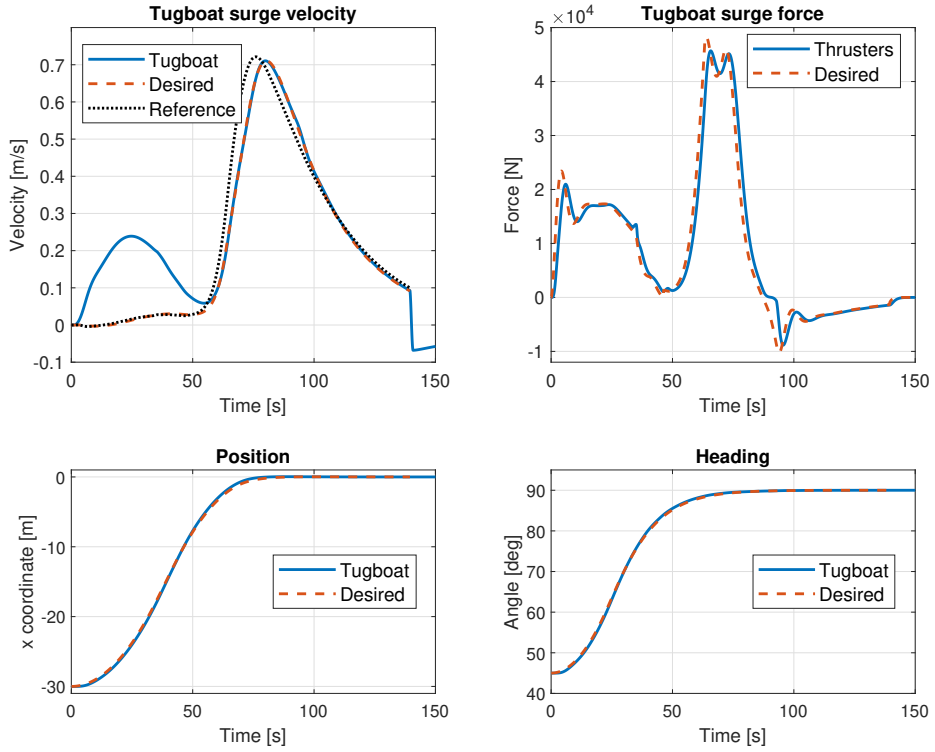

Figure 7.8: Simulation result of the surge controller in pushing mode when starting the tugboat away from the desired north coordinate and heading, similar to figure 7.3, and 30 [m] from the hull.

7.3 Control switching simulations

To test the switching logic between controllers, the tugboat was set to pushing, and after making contact with the hull and stabilising, set to pulling mode to get tension. The simulation results are shown in figure 7.9, where the first part until 90 [s] are similar to figure 7.6. From the tugboat azimuth angles, the rotation of the azimuth thrusters to reduce velocity before impact is shown with a peak around 50-100 [s] and valley around 250-300 [s]. For the change between pushing and pulling operation, the close-up in figure 7.9 shows the time delay used in the Stateflow chart. First, when the desired force crosses zero, the azimuths start to turn. After 5 [s], the desired velocity changes, which indicates that the transit to pull controller is activated. This results in a small overshoot of the desired surge velocity, which can be seen from the surge force around 170-180 [s].

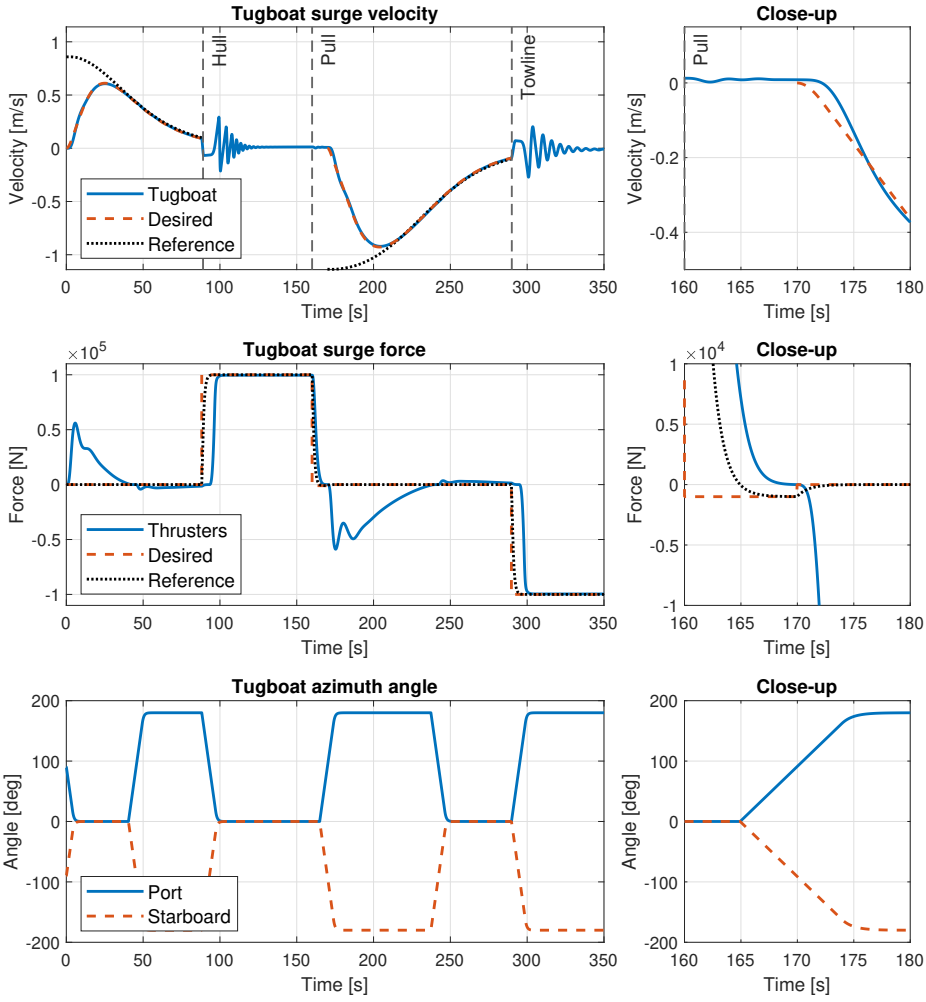

Figure 7.9: Simulation results for switching between controllers, with transition to push → pushing (Hull) → transition (Pull) → pulling (Towline). starting 30 [m] from the hull, with a towline length of 60 [m].

7.4 Force direction control simulation

7.4.1 Towing angle control simulations

The towing angle control simulations shows how the tugboat hold the desired angle of attack, while the bulk carrier is dead and while it moves ahead. To have a relatively large effect on the rotation of the bulk carrier, the towline connection was placed 70 [m] ahead of the CO, while the tugboat was set with a desired pulling force of 200 [kN]. The results are shown in figure 7.10, where the simulation starts with the tugboat at the stretching distance of the towline, at 60 [m], facing directly at the towline connection on the bulk carrier.

When the bulk carrier is dead (see figure 7.10a), the tugboat moves slightly ahead of the reference towline angle before settling. This require a small difference in thrust force, while the port thruster is rotated 1-2 [deg]. In figure 7.10b a desired force of 300 [kN] was set to the bulk carrier in surge direction when the simulation started. This caused the tugboat to lag after the towline connection point. While there is a small deviation in towing angle that slowly converges, the difference in azimuth thrust force is much larger. To follow the bulk carrier at an angle of attack $\alpha = -90^{\circ}$, the tugboat must move in a pure sway motion. This require the port thrust force to be double of the starboard thrust force, while the starboard thruster is rotated over 10°. In the last simulation, the results show how the controller manages to reach and follow an angle of attack away from the initial towline angle, while the bulk carrier moves ahead (see figure 7.10c). The towline angle deviates slightly from the desired angle, but reaches the reference angle with a small overshoot at around 230 [s]. To reach the new angle of attack, the starboard thruster peaks with three times as much force compared to the port thruster, while the port thruster angle peaks with a 20° rotation. The difference between the thruster force and angle is reduced and settles at around 170 [s], where the difference used to slowly converge to the towline reference angle is used to hold the angle.

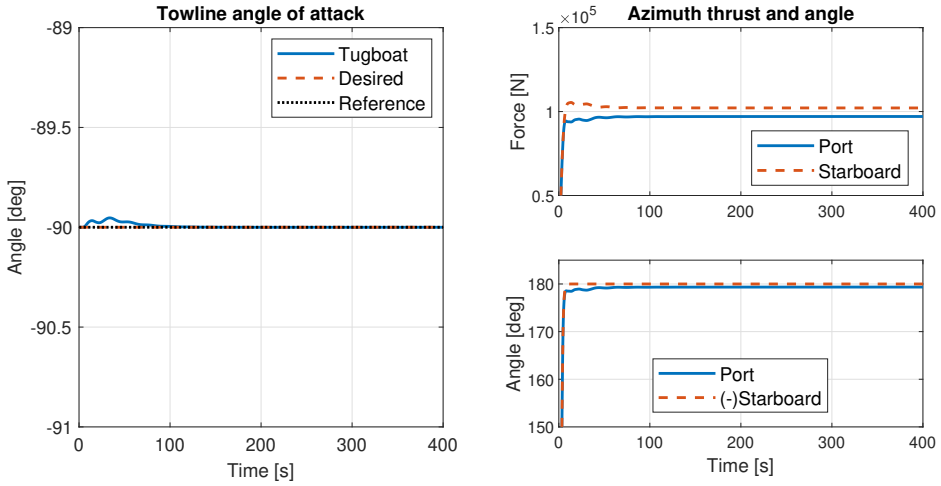

(a) Bulk surge force = 0, desired angle of attack = -90°

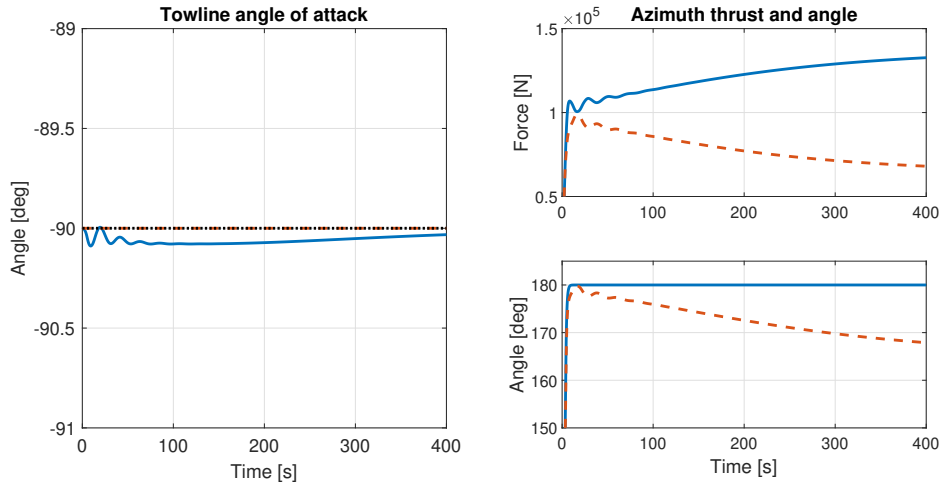

(b) Bulk surge force = 300 [kN], desired angle of attack = -90°

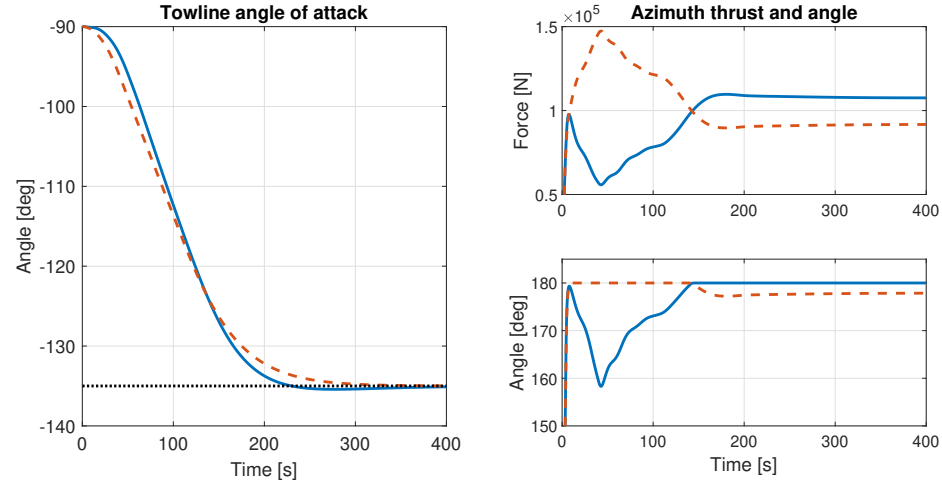

(c) Bulk surge force = 300 [kN], desired angle of attack = -135°

Figure 7.10: Simulation results of the towline angle controller, with towline connection at [70, -23] on the bulk carrier and a desired tugboat force of 200 [kN]. The azimuths start with an angle of attack $\alpha = \pm 90^{\circ}$ and no force.

7.4.2 Contact angle control simulations

To see how the contact angle controller could prevent the tugboat from slipping along the hull, the bulk carrier was starting still and set with a surge force of 300 [kN], while the tugboat started in contact with the hull with a desired pushing force of 40 [kN]. The simulation results are shown in figure 7.11 and shows that the tugboat slips at an angle of attack $\alpha = 50^{\circ}$ with contact force around 33 [kN] and friction force of 14 [kN]. Sliding is prevented with the controller, where the desired angle of attack $\alpha_d = 70^{\circ}$ have less difference in azimuth thrust and angle than $\alpha_d = 90^{\circ}$. With $\alpha_d = 90^{\circ}$, the tugboat follows along the hull in a pure sway motion, with negative friction force and holds the contact force at 40 [kN], while $\alpha_d = 70^{\circ}$ have a small reduction in contact force and a positive friction force.

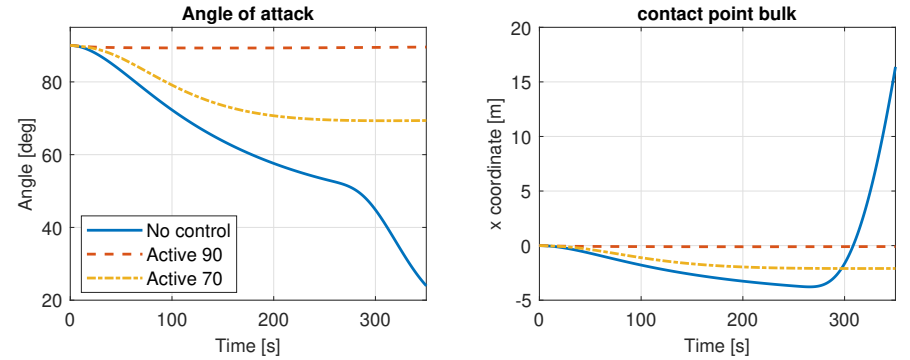

(a)

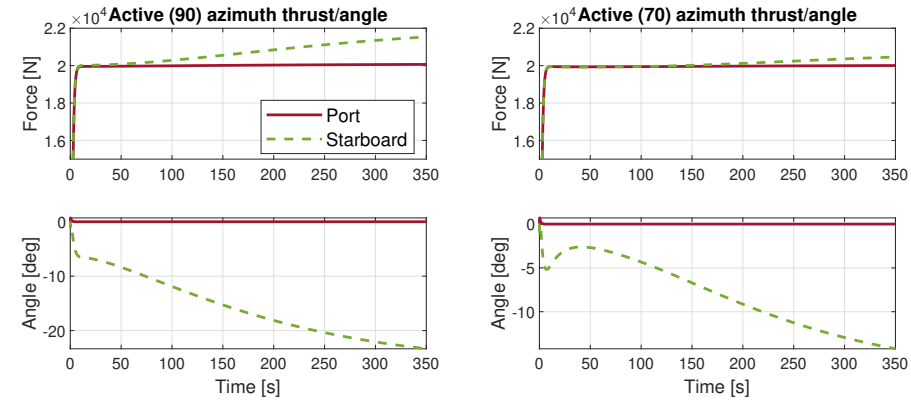

(b)

Figure 7.11: Simulation results of the contact angle controller. Comparing no controller and active with angle of attack $\alpha_d = 90^{\circ}$ and $\alpha_d = 70^{\circ}$ in (a), while (b) compare the azimuth thrusters for the active controllers. The azimuths angle of attack starts at $\alpha = 0$ with no force.

7.5 Tugboat control system discussion

7.5.1 Control allocation limitations and improvements

From the control allocation simulation results (see figure 7.1), there is a delay and peak in thrust force. While the peak was reduced by the delay, the delay should be removed. One method of reducing the delay could be to lower the rate of change in the QP-problem, to give more feasible desired thrust force for the thrusters to follow. Since the rate of change was set with a linear step, it would not be accurate in the entire range of the azimuth thruster, due to non-linear thrust force to rpm characteristics. By using the thrust force as input to the initial force in the control allocation, the desired force should be limited to the actual performance. Since the change in azimuth thrust force was calculated with a LP filter that saturated the rpm change, the performance was not accurate. While the rpm should correspond reasonable to the thrust force, the rate of change should instead be based on the torque required to change the rpm. However, this would require more data on the propulsion system to give realistic performance. The peak in desired thrust force should also be reduced, as it uses unnecessary power. A better response could be achieved by limiting the desired propulsion until the azimuth angles are close to their desired positions. However, this would require the control allocation to change limits based on the optimal azimuth angles.

The azimuth rotation limits were set to avoid the turbulent waterflow from the thruster to hit each other and reduce performance. By limiting the azimuth thrusters with 180° rotation to avoid a non-convex problem, some manoeuvrability was lost. This can be seen from the towing angle control simulations (see figure 7.10), were only one of the azimuths rotates to give sway force in their own direction. If both could rotate in the same direction, the force should be distributed more equally and require less rotation. This could be implemented with changing limitations on the azimuth angles, depending on the required operation, but it is uncertain how this would affect the performance. Another approach could be to include the hydrodynamic thruster interactions in the control allocation, and solving it based on non-linear SQP optimisation problem, which was used in another study to increase efficiency and performance (see section 1.2).

From the control switching simulations (see figure 7.9), the azimuth thrusters use relatively long time to turn to reduce the velocity before impact or stretching the towline. While rotation of the azimuth thrusters should be used for the main thrust direction, reversing could be a better solution for reducing the velocity. By allowing reversing of the thrusters, the transit operation could be improved, as it would be quicker to reduce the velocity before impact. However, by allowing the thrusters to reverse, the control allocation must be updated to decide between thruster rotation and reversing.

7.5.2 Transit controller limitations and improvements

While the controller shows reasonable performance for a still bulk carrier, the problems arise when the bulk carrier starts to move (see figure 7.4). The main problem is due to the limited sway force of the tugboat without rotation, which is limit by the tunnel thruster force. Since the force limit is not implemented in the controller, the desired sway force surpasses the limit, which causes undesired motion towards the bulk carrier hull. It should be possible to get a more feasible tugboat response with the pure sideways motion, by tuning the 3. order reference model to allow for a slower convergence. However, tracking a moving trajectory with only sideways motion was shown to have limitations, which should be a problem under certain operation conditions, like increased velocity and weather effects.

The sway velocity limit can be avoided by having a desired heading that changes depending on the motion of the bulk carrier. By having a heading that follow more in the direction of the motion, the tugboat could use more azimuth thrust force, which was seen by the simulation results of starting with an angle (see figure 7.5). It should also be possible to make contact with the bulk carrier hull at an angle, and then rotate the tugboat to push in the desired direction. However, this will cause a problem with the current surge controller, which is designed to use surge velocity to go straight for the hull. While the surge controller can be replaced, making contact at an angle could be difficult to control. If the tugboat make contact at a relatively large angle, the contact force from the impact velocity could give a moment that rotates the tugboat alongside the bulk carrier hull. This may be difficult to counteract if the navigation system has errors, where the exact impact moment can deviate from the predicted.

While there may be difficulties with the contact angle for transit to push, the transit to pull should be implemented with an angle to reduce positioning time. The reason for using the same path for both push and pull transit, was to simplify the implementation. The transit to pull should have been implemented with the desired angle of attack. However, this would not have worked with the implementation method of setting the error in east position $\tilde{y} = 0$ in the bulk carrier reference frame, since the angle would require both coordinates to change. Instead of 3-DOF trajectory tracking, the transit to pull may have worked with a velocity control in the direction of the angle of attack and a heading control to ensure that the tugboat bow pointed towards the towline connection. Since it should be less crucial to get the initial angle correct, compared to hull contact, the accuracy is not as important. The difficulty should be to implement and tune the velocity, which would depend on surge, sway and yaw motion.

7.5.3 Switching control limitations and improvements

The switching logic between control laws was based on desired force and if hull contact or towline tension was made. For this to be usable, these switching triggers need to be measurable in a real operation. While it should be possible to measure the towline tension, either

directly or with the towline winch, the hull contact may be more challenging. The contact could be registered by using an accelerometer to measure the impact, but it is uncertain on how reliable this would be.

To delay the control changes in the Stateflow chart, for changing from pushing to pulling or between transit and force control, the logic depended on time duration. The time duration to delay the change from force to transit control was set relatively long, with over 10 [s], to give the controller time to stabilise the "bouncing" from the impact forces (see figure 5.1). In this time, the tugboat may deviate from the desired contact positions, and cause damage to the vessels due to the large forces used. For the change from transit to force control, there should be several triggers to ensure that the tugboat is in the correct position and orientation before giving the desired force. Time duration would be operational dependant and should instead be replaced with physical limits. For the change in direction that require turning of the azimuths, it should be possible to measure the azimuth orientation to activate the switch between transit controllers.

7.5.4 Force direction control limitations and improvements

The towing angle controller show reasonable performance when following a desired angle or getting to a new angle, with a forward moving bulk carrier (see figure 7.10). However, the difference in azimuth thrust force required and the responsiveness to change desired angle could be a problem. The first problem may be solved by changing the azimuth rotation limits and are discussed in section 7.5.1. The other problem is seen from the change in desired angle to -135° (see figure 7.10c). While the change is relatively large, the tugboat uses 200 [s] to reach it. Tugboat docking operations are slow, but 200 [s] may be a long time in harbours that have limited space and may require faster changes. The response time could be changed by tuning the controller, but this would also increase the difference in azimuth thrust force and angle. In addition, the responsiveness to a desired angle would also depend on the towline length, as the controller use the arc length as error.

Simulation results shows that the contact angle controller had good performance that worked well for different angles (see figure 7.11). Since the contact angle control is based on a perfect half circular bow, the controller may not work in a real system. If the tugboat has a changing circular shape, the rolling motion would be different depending on the angle, which would be more difficult to control. Since the tugboat starts to slip when the friction force is to low, the velocity that the tugboat can follow would depend on the desired pushing force. The friction coefficients used was set low to show the slipping dynamics, where the friction between the wet hull and fender may be higher and would increase the contact to friction force ratio.

Chapter 8

Bulk carrier control system design

In this chapter, the implementation method for the bulk carrier control and guidance systems are described, while relevant Simulink models and Matlab codes are given in appendix D. The control system consists of a control law that was used to follow a given course from the guidance system, and control allocation to give desired forces to tugboats (see figure 8.1).

The guidance system in section 8.3 is based on section 4.2.3 in the specialisation project [2], and is updated with another method of computing the desired course / heading.

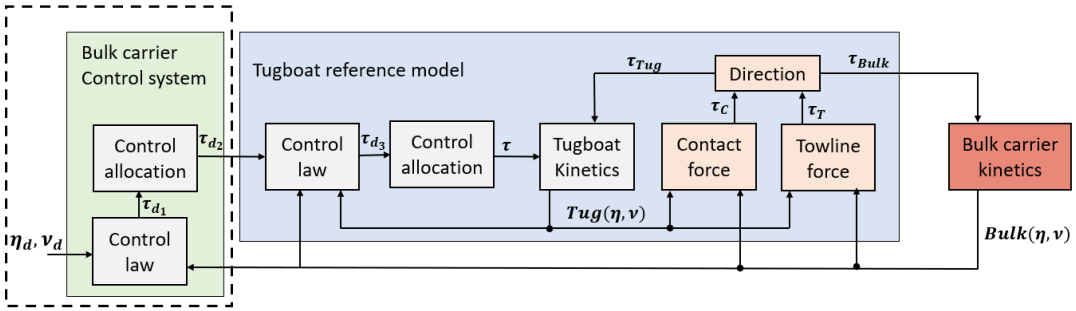

Figure 8.1: Illustration of the control systems in the Simulink model, with reference signal from the guidance system, covered in chapter 8, within the dotted line.

8.1 Bulk carrier control allocation

The control allocation was used to control a given number of tugboats, with the required pushing and towing forces. The control allocation was reused from the specialisation project [2], which allowed positive and negative forces without rotation.

8.1.1 Tugboat positions

The tugboats could be placed on either port or starboard side along the entire hull length of the bulk carrier (see figure 8.2). For each tugboat, the desired contact point and towing connection on the bulk carrier was set with the coordinate x^b on either port y_P^b or starboard y_S^b side. Since the control allocation was limited to positive and negative forces without rotation, the angle of attack was set perpendicular to the bulk carrier hull. This limited the control allocation to sway and yaw control. To get surge velocity on the bulk carrier, a desired force was set in the surge direction to simulate its own propulsion. This was implemented as a constant in the model, which resulted in a constant velocity without control.

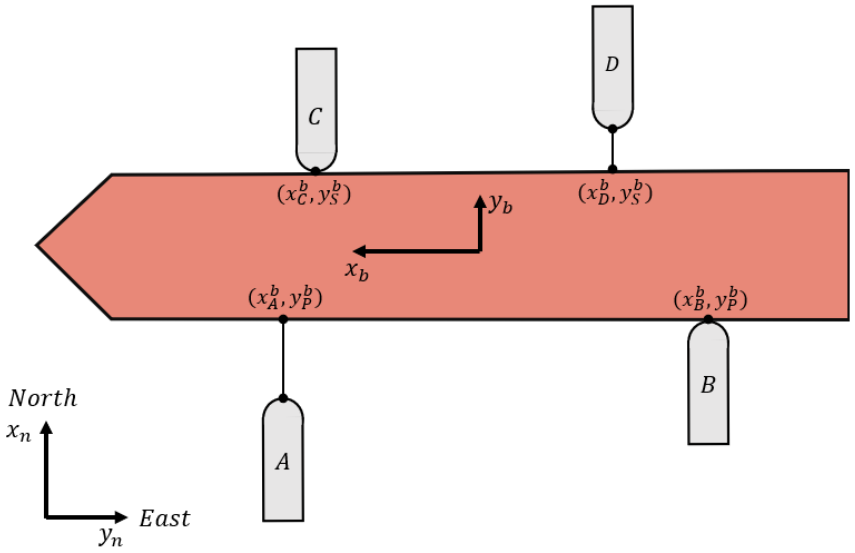

Figure 8.2: Illustration of possible positions for the tugboats to control as thrusters for the bulk carrier.

8.1.2 Bulk carrier control allocation optimisation problem

The control allocation was used to distribute forces among the tugboats to give a desired yaw moment τ_N to control the bulk carrier heading. This was solved based on the explicit constrained optimisation problem in section 3.3.1, with a constant thrust coefficient matrix $\boldsymbol{T}$. The thrust coefficient matrix was set with the position of the x^b coordinate and sign depending on the contact side, where port $y_P^b = (+)$ and starboard $y_S^b = (-)$. By using the tugboat configuration in figure 8.2 the thrust coefficient matrix would have been,

$$\boldsymbol{T} = \begin{bmatrix} x_A^b & x_B^b & -x_C^b & -x_D^b \end{bmatrix} \tag{8.1}$$

while only tug A and B was used in the model to simulate the operation from one side, as used in Narvik.

Since the tugboats was implemented from the same reference model used in Simulink, the tugboats were identical, and the weighting matrix $\boldsymbol{W}$ was set as the identity matrix. The tugboat thrust force was limited by the tugboat propulsion system, where the maximum pushing and pulling force was set to 500 [kN]. This was lower than the maximum thrust force for the tugboat, at 66.5 [t], which gave some deviations for the force required to move the tugboat. The forces were only allowed to change with a linear step Δf , which was set to give the maximum pushing force in 10 [s].

The optimisation problem was solved with the Matlab function "quadprog" (see appendix D.2 for implementation), on the form given in equation (8.2),

$$\min_{\mathbf{z}} \frac{1}{2}\mathbf{z}^T\mathbf{H}\mathbf{z} + (\mathbf{R}\mathbf{p})^T\mathbf{z} \text{ such that } \begin{cases} \mathbf{A}_1 \cdot \mathbf{z} = \mathbf{C}_1\mathbf{p} \\ \mathbf{A}_2 \cdot \mathbf{z} \leq \mathbf{C}_2\mathbf{p} \end{cases} \tag{8.2}$$

with the vectors,

$$\mathbf{z} = \left[\boldsymbol{f}^T, \mathbf{s}^T, \bar{f} \right]^T, \quad \mathbf{p} = \left[\boldsymbol{\tau}^T, \boldsymbol{f}_{\min}^T, \boldsymbol{f}_{\max}^T, \beta, \boldsymbol{f}_0^T, \boldsymbol{\Delta f} \right]^T$$

and the diagonal weighting matrix $\boldsymbol{H} = \text{diag}([\boldsymbol{W}, \boldsymbol{Q}, 0])$. The weights were chosen as $\boldsymbol{W} << \boldsymbol{Q}$, to ensure a feasible solution and ensure that the slack variables go to zero.

8.1.3 Changes to tugboat control system to avoid slipping

From the simulation results of the contact angle control (see section 7.4.2), there could be problems when the desired force was low compared to the bulk carrier velocity. This could be the case when the bulk carrier follows the desired heading, and the force is close to zero. To prevent the tugboat control system to switch back and forth between controllers, a lower limit was set on the desired force. When the force was lower than the limit, the desired force was set to zero. This results in the tugboat controller being set to idle in the Stateflow chart (see figure 6.4). To have the tugboat follow the bulk carrier, the idle mode was updated by activating the transit controller, without the surge controller. This made the tugboat follow the desired contact point, facing directly at the bulk carrier hull. Since the tugboat would follow facing the hull, the velocity was limited to the maximum sway velocity of the tugboat.

The friction coefficients were originally set relatively low, with values corresponding to the surface between wet asphalt and rubber, to simulate the slipping dynamics. To reduce the required contact force to stick to the bulk carrier hull, the static and kinetic friction coefficient was increased from $\mu_s = 0.40 \rightarrow 0.60$ and $\mu_k = 0.25 \rightarrow 0.40$. This allowed for a lower force limit, before switching between tugboat controllers.

8.2 Bulk carrier course autopilot

From the results with 3-DOF trajectory tracking in the specialisation project [2], it was assumed that the forces used to keep the bulk in north and east coordinates while turning was unnecessary, where a course autopilot could be a better solution.

The course autopilot was modelled from the mass-damper yaw dynamics as shown in section 3.2.1 $(I_z - N_{\dot{r}})\ddot{\psi} - N_r\dot{\psi} = \tau_N$, with parameters from the bulk carrier dynamics in section 4.1.1. This gave the control law,

$$\tau_N = -K_p(\tilde{\psi}) + K_d\dot{\psi} + K_i \int_0^t (\tilde{\psi})\, dt, \quad \tilde{\psi} = \psi - \psi_d \tag{8.3}$$

with gains,

$$K_p = (I_z - N_{\dot{r}})\omega_n^2, \quad K_d = 2\zeta\omega_n(I_z - N_{\dot{r}}) + N_r, \quad K_i = \frac{\omega_n}{10}K_p \tag{8.4}$$

where the natural frequency ω_n was set to give an overdamped and relatively fast response. The parameters were set with relative damping ration $\zeta > 1$ and a bandwidth $\omega_b = 0.1$, which is high for a large vessel. This response was tuned with the 3. order reference model given

in equation (3.2), similar to the one used for the 3-DOF trajectory tracking in the tugboat transit controller. The reference model was tuned based on using two tugboats on port side, at ±80 [m], to give a good response for a desired course change of 20°. To limit the maximum force from the controller, a saturation was set with limitation based on the tugboat maximum allowed pushing force and the position. The saturation limit was also used to cancel the integral action, to prevent integral windup.

While the course angle is controlled by setting the crab angle as disturbance and controlling the heading, the simulations was simplified by setting the crab angle $\beta_c = 0$. This was to avoid changes in desired course from tugboat impact and force changes, that could require a desired force from the tugboat in the opposite direction, which would require a position change. This turned the course autopilot into a heading autopilot.

8.2.1 Tugboat time delay control

From the simulation results of switching between tugboat controllers (see figure 7.9), there was over 100 [s] delay to start towing after pushing, with a bulk carrier at zero velocity. Since the time delay would depend on the responsiveness of the tugboat transit control and operation conditions, the time delay was implemented based on the tugboat transit control switching. To delay the control system, the course autopilot was implemented in an enabled subsystem that would activate when the transit controller to one of the tugboats was deactivated, and was implemented as shown in appendix D.

For the tugboat to deactivate the transit controller, it needed to get in position with either contacting the hull or stretching the towline. To get the tugboats in the desired positions, a simplified method of using the desired angle to choose either push or pull for the tugboats, depending on the contact point on the bulk carrier, and setting a constant desired force in that direction. The constant desired force was then active until the force from the course autopilot surpassed it.

8.3 Bulk carrier guidance system

The guidance system was used to create a path of straight lines with path course π_p, generated by waypoints from north and east coordinates, for the course autopilot to follow. To follow the path, a proportional LOS guidance law was implemented (see section 3.1.3), which gave a desired course,

$$\chi_d = \pi_p - \tan^{-1}(K_p y_e) \tag{8.5}$$

from the cross-track error y_e and the proportional gain K_p. The gain was calculated from $K_p = 1/\Delta$, with a lookahead distance $\Delta = 150$ [m]. The cross-track error was calculated by using the Matlab function "crosstrac", from the MSS toolbox [1]. This also gave the coordinates (x_p^n, y_p^n), which was used to find the point on the path given by the lookahead distance (see figure 8.3).

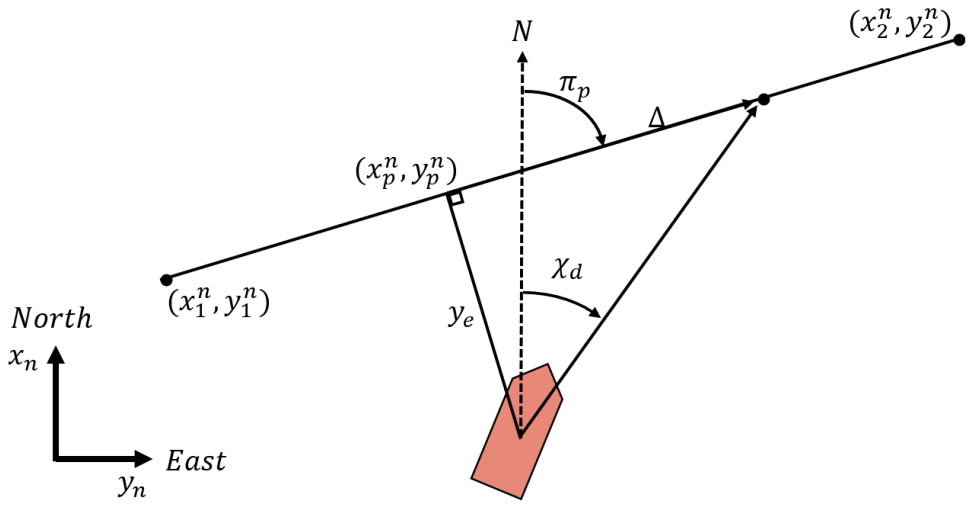

Figure 8.3: Illustrating the LOS guidance law used in the bulk carrier guidance system, where the lookahead distance Δ measures from (x_p^n, y_p^n). Figure based on reference [3]

To change from a straight line between waypoints to the next, a small radius where set on the point (x_2^n, y_2^n), where the waypoints was updated when the lookahead distance was within the radius. The waypoints were given in longitude and lateral coordinates, and was converted to NED reference frame with the function "llh2flat", from the MSS toolbox [1], to use in the guidance system. The waypoints used to generate a path was based on the movement of a bulk carrier from the live map at marinetraffic.com, under a tugboat operation in Narvik. Figure 8.4 show the desired path to the dock, where the initial coordinate is added to require a starboard turn before turning to port.

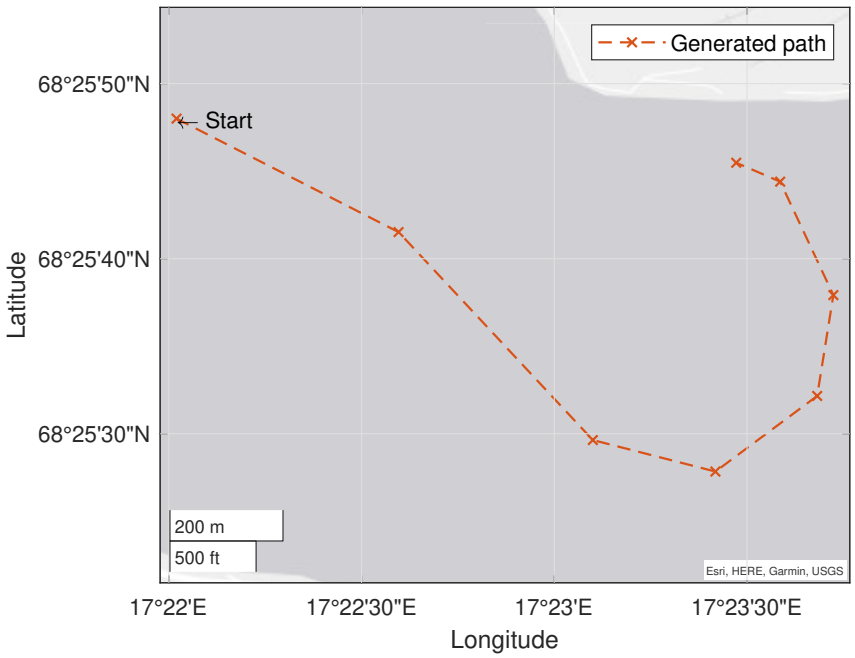

Figure 8.4: Generated path to the loading dock in Narvik, based on a live tugboat operation from Marinetraffic.com.

Chapter 9

Simulation result of the tugboat operation

Simulation results shown in this chapter was created with Simulink, by using automatic solver selection, which chose ode3, with fixed step size of 0.025. The results show the performance of the bulk carrier control system from chapter 8, by using two tugboats placed at ±80 [m] on the port side of the bulk, with 60 [m] towlines.

9.1 Course autopilot simulation

To see how the course autopilot performed with and without contact delay, to get the tugboats in positions, the bulk carrier was set with a force that resulted in a surge velocity just below 0.5 [m/s]. The tugboats started at a 30 [m] distance from the desired contact and towing point, with 60 [m] towlines. The reference heading for the bulk carrier was set to 10°, and then changed to -10° after 500 [s].

9.1.1 No contact delay

Figure 9.1 shows the simulation results of the course autopilot without contact delay. Without delay, the difference from change in desired heading to the actual change in bulk carrier heading is around 100 [s] for the initial reference heading, and around 150 [s] for the second reference heading at 500 [s]. While the time is increased for the second delay, the positioning distance is longer, at the full towline length, and the bulk carrier velocity is increased.

The immediate change in desired heading results in an error that cannot be accounted for, and results in a desired force from the integral action that is saturated. When the bulk carrier heading starts to change, the change is at the maximum turning rate, until it overshoots the desired heading. The slight overshoot requires the tugboats to change positions at around 170 [s]. The change in position is cancelled, and the same positions for contact and towing is achieved again at 200 [s], with a large force peak compared to the desired force.

The slight overshoot at 1100 [s] also need repositioning of the tugboats, as seen from the desired sway force, which is corrected by the impact force of Tug A. Tug B seems to be stuck with push before changing position, and therefore not reaching the desired position simultaneously as Tug A.

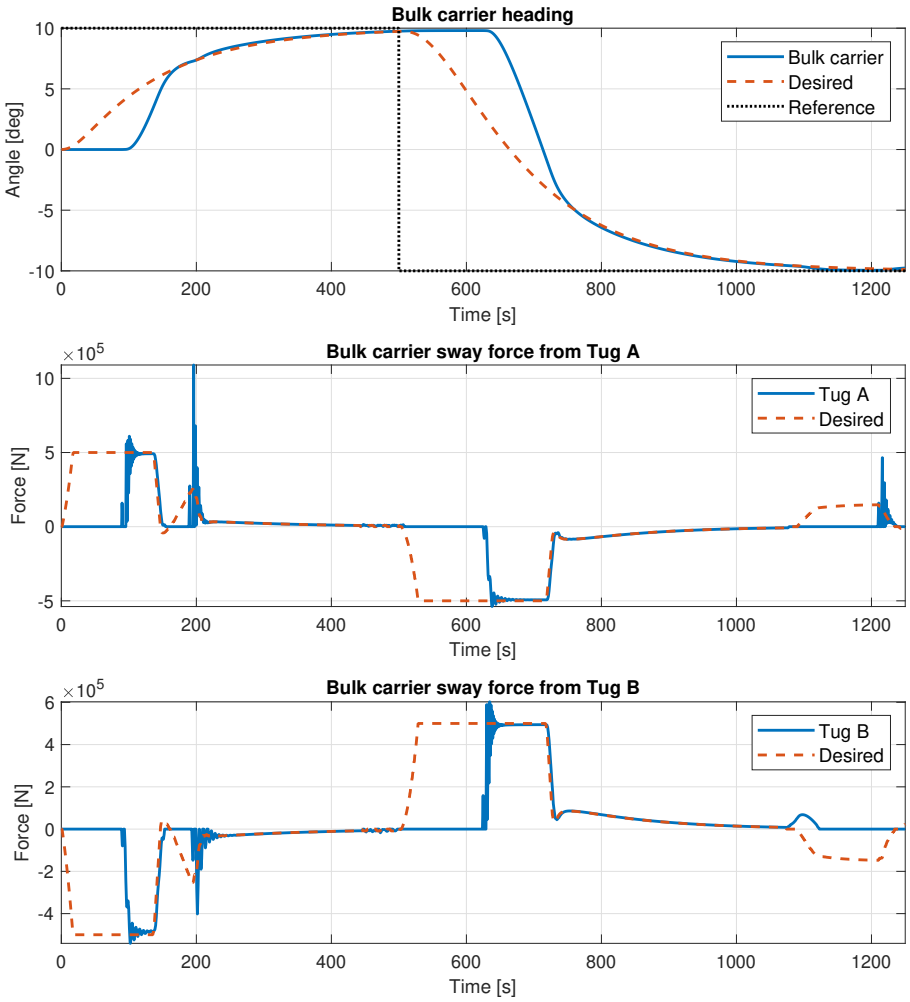

Figure 9.1: Simulation results of the course autopilot without contact delay. The hull contact point and towline connection of Tug A and B are illustrated in figure 8.2.

9.1.2 With contact delay

Figure 9.2 shows the results from the course autopilot with contact delay. The delay can be seen from the constant desired sway force from 0-100[s], until Tug A starts to push and Tug B starts to pull, and from 500-650 [s] where the opposite happens. Both tugboats have close to identical force on the bulk, except for the impulse caused by the impact force, where the sudden towline tension has a smoother transition. By delaying the course autopilot, the bulk carrier heading manages to follow the desired heading closely but require a relatively large moment in the beginning. The desired heading converges slowly to the reference heading, which require relatively low forces from the tugboats.

In the last part of the heading graph, shown in the close-up from 1140-1220 [s], the desired heading resets multiple times. The resets seem to correlate with the fluctuating sway force from both tugboats. This causes an undesired response, where the desired moment fluctuates in the opposite direction of the actual moment.

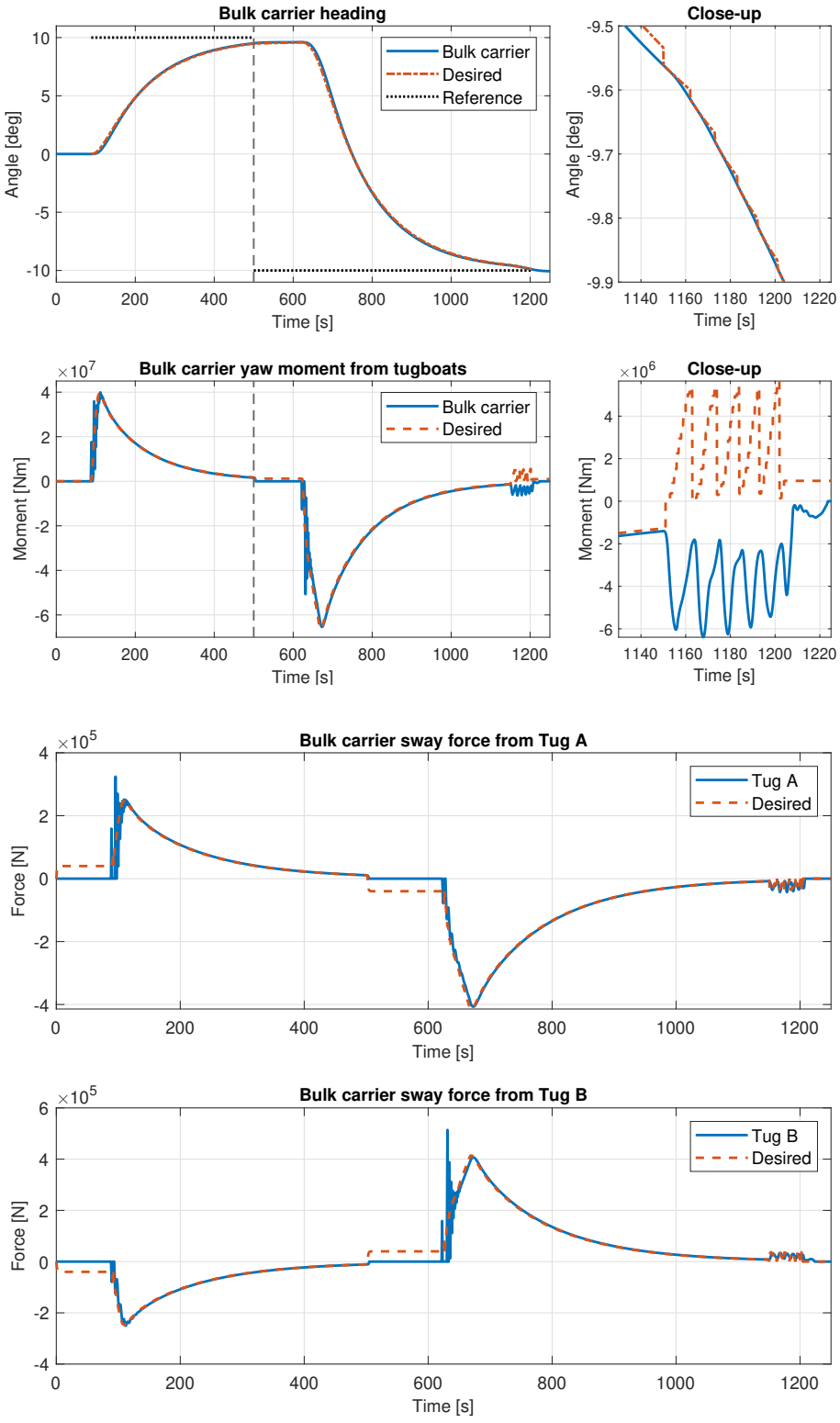

Figure 9.2: Simulation results of the bulk carrier course autopilot with contact delay. The hull contact point and towline connection of Tug A and B are illustrated in figure 8.2.

9.2 Path following simulation

To see if the course autopilot could be used to transport the bulk carrier to the dock in Narvik, the guidance system was used to generate a reference course to follow the the path created with set waypoints. The bulk carrier was starting with the initial course of the generated path, with both tugs 30 [m] away from the hull contact points. Figure 9.3 shows how the bulk carrier managed to follow the given path, while the corresponding heading, velocity and forces from tugboats are shown in figure 9.4.

From the first starboard turn, the bulk carrier surpasses the given path, before closing in on the path from the opposite side of the turn. This causes the tugboats to change positions, which can be seen from the desired sway force at around 1600 [s], and the impact at 1750 [s]. The change is performed before the new desired path would have required a shift in position, which can be seen from the change in reference course at around 1800 [s]. To keep up with the port side turn, the tugboat forces get relatively large compared to the maximum limit, where the force have a large increase at each new reference course. From the bulk carrier velocities, the surge velocity stays close to 0.5 [m/s] the entire turn, while there is a small increase in the sway velocity from 2400-3500 [s].

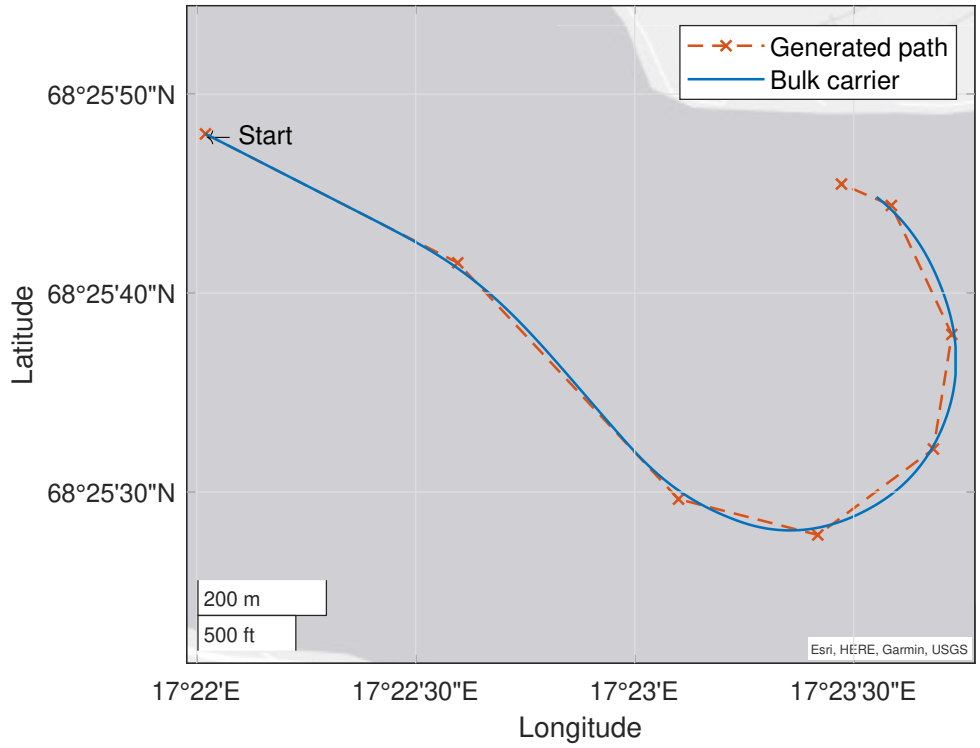

Figure 9.3: Path following simulation of the bulk carrier course autopilot following the set of waypoints given in figure 8.4, with relevant data shown in figure 9.4.

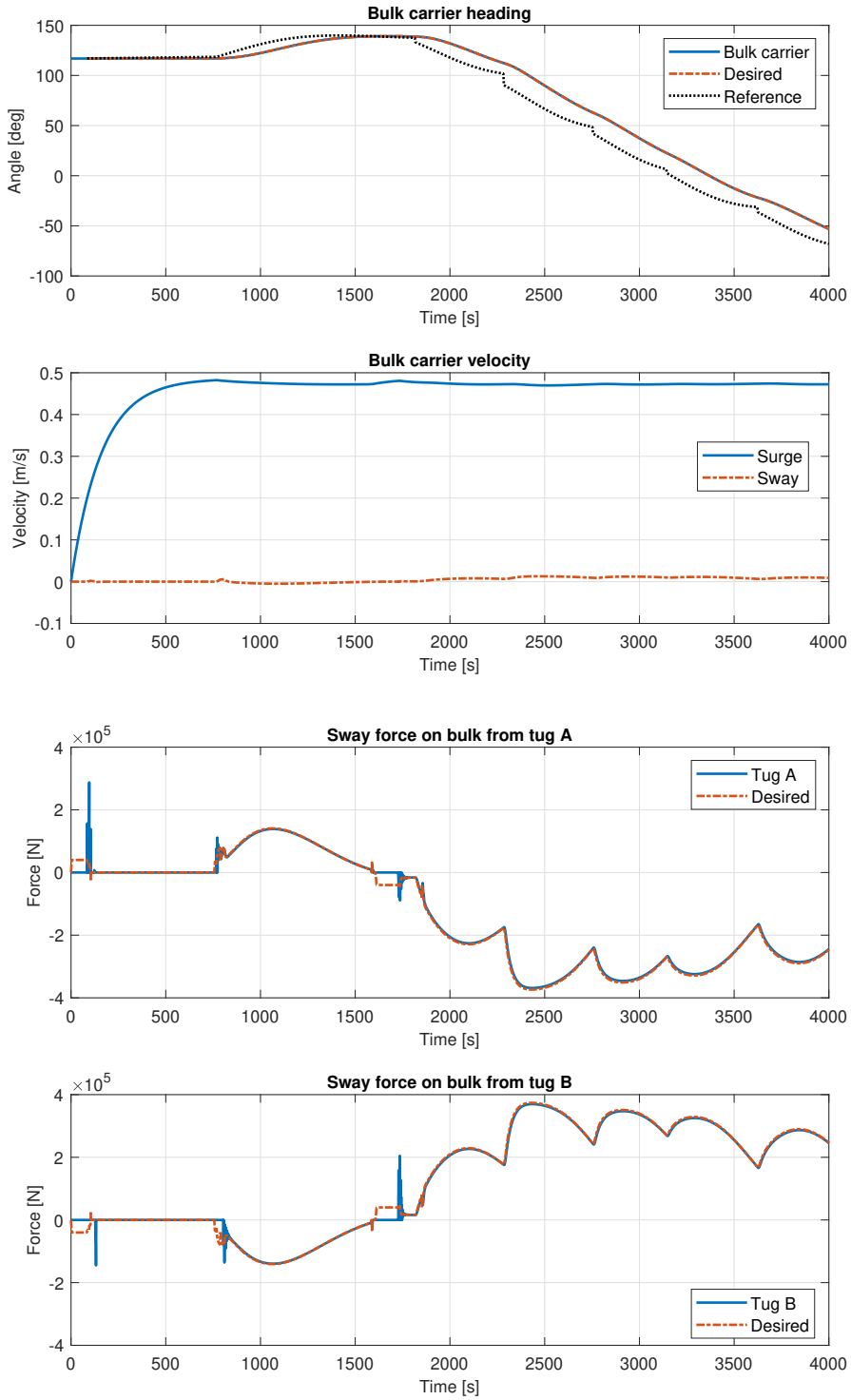

Figure 9.4: Simulation results corresponding to the trajectory shown in figure 9.3. The placement of Tug A and B are illustrated in figure 8.2.

9.3 Tugboat operation discussion

9.3.1 Course autopilot limitations and improvements

Since the crab angle was set to zero in the course autopilot, it only controlled the heading. The crab angle was neglected to prevent a small change in the course from sway velocity caused by the impact forces, or when the surge velocity was low. It should be possible to use a LP filter on the sway velocity to reduce fluctuating course, but since the simulation was under ideal conditions, removing the crab angle should not make much difference. This made it is easier to see other limitations of the controller, but the crab angle should be implemented to account for ocean currents and wind forces and/or when the sway velocity is increased.

The simulation results of the course autopilot without contact delay were used to illustrate the main problem that should be considered to control tugboats as thrusters, the time delay from control decision to thruster action (see figure 9.1). This problem is shown with a maximum desired thrust force, before the tugboats are in position. The change in desired heading could be slowed down with the 3. order reference model but this would be unnecessarily slow and situation dependant. The solution to the delay in this control system was to activate the course autopilot when Tug A first made contact or stretched the towline, such that the transit controller was deactivated. Since the tugboat control system changed control law depending on triggers, like contact or towline tension, it should be reasonable to depend the bulk carrier course autopilot on when the tugboats were ready. The course autopilot should depend on the positioning of each individual tugboat, to give a feasible moment. By only using one tugboat as trigger, the desired moment from the controller could be unachievable as the saturation limit was calculated based on the maximum moment from both tugboats. This could happen if one of the tugboats are in positions before the other, which was the case in the simulation results with no contact delay at 1200 [s] (see figure 9.1).

To be able to use a triggering mechanic to activate the course autopilot, another controller must be used to ensure that the tugboats arrive to their desired positions. This was implemented by setting a desired force to both tugboats, depending on the new course angle and positions of the tugboats. The idea of having a desired force was to ensure that the tugboat would start to stabilise quicker after impact, where the desired force from the control allocation would take over when the set force was surpassed. While the method of setting a desired force worked, it showed a problem for small changes to the bulk carrier heading. When the actual heading surpassed the desired heading (see figure 9.1), the desired force required the tugboats to change position, which only resulted in unnecessary movement of the tugboats. This could be improved by setting limits from the desired heading that would trigger a change in positions. From the close-up in figure 9.2, there is also a problem when the desired force is low while there is still deviation from the reference heading, where the course autopilot resets multiple times. The reset should be explained by the lower force limit

set. When the force is lower than a limit, the tugboat control system is changed to follow along the bulk carrier in a transit operation, to prevent the tugboats from sliding along the hull. While the contact angle controller was implemented to counteract sliding, this require a friction force limit to be large enough for the sideways motion and would therefore not be sufficient for a low desired force. If the reference heading is not reached, the desired force is activated again to get the tugboat in position, which resets the course autopilot. This could be improved by implementing another control law that ensures that the tugboat stays in contact and follow along until the reference course is achieved.

Since the autopilot was activated at the first impact, the course error should increase while the tugboat is on the rebound before making contact again, which may explain the large initial forces seen in the simulation results with contact delay (see figure 9.2). The large initial force could also be caused by an aggressive controller, but the time of the rebound should increase it. Another approach could be to wait until the tugboats had stabilised in the positions and then activated the course autopilot or lower the impact velocity of the surge controller to reduce the settling time.

9.3.2 Path following limitations and improvements

The guidance system used was implemented based on the specialisation project, with small modifications, and was not tuned or tested properly for the current operation due to time limitations. However, the simulation results of the path following guidance system gave some indications on problems that should be considered. Since the guidance system is based on the lookahead distance, the path should be created for a given speed and the turning capabilities. This was not accounted for, which can be seen from the first starboard turn in the operation. With the current lookahead distance the turn is initiated too late, which causes an overshoot on the desired path (see figure 9.3). The overshoot requires a change in position of both tugboats and gives around 150 [s] without yaw control (see figure 9.4). Since the next turn is a port turn, this gave an advantage. However, if the next turn had been a starboard turn, the tugboats would have needed to change position again, which would require another 150 [s] without control.

While a longer lookahead distance should have managed to close in on the path from the inner corner, the large time delay with control loss to counteract small changes would still be a problem. The lookahead distance would also impact the turning rate of the port turns, which should make it difficult to tune the controller for the given path. Instead of following coordinates, a desired path could have been designed with the use of Dubins path. By having a desired arch and resulting turning rate to follow, the tugboat thrust forces should have been more consistent instead of fluctuating in thrust force.

Since the simulations are performed in ideal conditions, wind and ocean currents are not accounted for. These are forces that can cause unforeseen movements of the bulk carrier,

especially close to the dock, that may need to be countered with the tugboats changing position. Based on the transition time delay, this can be crucial in a docking operation. In addition, forces from hydrodynamic interactions of the tugboat thrust forces could also affect the motion of the vessels, with larger effect close to the bulk carrier hull and bow. These can be more difficult to implement, where ensuring that the tugboats are position far enough away to have a negligible effect could be a better alternative.

To be more suited for unforeseen movements, the number of tugboats and formation should be improved for a safe operation. The real operation in Narvik uses three tugboats to assist the docking operation of large bulk carriers, with one leading on a towline, second in contact with the hull closer to the bow and the third closer to the aft with either push or pull. This formation would have come from experienced pilots and helmsmen in Narvik harbour, which is important to consider since every harbour could face their own challenges. However, this would have required a control allocation that could account for towing angles. Due to time limitations, the control allocation used was from the specialisation project and only allowed the thrust direction to change without rotation. Implementing a control allocation similar to the one used to control the tugboat, to account for azimuth thrusters rotation, could have worked on the towing angles by having a rate of change that depended on the towline distance and towing angle controller.

The force desired from the tugboats was close to identical, which is best seen from the path following simulation results (see figure 9.4). This should not be ideal, as the tugboats are placed an equal distance from the bulk carrier CO, while the CG is 3.9 [m] ahead of it. This gives a moment arm of 7.8 [m] in difference for the tugboats. In addition, the pivot point should also be moved further ahead due to the surge motion of the bulk carrier. Combined, this should have a significant impact on the efficiency of the tugboat forces, which should be considered in the control allocation problem.

Chapter 10

Conclusion and further work

The aim of the thesis was to develop guidance and control systems to manoeuvre a bulk carrier using multiple tugboats with their own dynamics as thrusters. In order to achieve this, the thesis was divided into three parts. First, creating a mathematical model in Simulink/Matlab with the dynamics of a bulk carrier and supporting tugboats, and the interaction forces between them to simulate towline forces and contact forces with stick-slip dynamics. Second, develop control systems with switching mechanics for the tugboats to get in positions and deliver the desired forces to the bulk carrier. Third, develop control and guidance systems for the bulk carrier to deal with time delays caused by the positioning time for the tugboats.

In the implementation of the mathematical model, the vessel dynamics used was based on rough assumptions and would not be suitable for real applications, while the interaction forces lack real data and should differ from real responses. Combined with stick-slip dynamics based on the implemented tugboat dynamics, the simulation results show that the model created should have plausible dynamics that enlighten certain problems that must be considered in the control and guidance system designs when using tugboats as thrusters.

The tugboat control system consisted of multiple linear and non-linear PID control laws, to get in position and perform towing or pushing operations, which was interchanged by using Stateflow logic. To distribute thrust force and allow azimuth thrust rotation, a local approximation of an implicit constrained control allocation was solved as a QP-problem, with thruster limitations and azimuth rotation constraints. From simulation results, the control system had reasonable performance, but had limitations in operations with increased velocity.

Simulation results for the control and guidance systems manage to show how the time delay could be handled by using Stateflow logic to activate the control system when the tugboats were in positions. It was also shown how small changes to the course could lead to long time delays with no control of the bulk carrier. This shows how vulnerable the tugboat operation could be in certain operations. Development of control and guidance system for the tugboat operations should therefore be focused on the real tugboat operations, from experienced pilots and helmsmen of each area, to use tugboat formations capable of handling disturbances and hydrodynamic interactions that can arise in harbours.

10.1 Further work

While the Simulink model have shown reasonable performance that can be used to develop control and guidance systems and strategies, more work is necessary to create a more realistic model environment and responses to control.

10.1.1 Improving vessel dynamics and interaction forces

- The inaccurate data on the vessel dynamics should be updated for more realistic responses of the vessels.
- The dissipative damping forces between the vessels should be investigated to simulate more realistic interaction forces.
- The constraints used to simulate contact forces should be updated to represent the real tugboat bow shape, while the sides should be included.
- Implement ocean currents and wind forces to develop and test control and guidance systems that can handle disturbances.
- Look more into hydrodynamic interactions between the bulk carrier and tugboats in harbours.

10.1.2 Improving the tugboat control system

- Implement thruster dynamics based on torque characteristics of the propulsion system and change the control allocation rate of change to the thruster dynamics.
- Look into the control allocation problem to improve azimuth thruster rotation, by changing the rotation constraints or implementing the hydrodynamic thruster interactions.
- Allow for azimuth thruster reversing to improve stopping time of the tugboats and develop a decision logic to decide between rotating the azimuth thrusters or reversing.
- Develop transit control system algorithms that are more robust to increased operational velocities and weather effects.
- The hull contact and towline force were assumed to be known in the simulations, to use as triggers in the switching logic, methods of measuring these triggers should be investigated.
- The Stateflow switching logic to change between control laws should be improved to handle various situations, by replacing the time duration logic used.
- The towing angle controller should be tuned for a more ideal response and account for various towline lengths.

- Update the contact angle controller to handle a more realistic bow geometry.
- Look into adaptive controllers to account for the tugboat model uncertainties.

10.1.3 Improving the bulk carrier control and guidance systems

- Include the crab angle in the course autopilot.
- Improve the activation of the course autopilot based on the number of tugboats.
- Look into the problem of the tugboats slipping due to low contact force and develop a control system to handle it.
- Develop a guidance system for the tugboat operation that considers the turning capabilities of the towed vessel and the time delay for positional changes.
- Implement control allocation for the bulk carrier that can account for the towing angles and considers the real moment based on CG and pivot point.
- Implement the formation of using three tugboats, based on the operation in Narvik, and compare against different formation configurations.

Bibliography

[1] Thor I. Fossen. *MSS toolbox, Github*. URL: https://github.com/cybergalactic/MSS (visited on 20/08/2021).

[2] Henning L. Ørke. *Autodock, Automated tugboat-assisted docking of large vessels. Unpublished specialisation project, NTNU*. 2021.

[3] Thor I Fossen. *Handbook of marine craft hydrodynamics and motion control*. eng. Second edition. Hoboken, NJ: Wiley, 2021. ISBN: 9781119575054.

[4] Clive Rees. *A master's guide to berthing*. 2021. URL: https://www.standard-club.com/knowledge-news/a-masters-guide-to-berthing-2021-3374/.

[5] Joel Esposito, Matthew Feemster and Erik Smith. 'Cooperative manipulation on the water using a swarm of autonomous tugboats'. In: *2008 IEEE International Conference on Robotics and Automation*. IEEE, 2008, pp. 1501–1506. ISBN: 1424416469.

[6] Van Phuoc Bui, Hideki Kawai, Young Bok Kim and Kwon Soon Lee. 'A ship berthing system design with four tug boats'. In: *Journal of mechanical science and technology* 25.5 (2011), pp. 1257–1264.

[7] Van Phuoc Bui, Sang Won Ji, Kwang Hwan Choi and Young Bok Kim. 'Nonlinear observer and sliding mode control design for dynamic positioning of a surface vessel'. In: *2012 12th International Conference on Control, Automation and Systems*. IEEE, 2012, pp. 1900–1904.

[8] Linying Chen, Hans Hopman and Rudy R. Negenborn. 'Distributed Model Predictive Control for cooperative floating object transport with multi-vessel systems'. In: *Ocean Engineering* 191 (2019), p. 106515.

[9] Anna Witkowska and Roman Śmierzchalski. 'Adaptive dynamic control allocation for dynamic positioning of marine vessel based on backstepping method and sequential quadratic programming'. In: *Ocean Engineering* 163 (2018), pp. 570–582.

[10] Felipe Arditti, Hans Cozijn, Ed F.G. Van Daalen and Eduardo A. Tannuri. 'Dynamic Positioning simulations of a Thrust Allocation Algorithm considering Hydrodynamic Interactions'. In: *IFAC-PapersOnLine* 51.29 (2018), pp. 122–127.

[11] Narvik Havn KF. *Om Narvik havn*. URL: https://www.narvikhavn.no/om-narvik-havn.aspx (visited on 16/09/2021).

[12] Bukser og Berging. *Our vessels*. URL: https://www.bube.no/our-vessels/ (visited on 16/11/2021).

[13] Raymond Kristiansen. private communication. Oct. 2021.

[14] Kartverket. *Resultat for Narvik vannstandsmåler (Narvik)*. URL: https://www.kartverket.no/til-sjos/se-havniva/resultat?id=1082327&location=#waterlevel-tab (visited on 30/05/2022).

[15] Olav Egeland and Jan Tommy Gravdahl. *Modeling and simulation for automatic control*. Marine Cybernetics Trondheim, Norway, 2002. ISBN: 8292356010.

[16] Sverre Steen. private communication. Oct. 2021.

[17] Tor A. Johansen and Thor I. Fossen. 'Control allocation—A survey'. eng. In: *Automatica* 49.5 (2013), pp. 1087–1103.

[18] Captain Henk Hensen and Dr. Markus van der Laan. *Towline friction and its consequences*. IMC Maritime System Development. 2017.

[19] Jamie Nicholson and Richard Erskine. *Guidance on the use of tugs for ship assist in the port of Southampton*. Associated British Ports. 2021.

[20] *Sea transport operations (VMO Standard - Part 2-2), DNV-OS-H202*. Det Norske Veritas, 2015. Chap. 4 Towing.

[21] *Modellingt and analysis of marine operation, recomended practice, DNV-RP-H103*. Det Norske Veritas, 2011. Chap. 7. Towing Operations.

[22] The Engineering Toolbox. *Technical Terms in Fluid Mechanics*. URL: https://www.engineeringtoolbox.com/technical-terms-fluid-mechanics-d_181.html (visited on 03/03/2022).

[23] Paulo Flores. *Contact Force Models for Multibody Dynamics*. 1st ed. 2016. Vol. 226. Cham: Springer International Publishing : Imprint: Springer, 2016. ISBN: 3319308971.

[24] The engineering toolbox. *Friction - Friction Coefficients and Calculator*. URL: https://www.engineeringtoolbox.com/friction-coefficients-d_778.html (visited on 12/04/2022).

[25] Anastasios Lekkas, Andreas R Dahl, Morten Breivik and Thor I. Fossen. 'Continuous-Curvature Path Generation using Fermat's Spiral'. eng. In: *Modeling, Identification and Control* 34.4 (2013), pp. 183–198.

[26] Tor A. Johansen, Thor I. Fossen and Svein P. Berge. 'Constrained nonlinear control allocation with singularity avoidance using sequential quadratic programming'. In: *IEEE Transactions on Control Systems Technology* 12.1 (2004), pp. 211–216.

[27] Benedetto Piaggio, Michele Viviani, Michele Martelli and Massimo Figari. 'Z-Drive Escort Tug manoeuvrability model and simulation'. In: *Ocean Engineering* 191 (2019), p. 106461.

[28] Wolfram Mathworld. *Positive Definite Matrix*. URL: https://mathworld.wolfram.com/PositiveDefiniteMatrix.html#:~:text=A%20Hermitian%20(or%20symmetric)%20matrix,part%20has%20all%20positive%20eigenvalues. (visited on 31/05/2022).

[29] Thor I. Fossen. private communication. Oct. 2021.

[30] Abaqus. *Contact damping*. URL: https://abaqus-docs.mit.edu/2017/English/SIMACAEITNRefMap/simaitn-c-contactdamping.htm (visited on 04/03/2022).

[31] Ltd Nanjing Deers Industrial Co. *Tug Boat Fender*. URL: https://www.chinarubberfender.com/tug-boat-fender/ (visited on 25/04/2022).

[32] Øyvind F. Auestad, Jan T. Gravdahl, Tristan Perez, Asgeir J. Sørensen and Trygve H. Espeland. 'Boarding control system for improved accessibility to offshore wind turbines: Full-scale testing'. In: *Control Engineering Practice* 45 (2015), pp. 207–218.

[33] Abaqus. *Frictional behavior*. URL: https://abaqus-docs.mit.edu/2017/English/SIMACAEITNRefMap/simaitn-c-friction.htm#simaitn-c-friction-coulomb (visited on 03/05/2022).

[34] *Rules for classification, ,Ships, Part 5 Ship types*. Det Norske Veritas, 2020. Chap. 10. Vessels for special operations, section 11.Tugs and escort vessels.

[35] Thor I. Fossen. *TTK4190: Control Forces and Moments, NTNU*. Online lecture on Panopto. Oct. 2021.

[36] Wärtsilä. *638 995-3600kW at 750-1000 min^{-1} Total service, Wärtsilä deutz mairine engines*. URL: https://www.quantiparts.com/wp-content/uploads/2015/06/deutz-D628.pdf (visited on 24/03/2022).

[37] Thrustmaster. *Tunnel Thrusters – Electric Motor or Diesel Engine Driven*. URL: https://www.thrustmaster.net/tunnel-thrusters/electric-motor-driven-tunnel-thruster/ (visited on 04/04/2022).

[38] Morten D. Pedersen. *TTK4230 UKE 2 - Sammenligningsmetoden, NTNU*. Online video on Blackboard. Aug. 2020.

Appendix A

Specifications for tugboat and towline

A.1 Bulldog fleet specifications - Buksér & Berging

Fleet Specifications

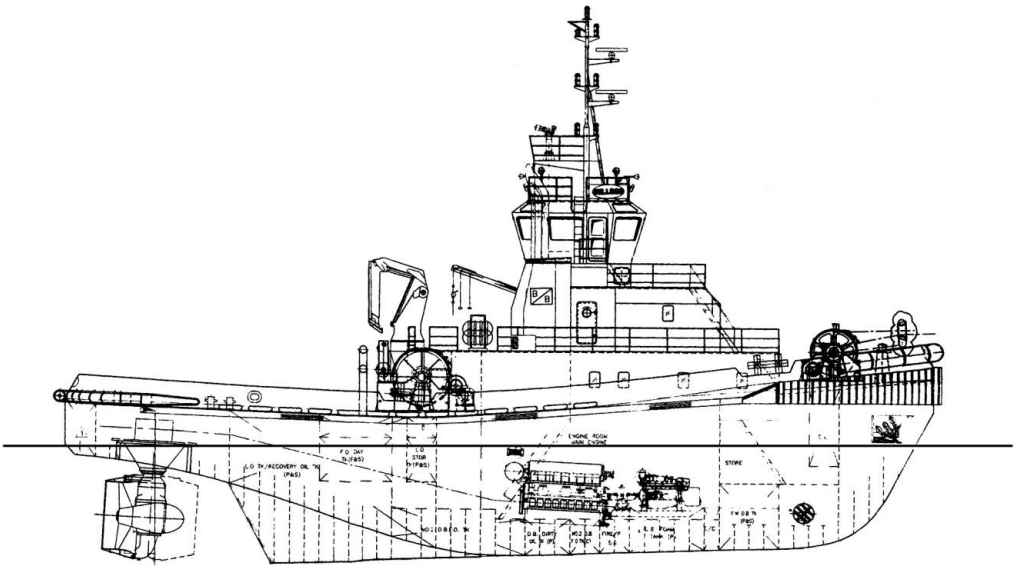

Type:		Azimuth Stern Drive	**Main engines:**	2 x Deutz SBV 9M 628
Built:		1999		5.508 bhp in total
Call sign:		LJMG	**Propulsion:**	FPP
IMO no.:		9200172	**Bowthruster**	252 hp
Port of registration:		Bergen	**Auxiliaries:**	400 kW
Class:		DNV +1A1 - E0 - Tug - OILREC	**Fire fighting:**	2 x water / foam monitors
Tonnage:		481 GRT		1.000 m^3/hr water
Speed:		13 knots	**Towing winch:**	Aft: 185 t brake
Bollard pull at MCR:		66.5 TBP		Fwd.: 175 t brake
Main dimensions:	Loa	35.00 m	**Deck equipment:**	Deck crane 64 tm
	Bmld	11.50 m		
	Dmld	5.30 m		
	Normal op.draft	5.20 m		

All the above particulars are believed to be correct, but not guaranteed

A.2 Towline specifications - TEHO ropes

FIBRE ROPE SPECIFICATIONS

MAGNARO®- HMPE Plus

PRODUCT PROPERTIES

Material	HMPE
Construction	12-strand
Jacketed	Yes
Rotating	No
Color of Rope	White
Specific Gravity	0.97 – 1.09
Melting Point	147°C / 260°C
Abrasion Resistance	Excellent
U.V. Resistance	Excellent
Chemical Resistance	Excellent
Dry & Wet Conditions	Identical wet & dry strength

FEATURES & BENEFITS

- Fibres are produced by gel-spinning ultra-high molecular weight polyethylene (UHMWPE)
- Higher strength compared to conventional steel wire rope
- Weight up to 7 times lower than wire rope
- Better handling
- Increased safety (no lash back)
- Cover can be made from polyester or HMPE
- Cover gives extra protection against abrasion, increasing the service life of the rope

APPLICATIONS

MOORING
- Main Line

TOWING
- Main Line

Dia. mm	Circ. inch	Weight* kg/100m	MBL	
			Ton	kN
28	3 ½	50.0	63.0	618.6
32	4	64.0	74.0	726.6
36	4 ½	78.9	93.0	913.2
40	5	94.8	114	1,002
44	5 ½	111	135	1,326
48	6	137	165	1,620
52	6 ½	160	195	1,915
56	7	183	230	2,258
60	7 ½	205	263	2,583
64	8	236	308	3,024
72	9	295	380	3,731
80	10	359	458	4,497
88	11	421	540	5,303
96	12	511	626	6,147

* Weights are with polyester cover, weights with HMPE cover are available upon request

Spliced Strength: -10%
MBL is in accordance with ISO 2307
Complies with OCIMF (MEG3)

Elongation at % of MBL :		
MBL	New	Used
25%	1.9%	0.5%
50%	2.8%	1.0%
100%	4.0%	2.0%

6

Appendix B

Simulink - Model dynamics

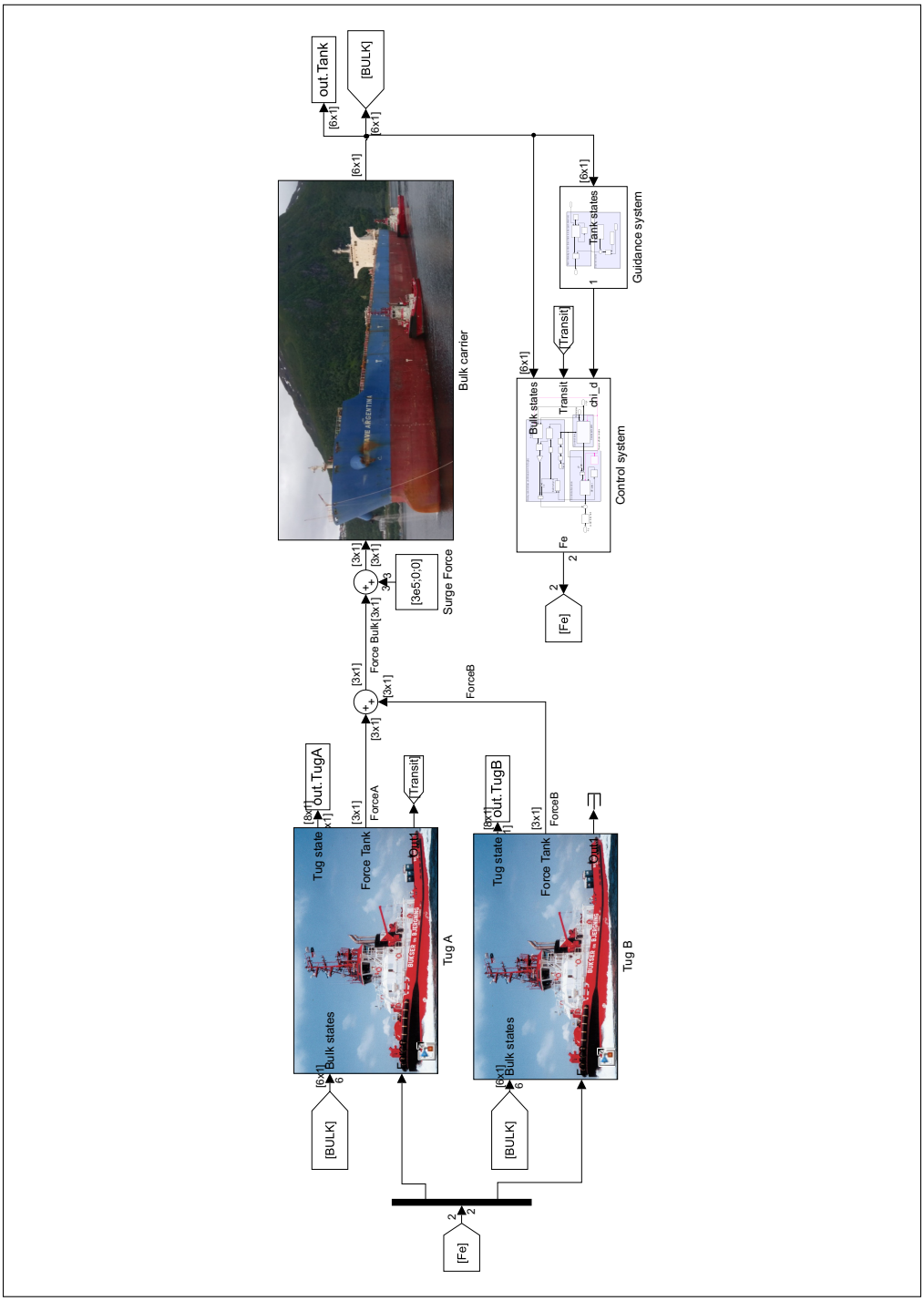

B.1 Tugboat reference model

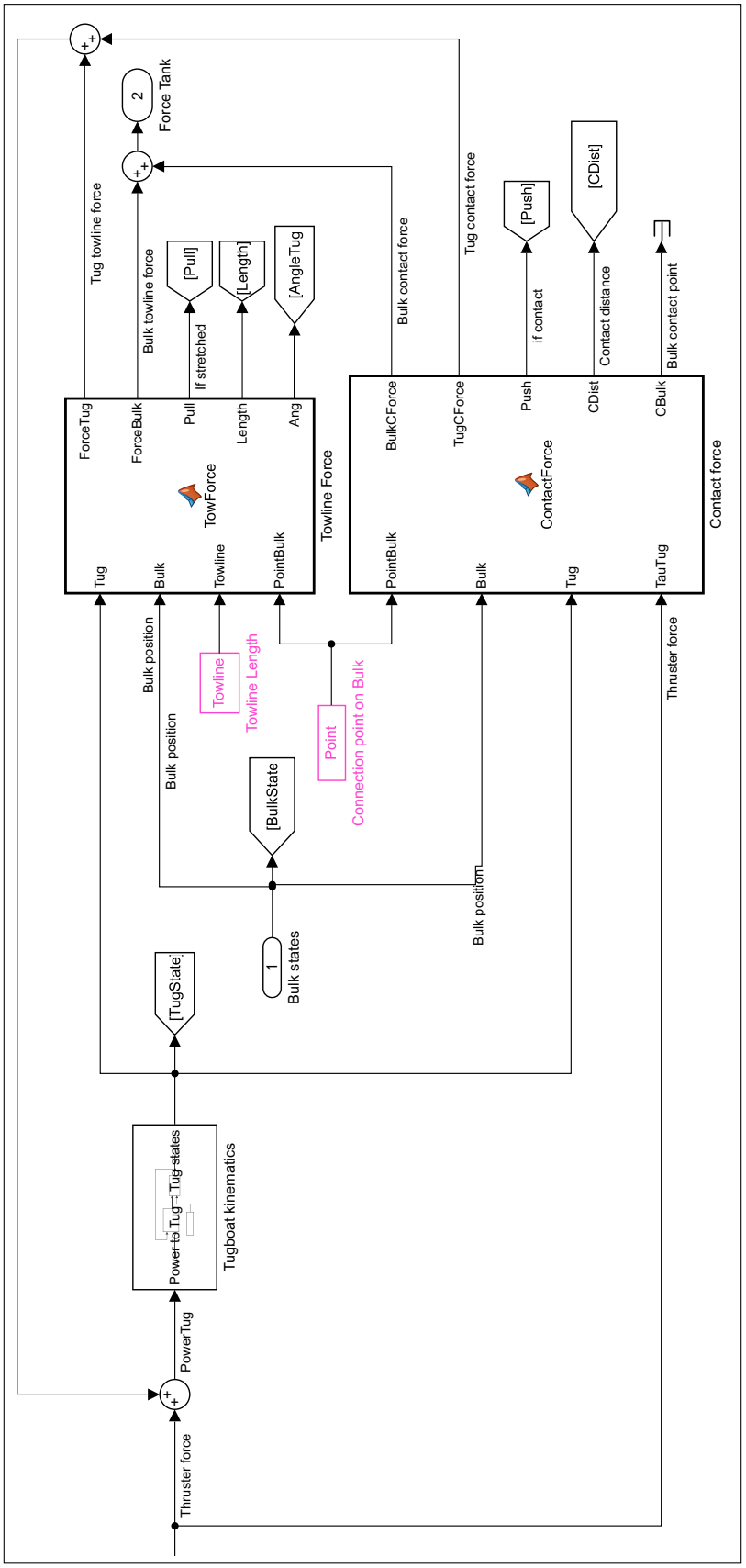

B.1.1 Function - Towline force

```
function [ForceTug,ForceBulk,Pull,Length,Ang]=TowForce(Tug, Bulk, ...
    Towline, PointBulk)
% ----Calculating distance between towline connections
k_E          = 6.63e7;
RBulk        = [cos(Bulk(3)), -sin(Bulk(3)); sin(Bulk(3)), cos(Bulk(3))];
RTug         = [cos(Tug(3)), -sin(Tug(3)); sin(Tug(3)), cos(Tug(3))];
PointTug     = [17.5;0];
PosBulk      = Bulk(1:2)+RBulk*PointBulk;
PosTug       = Tug(1:2)+RTug*PointTug;
Length       = sqrt((PosTug-PosBulk)'*(PosTug-PosBulk));
Vec          = (PosBulk-PosTug);
Ang          = atan2(Vec(2),Vec(1));
if Length ≥ Towline
% Calculating the relative velocity in the direction of the towline ...
    tension
     VBulk       = Bulk(4:5)+[-PointBulk(2);PointBulk(1)]*Bulk(6);
     VTug        =  Tug(4:5)+[-PointTug(2);PointTug(1)]*Tug(6);
     VelNed      = RTug*VTug-RBulk*VBulk;
     velTowline  = cos(Ang+pi)*VelNed(1)+sin(Ang+pi)*VelNed(2);
     Force       = ...
         (Length-Towline)/Towline*k_E+(0.01*sqrt(4*7.9e5*k_E)*velTowline);
     if Force <0
         Force   = 0;
     end
% Vector force from Bulk and Tug
     VecBulk     = RBulk'*(PosTug-PosBulk);
     AngBulk     = atan2(VecBulk(2),VecBulk(1));
     ForceBulk   = [1, 0; 0, 1; -PointBulk(2), ...
         PointBulk(1)]*[cos(AngBulk);sin(AngBulk)]*Force;
     VecTug      = RTug'*(PosBulk-PosTug);
     AngTug      = atan2(VecTug(2),VecTug(1));
     ForceTug    = [1, 0; 0, 1; -PointTug(2), ...
         PointTug(1)]*[cos(AngTug);sin(AngTug)]*Force;
     Pull        = true;
else
     ForceBulk   = zeros(3,1);
     ForceTug    = zeros(3,1);
     Pull        = false;
end
```

B.1.2 Function - Contact force

```
function [BulkCForce, TugCForce, Push,CDist,CBulk] = ...
    ContactForce(PointBulk, Bulk, Tug, TauTug)
% -----Calculating length between contact points -----%
RBulk   = [cos(Bulk(3)), -sin(Bulk(3)); sin(Bulk(3)), cos(Bulk(3))];
RTug    = [cos(Tug(3)), -sin(Tug(3)); sin(Tug(3)), cos(Tug(3))];
vec         = -sign(PointBulk(2))*RTug'*RBulk(:,2);
CTug        = [11.75;0]+5.75*vec;
CBulk1       = RBulk'*(Tug(1:2)+RTug*CTug-Bulk(1:2));
CBulk       = [CBulk1(1);PointBulk(2)];
CTug1       = RBulk'*(Tug(1:2)+RTug*CTug-Bulk(1:2));
CDist       = -sign(PointBulk(2))*(CBulk(2)-CTug1(2));
frontback   = abs(CBulk(1))-123;
if CDist <0 &&  frontback<0
    VBulk       = Bulk(4:5)+[-CBulk(2);CBulk(1)]*Bulk(6);
    VTug        =  Tug(4:5)+[-CTug(2);CTug(1)]*Tug(6);
    vRsway     = sign(PointBulk(2))*(VBulk(2)-[0,1]*RBulk'*RTug*VTug);
    vRsurge      = VBulk(1)-[1,0]*RBulk'*RTug*VTug;
    velD = [RTug.'*RBulk*[VBulk(1);0];0];
    dt=0.1;
    velD_dot = [RTug.'*RBulk*[vRsurge/dt;0];0];

    TugForce    = RBulk'*RTug*TauTug(1:2);
    [M,C,D,Dn]=ContactFriction(velD);
    stickForce = M*velD_dot+(C+D)*velD+Dn;
    stickDir = RBulk.'*RTug*stickForce(1:2);
    VelDFric= (stickForce(1)^2+stickForce(2)^2)^(0.5)*sign(stickDir(1));
    %Curve fitting for the M-fender stiffness and resulting displacement
    %force.
    A =abs(CDist)-[0; 0.05; 0.08; 0.095];
    C=A>0;
    Steps = [4500e3;2167e3;5000e3;8333e3];
    StiffForce=sum(A.*C.*Steps);
    Stiff = StiffForce/abs(CDist);

    CForce      = (StiffForce+0.1*sqrt(4*7.9e5*Stiff)*vRsway);
    if CForce<0
        CForce=0;
    end
    CForce=-sign(PointBulk(2))*CForce;
    CFric       = (exp(-7*abs(vRsurge))*0.15+0.25)*abs(CForce);
    MaxFriction =   VelDFric-TugForce(1);
    if abs(MaxFriction)≤CFric
        CFric       = MaxFriction;
        BulkForce   = -CFric;
    else
        CFric       = CFric*sign(MaxFriction);
        BulkForce   = -CFric;
```

```
47      end
48      FricTug      = [1,0;0,1,;-CTug(2),CTug(1)]*(RTug'*RBulk(:,1)*CFric);
49      BulkCForce   = [1,0;0,1;-CBulk(2),CBulk(1)]*[BulkForce;CForce];
50      TugCForce1   = [1,0;0,1;-CTug(2),CTug(1)]*(-vec*abs(CForce));
51      TugCForce    = TugCForce1+FricTug;
52      Push         = true;
53  else
54      BulkCForce   = zeros(3,1);
55      TugCForce    = zeros(3,1);
56      Push         = false;
57  end
```

B.1.3 Symbolic Matlab function - Tugboat dynamics

```
1  %==========Tugboat Dynamics====================%
2  syms xn yn psi  % Position and orientation
3  syms u v r      % linear and angular velocity
4  syms X Y N      % Forces and moments
5  eta      = [xn;yn;psi];      % Position and orientation (NED)
6  nu       = [u;v;r];          % Linear and angular velocity (NED)'
7  tau      = [X;Y;N];          % Forces and moments (BODY)
8  % measured values from BB bulldog drawing.
9  Pos      = [0.5,0.6, 5.1, 13.2, 16.7, 20.9, 29.9, 31.1, 32.3,32.9, ...
       34]-17.5;
10 Draft    = [0,0.4, 1.2, 3.7, 4.4, 4.3, 4.1, 3.9, 3.1, 2.3, 0];
11 PosKjol      = [6.7, 7.2, 7.8, 8.3, 12.6, 16.7]-17.5;
12 DraftKjol    = [0, 1.1, 1.9, 2.7, 1.2, 0];
13 % Position of endpoints (under the waterline) with respect to the CO
14 xq=-17:0.5:16.5;
15 vq = interp1(Pos,Draft,xq);
16 vqK = interp1(PosKjol,DraftKjol,xq);
17 vqK(isnan(vqK))=0;
18 % Calculating the side area of the hull under the waterline.
19 Lsection = diff(xq);
20 n = length(Lsection);
21 A = zeros(n,1);
22 for i=1:n
23     A(i) =(vq(i)+vq(i+1))/2*Lsection(i);
24 end
25 B = 11.5;            Volume   = sum(A)*B*0.7854*0.9;
26 rho      = 1025;      m        = Volume*rho*0.90;
27 T        = max(vq);   L        = 33.5;
28 CG       = [0,0,0];   R44      = 0;
29 R55      = 0;         Iz       = 1/12*m*(B^2+L^2)+m*CG(1)^2;
30 R66      = sqrt(Iz*0.6/m);
31 % Rigid body inertia and coriolis matrix
32 [MRB_CO, CRB_CO] = rbody(m,R44,R55,R66,[0;0;r],CG);
33 MRB_CO  =   [MRB_CO(1,1),MRB_CO(1,2),MRB_CO(1,6);
```

```
              MRB_CO(2,1), MRB_CO(2,2), MRB_CO(2,6);
              MRB_CO(6,1), MRB_CO(6,2),MRB_CO(6,6)];

CRB_CO  =   [CRB_CO(1,1),CRB_CO(1,2),CRB_CO(1,6);
              CRB_CO(2,1), CRB_CO(2,2), CRB_CO(2,6);
              CRB_CO(6,1), CRB_CO(6,2),CRB_CO(6,6)];
% Added mass and coriolis matrix
M_A     =   [8e4, 0, 0;
              0 , 3.9e5, 1e6;
              0, -5e5, 3e7];

           % Rotation matrix from Body to NED
C_A     =   m2c(M_A,nu);
C       =   CRB_CO+C_A;
M       =   MRB_CO+M_A;
%linear damping
D       = zeros(3,3);
D(1,1)=M(1,1)/50; D(2,2)=M(2,2)/80; D(3,3)=M(3,3)/10;
% Nonlinear surge damping
S       = 2*sum(A)+B*L+2*B*T*0.75;
kinVisc = 1e-6;
ur      =u;
Rn      = L/kinVisc*abs(ur);
eps     =0.001;
CR      = 0.02;              % Surface friction
Cf      = 0.075/((log10(Rn)-2)^2+eps)+CR;
Xdamp   = -0.5*rho*S*(1+0.25)*Cf*abs(ur)*ur;
% Cross-flow drag principle, with K defining the extra "Keel"
Cd=zeros(1,length(xq));
for k=1:length(Cd)
    Check = B/(2*vq(k));
    if Check>4
        Cd(k)=0.5;
    else
        Cd(k)= Hoerner(B,vq(k));
    end
end
CdK = zeros(1,length(xq));
B2=1;
for k2=1:length(CdK)

    if  vqK(k2)<0.1
        CdK(k2)=0;
    else
        CdK(k2)= Hoerner(B2,vqK(k2));
    end
end
gain =ones(1,length(xq)); gain(2:end-1)=2;
dx=0.5;
vr=v;
Ydamp = sum(-rho*0.5*dx*0.5*gain.*Cd.*vq.*abs(vr+xq*r).*(vr+xq*r));
```

```
85 Ndamp = sum(-rho*0.5*dx*0.5*gain.*Cd.*vq.*xq.*abs(vr+xq*r).*(vr+xq*r));
86 YKdamp= sum(-rho*0.5*dx*0.5*gain.*CdK.*vqK.*abs(vr+xq*r).*(vr+xq*r));
87 NKdamp= sum(-rho*0.5*dx*0.5*gain.*CdK.*vqK.*xq.*abs(vr+xq*r).*(vr+xq*r));
88 Ydamp = Ydamp+YKdamp;
89 Ndamp = Ndamp+NKdamp;
90 Dn    = -[Xdamp;Ydamp;Ndamp];
91 % ------- Creating dynamic functions------%
92 R       =   Rzyx(0,0,eta(3));
93 eta_dot = R*nu;
94 states  = [eta;nu];
95 matlabFunction(M,C,D,Dn,eta_dot,'file','TugDynamicsCALC',...
96     'vars',{states},'Comments',"in1=states=[xn;yn;psi;u;v;r]")
97 %%  Sliding friction
98 matlabFunction(M,C,D,Dn,'file','ContactFriction',...
99     'vars',{nu},'Comments',"in1=states=[uM;vM;0]")
```

B.2 Bulk carrier subsystem

B.2.1 Symbolic Matlab function - Bulk carrier dynamics

```
%==========Bulk carrier Dynamics ====================%
% Data obtained from MSS toolbox, wamit file Tanker, by T. I. Fossen.
syms xn yn psi  % Position and orientation
syms u v r      % linear and angular velocity
syms X Y N      % Forces and moments
eta     = [xn;yn;psi];      % Position and orientation (NED)
nu      = [u;v;r];          % Linear and angular velocity (NED)'
tau     = [X;Y;N];          % Forces and moments (BODY)
load tanker% Tanker specifications
m       = vessel.main.m;     T       = vessel.main.T;
B       = vessel.main.B;     Lpp     = vessel.main.Lpp;
nabla   = vessel.main.nabla; rho     = vessel.main.rho;
CG      = vessel.main.CG;    R44     = vessel.main.k44;
R55     = vessel.main.k55;   R66     = vessel.main.k66;
A0      = vessel.A(:,:,1);   B0      = zeros(3);
% -------Hydrodynamic forces from------%
[MRB_CO, CRB_CO] = rbody(m,R44,R55,R66,[0;0;r],CG);
MRB_CO  =   [MRB_CO(1,1),MRB_CO(1,2),MRB_CO(1,6);
             MRB_CO(2,1), MRB_CO(2,2), MRB_CO(2,6);
             MRB_CO(6,1), MRB_CO(6,2),MRB_CO(6,6)];
CRB_CO  =   [CRB_CO(1,1),CRB_CO(1,2),CRB_CO(1,6);
             CRB_CO(2,1), CRB_CO(2,2), CRB_CO(2,6);
             CRB_CO(6,1), CRB_CO(6,2),CRB_CO(6,6)];
M_A     =   [A0(1,1), 0, 0;
             0 A0(2,2), A0(2,6);
             0, A0(6,2), A0(6,6)];
R       =   Rzyx(0,0,eta(3));
C_A     =   m2c(M_A,nu);
C       =   CRB_CO+C_A;
M       =   MRB_CO+M_A;
D       = zeros(3,3);
D(1,1)=M(1,1)/160; D(2,2)=M(2,2)/19; D(3,3)=M(3,3)/21;
% -------  functions------%
eta_dot = R*nu;
nu_dot  =M\(tau-C*nu-D*nu);
states = [eta;nu]; input = tau;
matlabFunction(eta_dot,nu_dot,'file','TankerDynamics',...
    'vars',{states,input},'Comments','in1=states=[xn;yn;psi;u;v;r], ...
       in2=inputs=[X;Y;N]')
```

Appendix C

Simulink - Tugboat control system

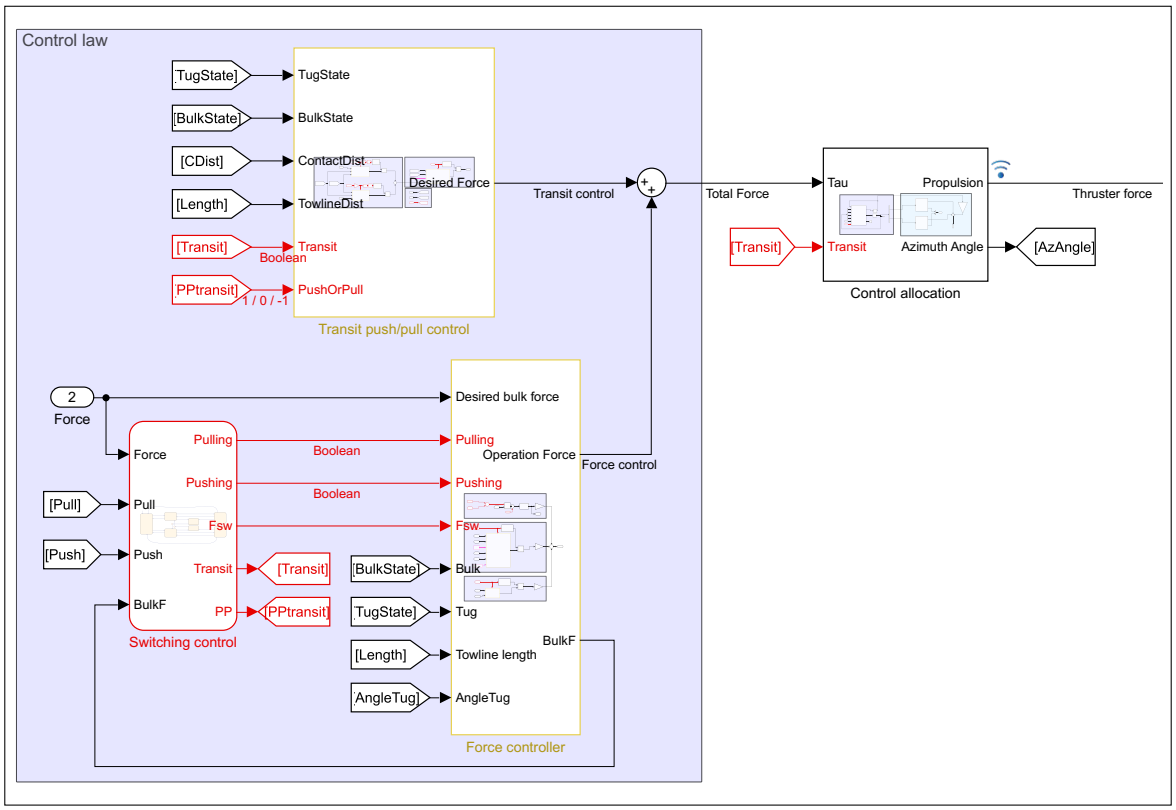

C.1 Simulink - Tugboat control allocation

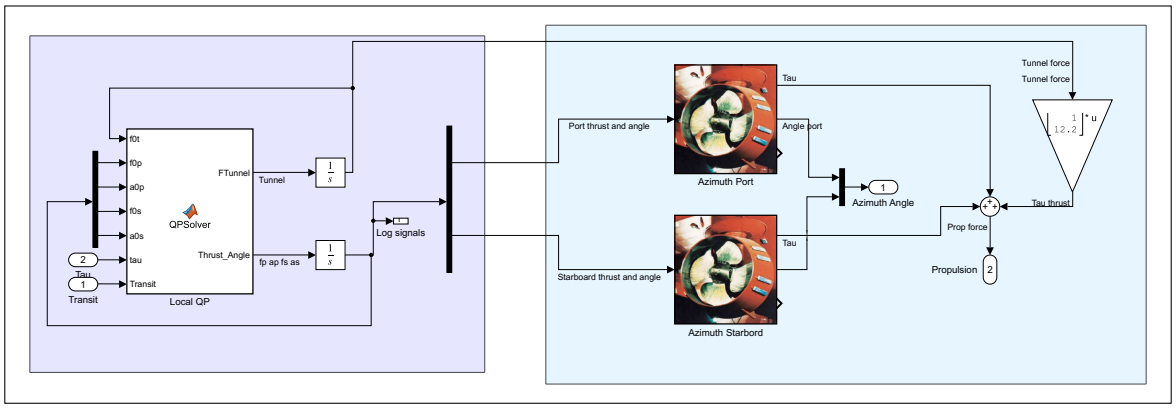

C.1.1 Simulink - Azimuth thruster

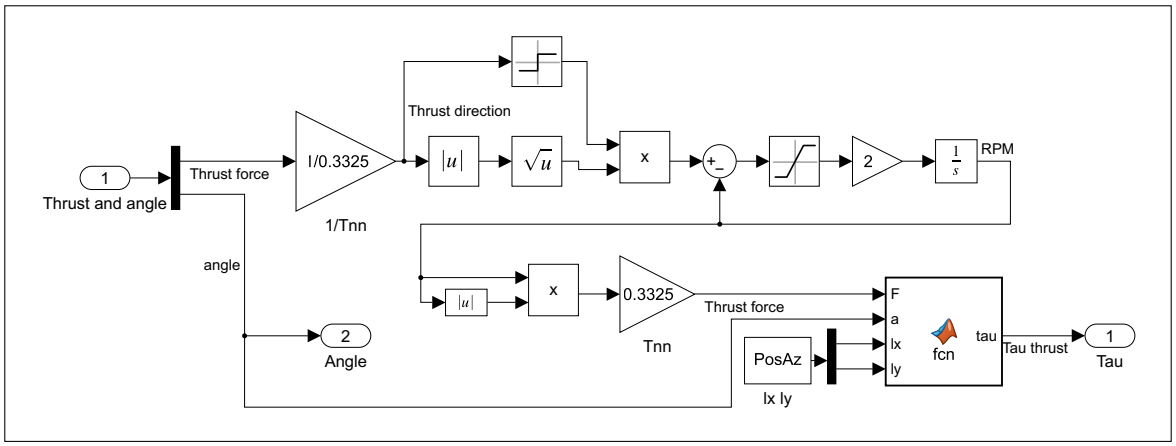

C.1.2 Function - Local QP solver

```
function [FTunnel,Thrust_Angle]    = QPSolver(f0t,f0p, a0p, f0s, a0s, ...
    tau, Transit)
f0 = [f0t;f0p;f0s]; a0 = [a0p;a0s];
lyp = -3; lxp = -13.9; lys = 3; lxs = -13.9;
Tunnel = [0;1;12.2]*Transit;
T =     [Tunnel,    [cos(a0p),cos(a0s);
                     sin(a0p),sin(a0s);
                    -lyp*cos(a0p)+lxp*sin(a0p),-lys*cos(a0s)+lxs*sin(a0s)]];
dT = [-sin(a0p)*f0p,-sin(a0s)*f0s;
          cos(a0p)*f0p,cos(a0s)*f0s;
          (lyp*sin(a0p)+lxp*cos(a0p))*f0p,(lys*sin(a0s)+lxs*cos(a0s))*f0s];
fLim = [-27e3,27e3; 0.01,25e4; 0.01,25e4]; aLim = deg2rad([0,180; ...
    -180,0]);
fRate = [27e3/2; 25e4/10; 25e4/10];        aRate = deg2rad([18;18]);
[df,da,s] = TugAlloc_lbub(tau,T, dT,f0,a0,fLim,aLim,fRate,aRate); % ...
    solver
FTunnel = df(1); Fp=df(2); Fs = df(3); Ap=da(1); As=da(2);
Thrust_Angle = [Fp;   Ap;   Fs;   As];
%%%%%%%%%%%%%%%%%%%%%%%%%%%%%%%%%%%%%%%%%%%%%%%%
function [df,da,s] = TugAlloc_lbub(tau,T, dT,f0,a0,fLim,aLim,fRate,aRate)
ne      = length(f0);   % Number of effectors
na      = length(a0);   % Number of rotating thrusters
nd      = length(tau);  % Number of DOF (forces and moments)
% Parameters for azimuth thrusters
f_min   = fLim(:,1);    f_max   = fLim(:,2);
df_min  = -fRate;       df_max  = fRate;
a_min   = aLim(:,1);    a_max   = aLim(:,2);
da_min  = -aRate;       da_max  = aRate;
lb =    [df_min; da_min; ones(nd,1)*-inf];
ub =    [df_max; da_max; ones(nd,1)*inf];
% Weighting matrices
 W  = eye(ne)*diag([5,80,80]); Ohm = eye(na)*1;
```

```
30   Q  = eye(nd)*diag([1e4,1e4,1e5]);
31  PHI =   [W, zeros(ne,na), zeros(ne,nd);
32           zeros(na,ne), Ohm, zeros(na,nd);
33           zeros(nd,ne), zeros(nd,na), Q];
34  P = [tau', f_min', f_max', a_min', a_max',a0', f0']';
35  R = zeros(size(PHI,1),size(P,1));
36  R(1:ne,end-(ne-1):end) = W;
37  % Equalities
38  A1          = [T, dT, eye(nd)]; C1 =  zeros(nd,length(P));
39  C1(1:nd,1:nd) = eye(nd);        C1(1:nd,end-(ne-1):end) = -T;
40  % Inequalities
41  A2      =  [-eye(ne), zeros(ne,na), zeros(ne,nd);
42               eye(ne), zeros(ne,na), zeros(ne,nd);
43               zeros(na,ne),-eye(na), zeros(na,nd);
44               zeros(na,ne), eye(na), zeros(na,nd)];
45  C2      = [zeros(ne,nd), -eye(ne), ...
        zeros(ne,ne),zeros(ne,na),zeros(ne,na),zeros(ne,na), eye(ne);
46              zeros(ne,nd), zeros(ne,ne), eye(ne), ...
                    zeros(ne,na),zeros(ne,na),zeros(ne,na),-eye(ne);
47              zeros(na,nd), zeros(na,ne), zeros(na,ne), -eye(na), ...
                    zeros(na,na),eye(na),zeros(na,ne);
48              zeros(na,nd), zeros(na,ne), zeros(na,ne), zeros(na,na), ...
                    eye(na), -eye(na),zeros(na,ne)];
49  options = optimoptions( 'quadprog', 'Algorithm','active-set');
50  x0 = [f0;a0;zeros(nd,1)];
51  X = quadprog(PHI,(R*P).',A2,C2*P,A1,C1*P,lb,ub,x0, options);
52  df = X(1:ne);   da = X(ne+1:ne+na); s = X(ne+na+1:na+ne+nd);
53  end
```

C.2 Simulink - Transit push/pull control law

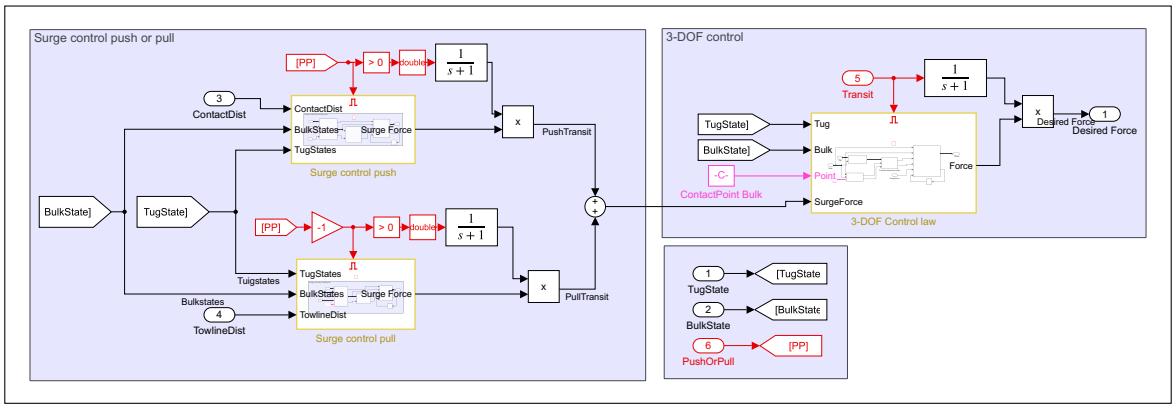

C.2.1 Enabled subsystem - 3-DOF control law

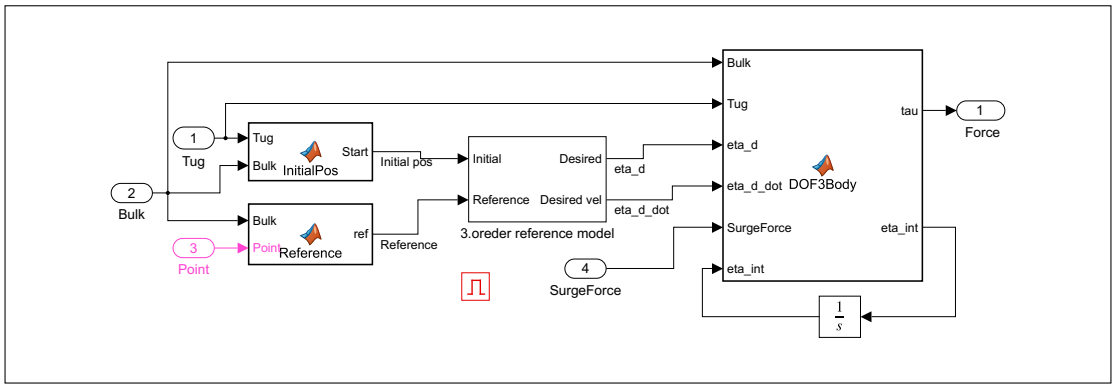

3. order reference model

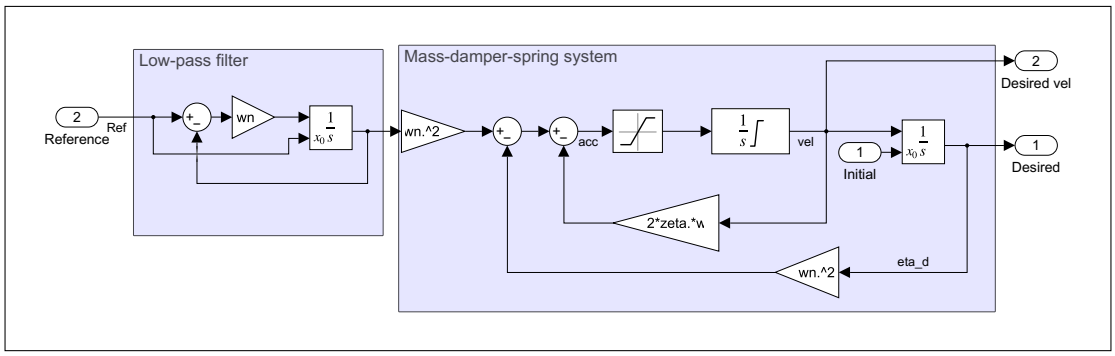

Function - DOF3Body

```
function [tau,eta_int]    = DOF3Body(Bulk, Tug, eta_d,eta_d_dot, ...
    SurgeForce,eta_int)
eta = Tug(1:3); nu  = Tug(4:6); wb = [0.2;0.2;0.3]; zeta = ones(3,1);
%From NED to Body
[Kp,Kd,Ki] = TugPID_Gains(wb,zeta,eta(3)-Bulk(3),nu);
RTug    = [cos(Tug(3)), -sin(Tug(3)); sin(Tug(3)), cos(Tug(3))];
RBulk   = [cos(Bulk(3)), -sin(Bulk(3)); sin(Bulk(3)), cos(Bulk(3))];
Dist =  RBulk.'*(Tug(1:2)-Bulk(1:2));
eta_tilde = [Dist(1)-eta_d(1);0;eta(3)-eta_d(3)];
ye_dot = RBulk'*RTug*nu(1:2)-Bulk(4:5);
eta_tilde_dot =  [ye_dot(1);0;nu(3)]-eta_d_dot;
eta_tilde(3) = ssa(eta_tilde(3));
RRTug =Rzyx(0,0,eta(3)); RRBulk =Rzyx(0,0,Bulk(3));
PIDtau = -Kp*eta_tilde-Kd*eta_tilde_dot-Ki*eta_int;
    eta_int =eta_tilde;
    tau=RRTug'*RRBulk*PIDtau+[SurgeForce;0;0];
%%%%%%%%%From tugboat symbolic %%%%%%%%%%%%%
%==========Tug 3-DOF PID controller====================%
 syms wb1 wb2 wb6 zeta1 zeta2 zeta6
 Skew = Smtrx([0;0;r]);
```

```
20  Wb=[wb1; wb2; wb6];
21  Zeta = [zeta1; zeta2; zeta6];
22  Omega_b = diag([wb1,wb2, wb6]);
23  Z = diag([zeta1,zeta2, zeta6]);
24  wn1=1/((1-2*zeta1^2+(4*zeta1^4-4*zeta1^2+2)^(1/2))^(1/2))*wb1;
25  wn2=1/((1-2*zeta2^2+(4*zeta2^4-4*zeta2^2+2)^(1/2))^(1/2))*wb2;
26  wn6=1/((1-2*zeta6^2+(4*zeta6^4-4*zeta6^2+2)^(1/2))^(1/2))*wb6;
27 Omega_n = diag([wn1,wn2,wn6]);
28 Kp = R*M*R.'*(Omega_n.'*Omega_n);
29 Kd = 2*R*M*R.'*Z*Omega_n-R*(C+D)*R.'+R*M*R.'*Skew;
30 Ki = 1/10*Kp*Omega_n;
31 matlabFunction(Kp,Kd,Ki,'file','TugPID_Gains','vars',{Wb,Zeta,psi,nu});
```

C.2.2 Enabled subsystem - Surge control

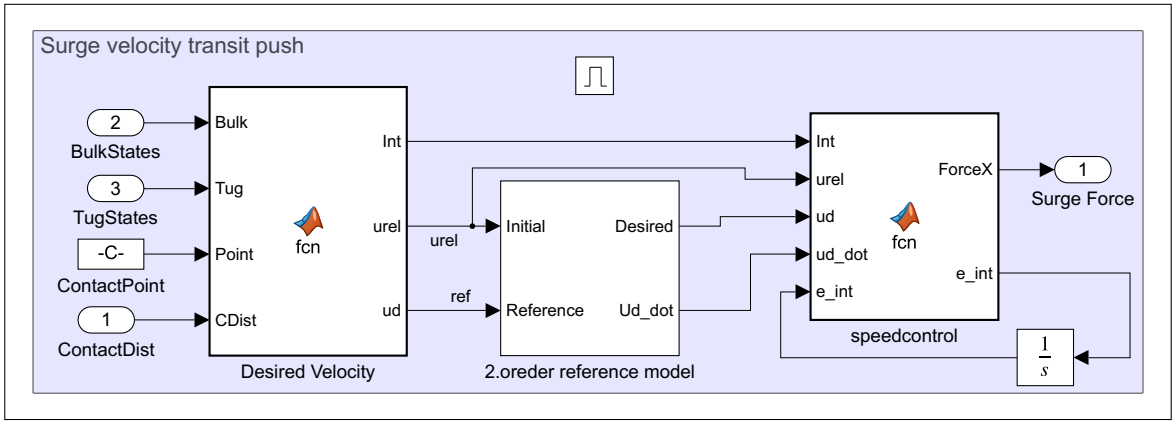

2. order reference model

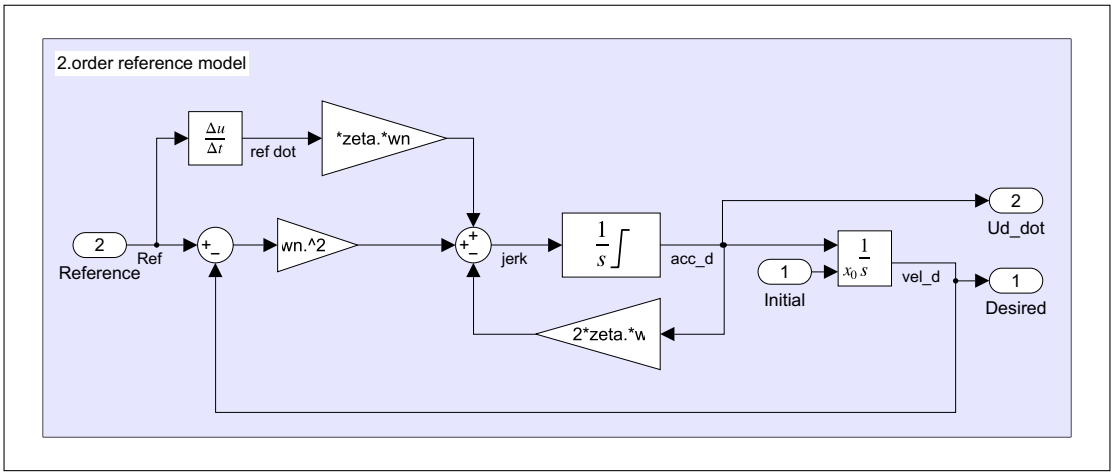

C.3 Stateflow - Switching control

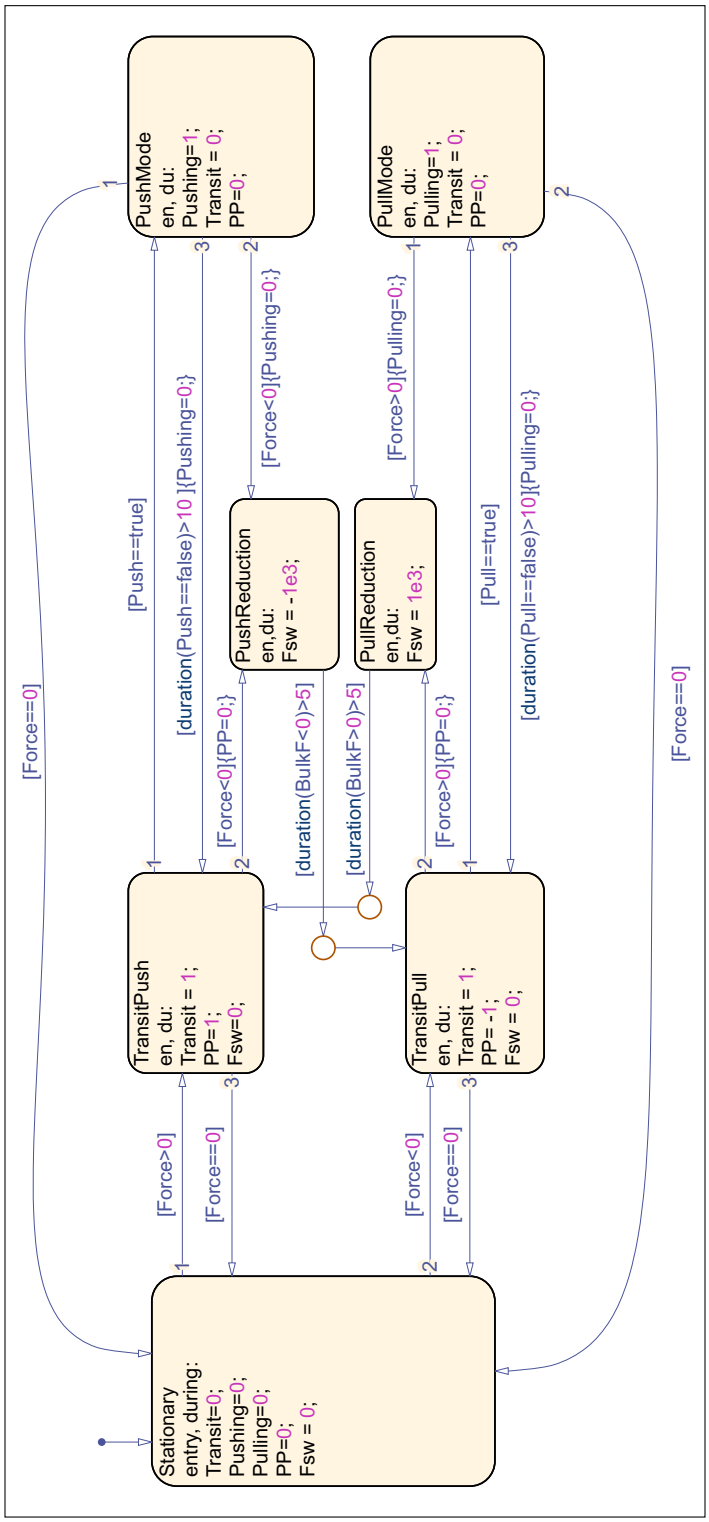

C.4 Simulink - Force control

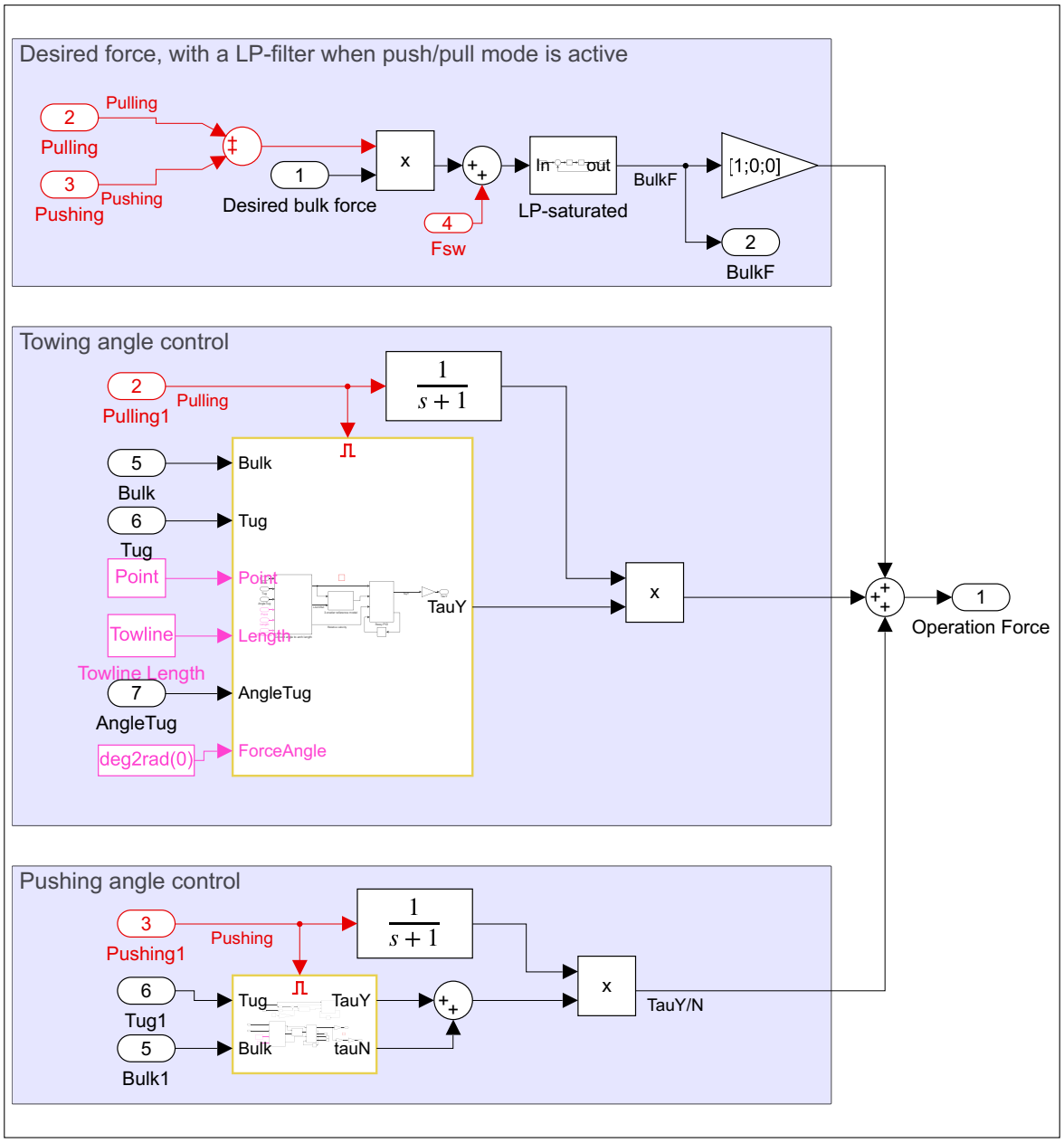

C.4.1 Enabled subsystem - Towing angle control

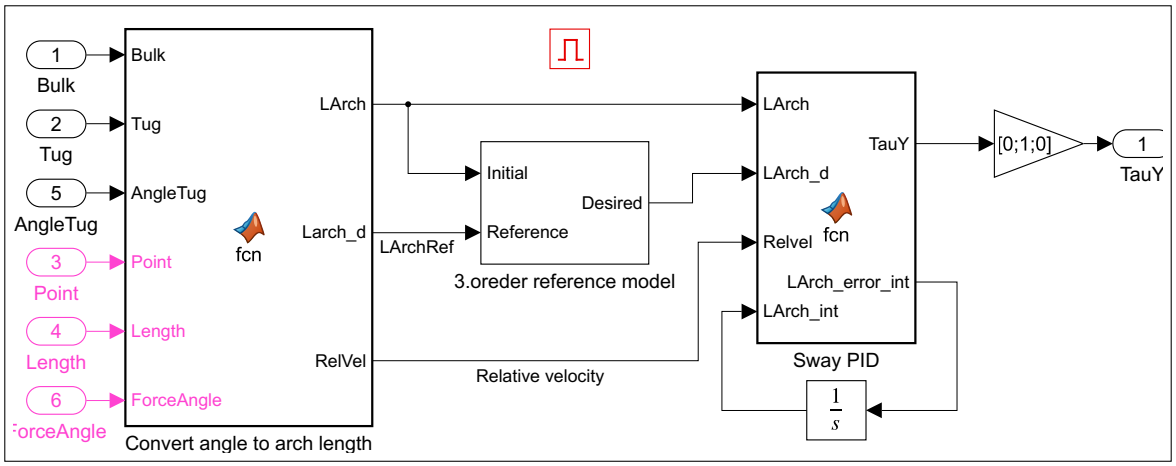

Convert angle to arch length

```
function [LArch,Larch_d,RelVel] = ...
    fcn(Bulk,Tug,AngleTug,Point,Length,ForceAngle)
alpha = AngleTug-Bulk(3);
alpha_d  = sign(Point(2))*pi/2+ForceAngle;
% Velocity of desired angle of attack
TowPBulk = Point+(Length+17.5)*[cos(alpha_d);sin(alpha_d)];
Ralpd = [cos(alpha_d),-sin(alpha_d); sin(alpha_d),cos(alpha_d)];
TowPointVel = ...
    [0,1]*Ralpd'*(Bulk(4:5)+[-TowPBulk(2);TowPBulk(1)]*Bulk(6));
% Velocity of  angle of attack
Ralph = [cos(alpha),-sin(alpha); sin(alpha),cos(alpha)];
RTug = [cos(Tug(3)),-sin(Tug(3)); sin(Tug(3)),cos(Tug(3))];
RBulk = [cos(Bulk(3)),-sin(Bulk(3)); sin(Bulk(3)),cos(Bulk(3))];
TugpointVel = [0,1]*Ralph'*RBulk'*RTug*(Tug(4:5));

RelVel = TowPointVel-TugpointVel;
LArch   = alpha*(Length+17.5);
Larch_d = alpha_d*(Length+17.5);
```

Appendix D

Simulink - Bulk carrier control system

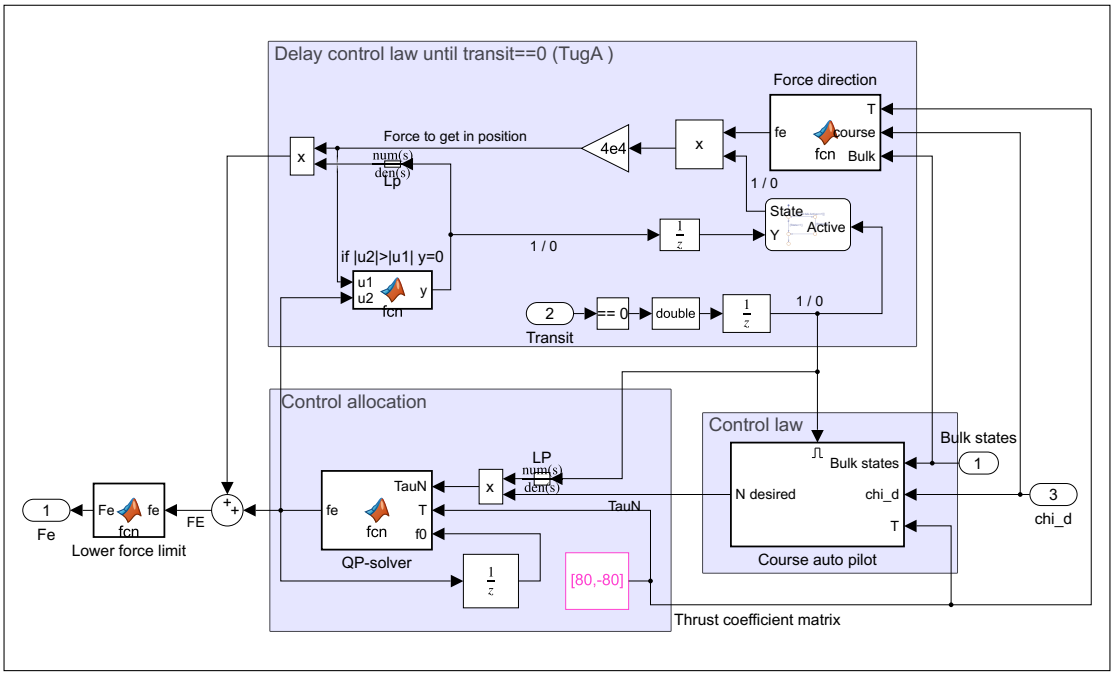

D.1 Enabled subsystem - Course autopilot

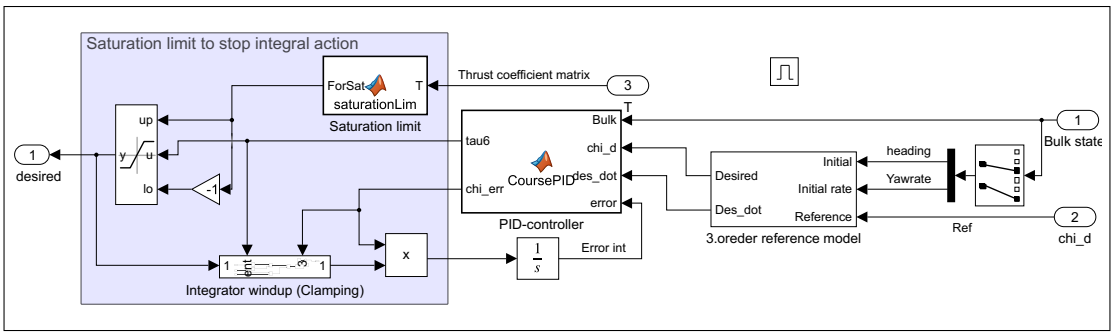

D.2 Matlab code - QP-solver

```
function fe = fcn(TauN,T,f0)
dMax = 50e4/10*0.025;
f_max=ones(length(T),1)*50e4;
f_min=-f_max;
fe = QPsovler_Bulk(TauN,Te,f0,dMax,f_max,f_min);
function fe = QPsovler_Bulk(tau,Te,f0,dMax,f_max,f_min)
r       = size(Te,2);
n       = size(Te,1);
Df = ones(r,1)*dMax;
beta    = 1;
P = [tau',f_min',f_max',beta,f0',Df']';
W = eye(r)*1;
Q = eye(n)*1000;
PHI =   [W, zeros(r,n), zeros(r,1);
         zeros(n,r), Q, zeros(n,1);
         zeros(1,r), zeros(1,n), 0];
R = [zeros(r+n+1,n+2*r), [zeros(r+n,1);1],zeros(r+n+1,r),zeros(r+n+1,r)];
%----Equalities----------%
A1 = [Te,-eye(n), zeros(n,1)];
C1 = [eye(n),zeros(n,2*r+1),zeros(n,r),zeros(n,r)];
%-----Inequalities---------%
A2 =    [-eye(r), zeros(r,n), zeros(r,1);
         eye(r), zeros(r,n), zeros(r,1);
         -eye(r), zeros(r,n),-ones(r,1);
         eye(r), zeros(r,n),-ones(r,1);
         eye(r), zeros(r,n),zeros(r,1);
         -eye(r), zeros(r,n), zeros(r,1)];
C2 = zeros(6*r,4*r+n+1);
C2(1:r,n+1:n+r)=-eye(r);                % fmin
C2(r+1:2*r,r+n+1:n+2*r)=eye(r);         % Fmax
C2(4*r+1:5*r,n+2*r+2:n+3*r+1)=eye(r); % F0
C2(4*r+1:5*r,n+3*r+2:n+4*r+1)=eye(r); % Df
C2(5*r+1:6*r,n+2*r+2:n+3*r+1)=-eye(r); % -F0
C2(5*r+1:6*r,n+3*r+2:n+4*r+1)=eye(r); % Df
options = optimoptions( 'quadprog', 'Algorithm','active-set');
X = quadprog(PHI,(R*P)',A2,C2*P,A1,C1*P,[],[],zeros(n+r+1,1), options);
fe=X(1:r);
end
```

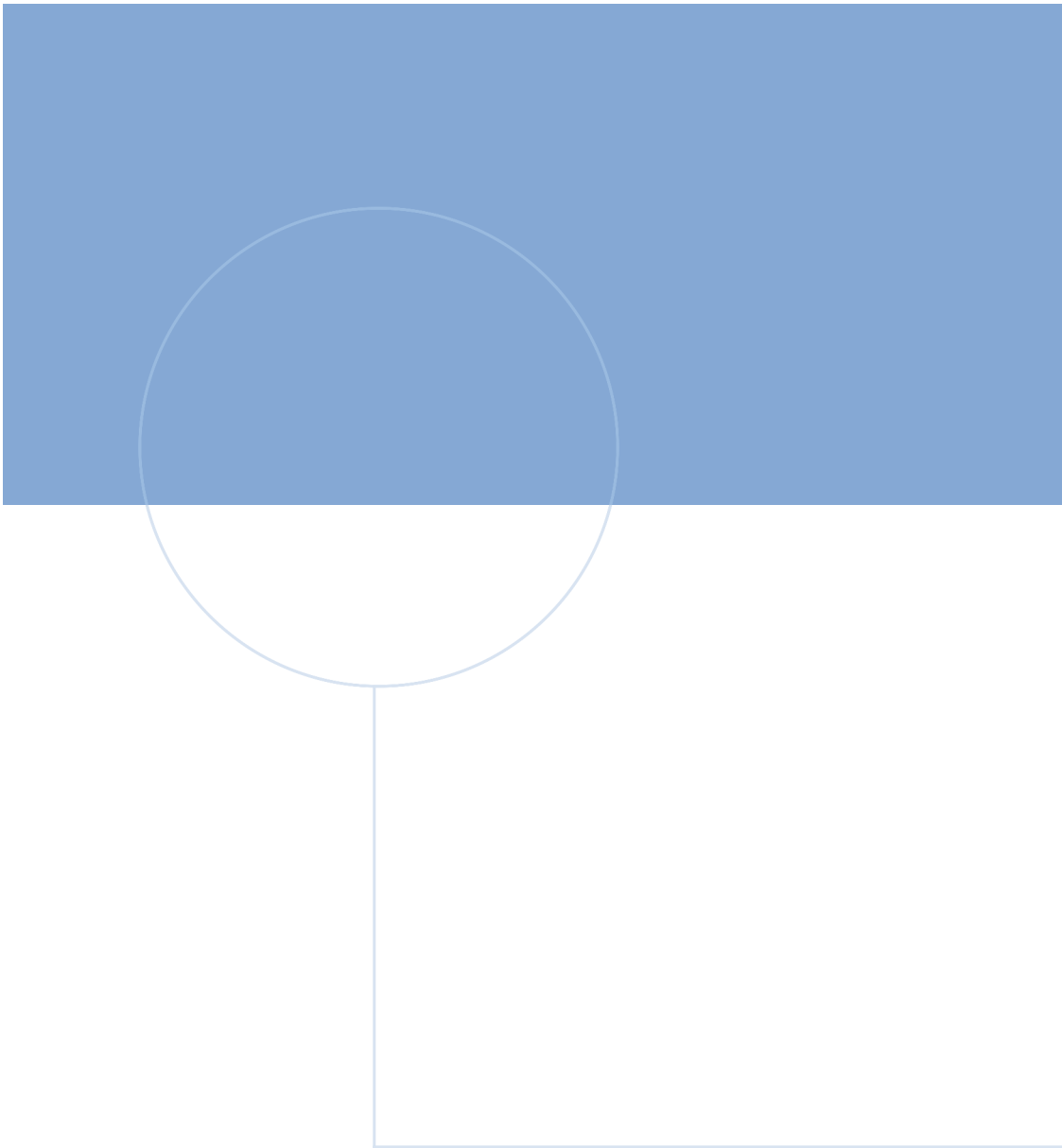

NTNU

Norwegian University of
Science and Technology